ERASMUS MUNDUS MSC PROGRAMME

COASTAL AND MARINE ENGINEERING AND MANAGEMENT
COMEM

ADAPTATION OF SECOND ORDER WAVEMAKER THEORIES TO THE CIEMITO WAVE FLUME

Claudio Gillen
1550276

Universitat Politècnica de Catalunya
16/06/2010

The Erasmus Mundus MSc Coastal and Marine Engineering and Management is an integrated programme organized by five European partner institutions, coordinated by Delft University of Technology (TU Delft).
The joint study programme of 120 ECTS credits (two years full-time) has been obtained at three of the five CoMEM partner institutions:

- Norges Teknisk- Naturvitenskapelige Universitet (NTNU) Trondheim, Norway
- Technische Universiteit (TU) Delft, The Netherlands
- City University London, Great Britain
- Universitat Politècnica de Catalunya (UPC), Barcelona, Spain
- University of Southampton, Southampton, Great Britain

The first year consists of the first and second semesters of 30 ECTS each, spent at NTNU, Trondheim and Delft University of Technology respectively.
The second year allows for specialization in three subjects and during the third semester courses are taken with a focus on advanced topics in the selected area of specialization:

- Engineering
- Management
- Environment

In the fourth and final semester an MSc project and thesis have to be completed.
The two year CoMEM programme leads to three officially recognized MSc diploma certificates. These will be issued by the three universities which have been attended by the student. The transcripts issued with the MSc Diploma Certificate of each university include grades/marks for each subject. A complete overview of subjects and ECTS credits is included in the Diploma Supplement, as received from the CoMEM coordinating university, Delft University of Technology (TU Delft).

Information regarding the CoMEM programme can be obtained from the programme coordinator and director

Prof. Dr. Ir. Marcel J.F. Stive
Delft University of Technology
Faculty of Civil Engineering and geosciences
P.O. Box 5048
2600 GA Delft
The Netherlands

EXECUTIVE SUMMARY

Coastal engineering deals with complex systems that involve processes that are not fully understood. Physical modeling has become an important tool in the study of these processes. It allows researchers to control the conditions that are being studied, and simplify the system to include only what is desired. In a coastal system waves are often one of the main driving forces of these processes. Because of this it is of great importance to have the ability to reproduce the natural wave conditions in the laboratory settings.

When generating waves with a low relative water depth, and/or a high wave steepness using first order wavemaker theory the resulting waves are contaminated with an unwanted secondary wave, which causes the generated wave profile to change as the wave travels along the wave flume. The aim of this study is to find under which conditions this issue takes place in the CIEMito wave flume of the Laboratori d'Enginyeria Marítima (LIM), and to implement a second order wavemaker theory capable of suppressing it.

Several wavemaker theories were studied, the first order wavemaker theory, and several second order wavemaker theories. Due to issues arising with the implementation of most of the second order theories, only the first order wavemaker theory and the second order wavemaker theory given by Madsen (1971) were applied to the CIEMito wave flume.

Thirty-seven different wave conditions were tested in the CIEMito wave flume using first order wavemaker theory. From this the issues with first order wave generation were studied. Due to issues with the physical wave flume the second order theory could not be tested there. Instead, a numerical wave flume based on PFEM (particle finite element method) was validated so that the CIEMito wave flume could be simulated with this numerical model. Four of the wave conditions tested in the physical wave flume were simulated using both first order and second order Madsen wavemaker theory. From this the capability of Madsen's second order wavemaker theory of suppressing the unwanted secondary waves was assessed.

ACKNOWLEDGEMENTS

Firstly I would like to give a big thank you to Xavi Gironella and Tiago Oliveira for their patience, guidance and support through this master thesis. To my family and friends, thank you for giving me the encouragement I needed to finish this master thesis. I would also like to thank the staff of UPC and LIM who have welcomed me in their institution. Finally, I would like to thank the people of NTNU, TUDelft, and UPC, and everyone who made the CoMEM Erasmus Mundus program possible, and an amazing experience. Thank you, tussen takk, dank je wel, merci, pura vida.

TABLE OF CONTENTS

LIST OF TABLES

LIST OF FIGURES

1. INTRODUCTION

1.1. PROBLEM DEFINITION

Physical modeling has been a very important tool for coastal engineers for many years. The coastal system is a very complex system, and the processes that take place within it are not completely understood. Having a physical model of the system to study these processes, in which the conditions may be controlled, is a great advantage to having to go out in the field to obtain the data. It also provides a way to study how a coastal work will react to the system, and the effects it could have on the coastal system, before it is actually done.

In the coastal environment very often one of the most important driving forces to the processes that take place within the system are waves. Waves drive longshore sediment transport, they are one of the main design factors for costal structures, and they create currents, amongst other things. Because of this it is very important to have the ability of generating the same wave conditions that are found in nature in the laboratory environment.

Over the years laboratory wave generation has evolved from a simple board moving sinusoidally with a given amplitude and period, to complex wavemaker theories that predict the resulting waves from different wave paddle motions. Havelock (1929) is said to provide the beginning of wavemaker theory, where a general theory for wave generation is given. Bièsel and Suquet (1954) were the first to give the solution to the first order wavemaker problem for a hinged and piston paddle, and it has since been given by several others.

The waves generated by using the first order wavemaker theory coincide quite well with those predicted by the theory, except when the waves have a large wave steepness, H/L, and/or a small relative water depth, h/L. In these cases an unwanted secondary wave is generated along with the desired primary wave. As described by Goda (1967) the secondary wave travels at a slightly slower speed than the primary wave. This causes the secondary wave crest to be present in the trough of the primary wave, then slowly drift back and be absorbed by the primary wave crest, and then move into the

trough of the primary wave again. This will happen over and over along the length of the wave flume, causing the profile of the generated wave, as well as its height to change over the length of the wave flume.

Coastal engineers study processes that take place close to the coast, where the water is shallow. Unfortunately, it is under these conditions that the unwanted secondary waves are generated. Although for some studies the unwanted secondary wave is not considered an issue, there are certain cases where a more precise wave generation is required. This has driven the development of new wavemaker theories, such as the Stoke's second order wavemaker theories, cnoidal wavemaker theory, and stream function wavemaker theory.

This study will study the wavemaker theories and adapt them to the CIEMito wave flume, the small-scale wave flume of the Laboratori d'Enginyeria Marítima (LIM), located at the Universitat Politècnica de Catalunya (UPC) in Barcelona. This way, the conditions under which the unwanted secondary waves are generated along with the desired waves, and to what degree, will be found. Also, it will be seen if the second order wavemaker theory is capable of suppressing the generation of the unwanted waves.

Other reports that study the capability of different wavemaker theories to suppress the unwanted waves have been performed, such as Calabrese *et al*. (2009). Still, the CIEMito wave flume is a specific facility, and it is important to study how different wavemaker theories will affect its performance in particular. The wave flume is fairly new, it was inaugurated in 2009, therefore not many studies have been performed with it.

1.2. DEFINITION OF OBJECTIVES

The aim of this study is to adapt different wavemaker theories to the CIEMito wave flume of the Laboratori d'Enginyeria Marítima (LIM), and find under what conditions the secondary unwanted waves are generated, and to what degree, and to implement a second order wavemaker theory capable of suppressing the appearance of the unwanted waves.

To achieve the aim of this study the following objectives were established:

- Analyze the state of the art of first and second order wavemaker theory.

- Implement the first order wavemaker theory in the CIEMito wave flume.
- Study the waves generated using first order wavemaker theory in the CIEMito wave flume to find the conditions under which the unwanted secondary waves appear, and their effects.
- Validate a numerical wave flume based on PFEM for the study of unwanted secondary waves.
- Implement an effective second order wavemaker theory in the CIEMito wave flume.

1.3. OUTLINE OF CONTENTS

Chapter 2 gives some information about the importance of modeling, more specifically physical modeling, in coastal engineering. Also, the importance, as well as the evolution, of wave generation theories is dicussed.

In Chapter 3 the wavemaker problem is described. Then the first order solution and several second order solutions are discussed. The application of these wavemaker theories to the CIEMito wave flume is also discussed.

In Chapter 4 the modeling tools that were used in this study, the CIEMito wave flume and the PFEM numerical model, are described. The history and specifications of the CIEMito wave flume are given. Then the PFEM numerical model is described.

In Chapter 5 the first order wave generation experiment is described, both the physical experiment and the numerical simulation. For both the experiment set-up is given, the way the data was analyzed is described, and the results obtained are given. Also, the results of the first order numerical wave generation simulation are compared to the results of the first order physical wave generation experiment in order to find if the simulation correctly represents the CIMEito wave flume.

In Chapter 6 the second order wave generation experiment using Madsen's second order wavemaker theory is described. The set-up for the simulation is given, the data analysis is described, and the results are given. Also, the results of the second order numerical wave generation simulation are compared to the results of the first order

numerical wave generation simulation to find if the second order wavemaker theory reduced the appearance of the unwanted secondary waves.

In Chapter 7 the conclusions obtained from this study are given. Also some recommendations for future studies are discussed.

2. PHYSICAL MODELING AND WAVE GENERATION

Physical modeling has been one of the most important tools for the development of coastal engineering. Being able to reproduce complex systems in a controlled laboratory setting has allowed for a better understanding of coastal processes, and the generation of engineering solutions to coastal issues. Wave generation, and wavemaker theories, is an essential part of physical modeling, enabling the natural wave conditions to be reproduced in the laboratory.

In this chapter the different modeling techniques used, and their importance to coastal engineering are discussed. Also, the history and development of different wavemaker theories are talked about.

2.1. MODELING IN COASTAL ENGINEERING

Coastal engineers always have to deal with water, and its interaction with the coast or coastal structures. This can lead to very complex systems that make it very difficult to understand the processes that take place within the system. Also, when a problem rises in the coastal zone, it may be difficult to come up with good engineering solutions. Leonardo da Vinci, who is thought to have been one of the first to experiment with water, is quoted as saying, "when dealing with water, first experiment then use judgment" (Hughes, 1993).

In order to understand the coastal systems engineers have used three different techniques, field research, physical modeling, and numerical modeling. Field research is where researchers obtain data directly from the field. It is the oldest technique, but it is still of great importance. Physical modeling is the study of a system by using a model representation of it in a laboratory setting. Numerical modeling is the study of a system by using a mathematical representation of it. Here the system is defined by its governing equations, which are discretized and solved using computers.

During field research engineers gather data out in the field to study a given phenomenon. This may result in very good data, since it is the actual process that is being studied. Still, field research has its disadvantages. Analyzing the data obtained

from a field research can be difficult. Researcher cannot control the conditions during the data collection, so that the process being studied may be affected by other factors that are not being considered.

The other two techniques, physical and numerical modeling, have become a primary tool in the development of coastal engineering. They have an advantage over the field research since through this methods researchers can control the conditions being studied, and change them if wanted, it is less expensive, and it may simplify the system in order to isolate the process that is of interest.

Still, these three techniques compliment one another and all help in the understanding of the complex coastal processes. Field data is used to validate numerical and physical models, to show that their results reflect the actual conditions in the field. Results of physical models are also used to validate numerical models. Hybrid models have also been developed, where both numerical and physical models are used to solve the processes in a system (Hughes, 1993). Here the results from the numerical model may be entered as a boundary condition to the physical model, or vice versa, depending on the situation.

Numerical modeling has gained popularity, especially with the development of faster and more capable computers. Numerical models do not need infrastructure, and have shown to provide good results. Still, for some processes where the governing equations are too complex, or not well understood, it is not possible to represent them in a numerical model. In these cases physical modeling is still required. In this study the focus will be given to physical modeling.

The physical models have their advantages and disadvantages. Hughes (1993) states some of the advantages of physical modeling. Physical modeling includes the governing equations of the process without having to use simplifications as in numerical models. Since the model is of a small size data may be collected much easier than in the field. The researcher has control of the conditions being studied, and may reproduce a variety of conditions, even the ones that rarely occur in the field but may be of great importance. Finally, in the physical model researchers get to observe the system as the experiment develops. This gives them a better understanding of the processes.

The disadvantages of the physical models discussed by Hughes (1993) include the problem with scale effects. The scale effects may become an issue when the model is of a smaller size that the prototype (the system being studied), which is most times the case. This causes differences between the response of the prototype and the response of the model because all the relevant variables cannot be given the correct scale. Another issue is that laboratories have a limitation to what they can simulate. Because of this not all the processes that affect a system can be included in one physical model, making it an approximation of the system. Also, the laboratory effects can cause the model to give incorrect results. The laboratory effects occur because it is not possible to recreate the exact conditions in nature in the laboratory. An example of this is the use of unidirectional waves instead of multidirectional waves as in nature. In this study issues with wave generation in a wave flume are dealt with. If the waves generated do not have the characteristics that are desired, then it could lead to laboratory effects.

2.2. WAVE GENERATION FOR PHYSICAL MODELING

When studying any type of phenomenon that is caused or affected by waves by using a physical model, one of the most important aspects of the modeling process is the wave generation. It is essential to be able to recreate the natural wave conditions that are being studied within the physical model.

One of the most common methods for generating waves is the mechanical wave generation, where a wave paddle is placed in the physical model and given a certain oscillatory motion to generate the desired waves. Over the years wave generation has evolved from simply moving a wave paddle in sinusoidal motion with a given amplitude and period, to the development of complex wavemaker theories that describe the waves generated by a specific paddle motion for different types of wave paddles. The wave paddles are now driven by a hydraulic motor, which gives a much better control of the wave paddle movement.

The beginning of the wavemaker theories was given by Havelock (1929) when he developed a theory for forced waves in both infinite and finite water depth. From this the wavemaker problem was defined. The first order solution to the wavemaker problem for a piston and a hinged paddle was first given by Bièsel and Suquet (1954), and has since

been given by several others, including Ursell et al. (1960), Flick and Guza (1980), Schäffer (1996) and others, and for other more complex paddle configurations.

The first order solution gave relatively good results between the desired waves, and the generated waves. Still, when trying to generate certain wave conditions, especially waves with high steepness, H/L, and/or very small relative depth, h/L, the wave generated by the first order paddle motion is contaminated by at least one unwanted secondary wave. The secondary waves generated travel at a lower speed than the primary, or desired, wave. Because of this, as the wave propagates along the wave flume, the crest of the secondary wave will recede relative to the main wave crest. This causes the wave profile to change as the wave propagates, and the wave height will also vary (Goda, 1967). Figure 2.1, taken from Goda (1967), shows a wave profile that has an unwanted secondary wave present. It can be seen how both the wave height and the wave profile change according to the location.

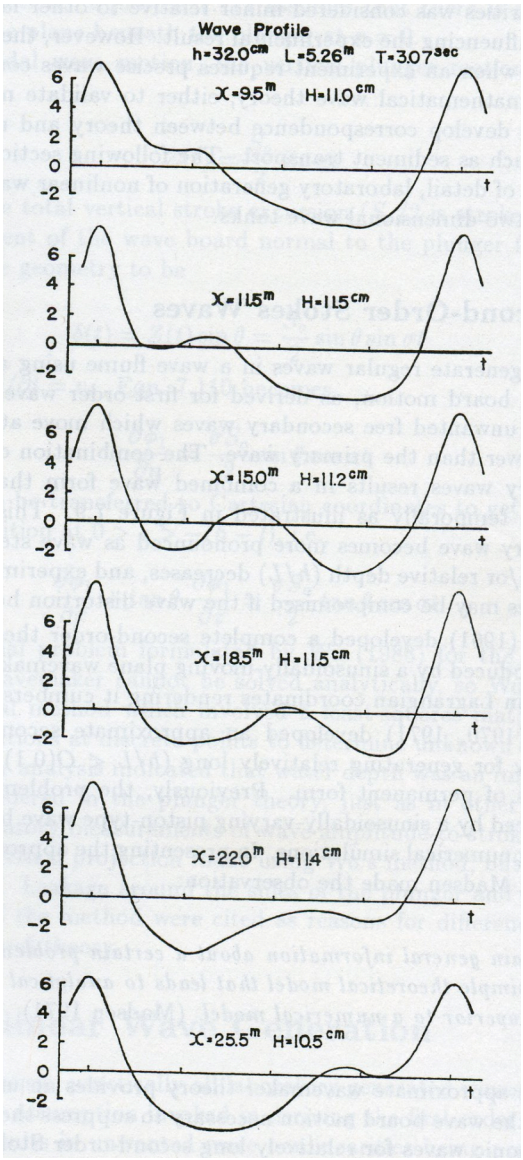

Figure 2.1. Wave profile at several locations with the presence of an unwanted secondary wave (Goda, 1967).

This unwanted secondary wave is generated due to the disagreement between the velocities the paddle forces on the water, and the theoretical wave velocity profile (Calabrese *et al*., 2009). This is also the cause of the exponentially decaying standing waves that are generated close to the paddle. When the relative water depth decreases, the difference between the sinusoidally moving paddle and the wave velocity profile is increased, generating secondary waves with a frequency multiple of the desired wave frequency (Calabrese *et al*., 2009). Goda (1967) states that unwanted secondary waves

will be generated when the relative water depth, h/L, is lower than 0.15, above this the unwanted secondary waves are not an issue.

Coastal engineering mainly deals with processes that occur close to the coast, where the relative water depth is low. This means that often the waves that need to be generated for a physical model of coastal engineering interest have a low relative water depth, and therefore have the issue of unwanted secondary waves. For some studies these effects can be neglected, still, in some cases it is necessary to generate more accurate waves, which coincide perfectly with the waves predicted by the theory. With this objective other wavemaker theories were developed to try and eliminate the unwanted waves completely.

By using second order wavemaker theories the generation of the unwanted secondary waves could be prevented. The first to give a complete solution to the second order wavemaker problem was Fontanet (1961). It was given using Lagrangian coordinates, which made it too complicated to use. Madsen (1971) derived an approximate solution to the second order wavemaker problem. He gave an explicit expression of the wave paddle motion required to eliminate the secondary waves. Still, it was applicable only for certain types of waves, where his simplifying assumptions would hold.

Daugaard (1972) gave a solution to the second order wavemaker problem for a piston paddle including the standing wave summation term of the first order solution, but still neglected this term for the free surface boundary condition near the wave paddle. Flick and Guza (1980) found the second order wavemaker problem solution for wave paddle that is hinged at or below the bottom of the flume. Their solution also included the standing wave summation term of the first order solution except in the free surface boundary. Because of this it was still an approximate solution to the second order wavemaker problem.

Hudspeth and Sulisz (1991) gave the complete analytical solution for the second order wavemaker problem using a generic planar wave paddle moving in a monochromatic oscillation. Moubayed and Williams (1994) expanded this solution to include bichromatic paddle motion.

Schäffer (1996) gives the complete second order solution to the wavemaker problem including superharmonics (sum frequencies) and subharmonics (difference frequencies) for a piston and a hinged wave paddle. From this theory the wave paddle motion necessary to suppress the unwanted secondary wave is provided.

Other theories have been developed to generate waves with a constant profile, which have a high steepness, H/L, or a very small relative depth, h/L. Goring (1979) developed a wavemaker theory based on cnoidal wave theory using a piston type wave board. This theory was developed in order to accurately simulate tsunami waves. Zhang and Schäffer (2006) developed a wavemaker theory based on stream wave theory, which can be used to generate higher order waves.

3. WAVEMAKER THEORIES

In order to apply the wavemaker theories to the CIEMito wave flume, it is first necessary to study them.

From the solution of the wavemaker problem the description of the waves generated by a wavemaker, and the paddle motion required to obtain it, is found. The boundary conditions for the wavemaker problem are similar to the ones used to describe a regular wave, with the addition of a new boundary condition; the boundary condition imposed by the wave paddle that drives the wave generation. Several solutions have been given for the wavemaker problem, to different order of accuracy, and using different simplifying assumptions.

In this chapter the different wavemaker theories will be discussed. First the first and the second order wavemaker problem will be defined by the boundary conditions. Then the solutions that have been studied will be described and discussed. In the cases where the wavemaker theory was applied to the CIEMito wave flume, the application will be described. In the other cases, where the application of the theory to the CIEMito wave flume was not possible, the theories, and the issues that prevented their application, will be discussed.

3.1 THE WAVEMAKER PROBLEM

Figure 3.1 shows the scheme of a two-dimensional wave flume, with a planar paddle that moves in a combination of rotation and back and forth translation, taken from Hughes (1993). Figure 3.1 defines the Cartesian coordinate system that will be followed. As defined in the figure, the x-axis has its origin at the mean paddle position and runs along the length of the wave flume, and the z-axis has its origin at the mean water surface elevation and runs along the height of the wave flume. The water depth is h, the distance from the bottom of the wave flume to the center of rotation is l, and $X(z,t)$ is the position of the paddle, which is dependent on the z location and the time t, with $X_0(t)$ being the position of the paddle at a given time t at the water surface elevation ($z = 0$).

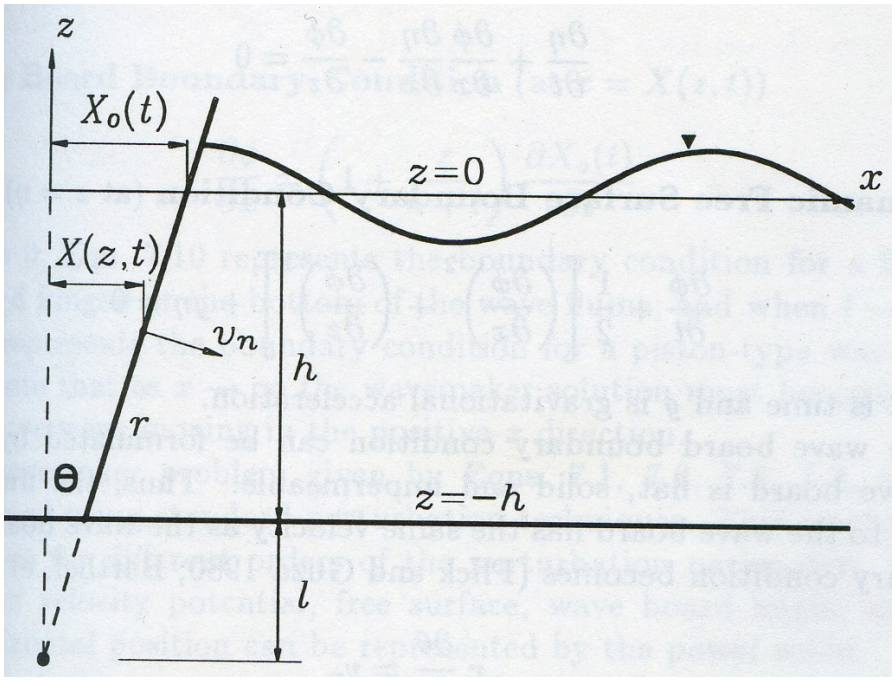

Figure 3.1. Scheme of a two-dimensional wave flume (Hughes, 1993).

The CIEMito wave flume uses a piston paddle, which is the case when $l \to \infty$. This way the position of the paddle depends only on the time, t. This will simplify the boundary conditions of the problem and therefore the solutions found for it.

In order to find a solution to the motion of the waves generated by the paddle, the fluid is assumed to be inviscid and irrotational. With this, the Laplace equation, along with several boundary conditions may be solved in order to describe the motion of the waves. The Laplace equation and the boundary conditions will be given in terms of the velocity potential $\phi(x,z,t)$.

The velocity potential is a scalar function whose gradient at any point (x,z) of the fluid, at any given time, t, gives the velocity vector. So that the following is true,

$$u = \frac{\partial \phi}{\partial x} \qquad \text{and} \qquad w = \frac{\partial \phi}{\partial z} \qquad \text{Equation 3.1}$$

where u is the velocity of the velocity of the fluid in the x-direction, and w is the velocity of the fluid in the z-direction.

The Laplace equation, in terms of the velocity potential, is given by Equation 3.2, and it should hold true for the entire domain of the fluid.

$$\frac{\partial^2 \phi}{\partial x^2} + \frac{\partial^2 \phi}{\partial z^2} = 0 \qquad \text{Equation 3.2}$$

Next the bottom boundary condition states that the bottom of the wave flume is an impermeable boundary, therefore the vertical velocity at the bottom, that is $z = -h$, is zero (Equation 3.3).

$$\frac{\partial \phi}{\partial z} = 0 \qquad \text{Equation 3.3}$$

There are two free surface boundary conditions, the kinematic free surface boundary condition, and the dynamic free surface boundary condition. The kinematic free surface boundary condition states that the particles that are at the surface must remain at the surface (Equation 3.4). The dynamic free surface boundary conditions states that the pressure at the surface must be equal to the atmospheric pressure, which is assumed to be constant (Equation 3.5). These two boundary conditions must hold at the free surface, that is $z = \eta$.

$$\frac{\partial \eta}{\partial t} + \frac{\partial \phi}{\partial x} \cdot \frac{\partial \eta}{\partial x} - \frac{\partial \phi}{\partial z} = 0 \qquad \text{Equation 3.4}$$

$$\frac{\partial \phi}{\partial t} + \frac{1}{2} \cdot \left[\left(\frac{\partial \phi}{\partial x} \right)^2 + \left(\frac{\partial \phi}{\partial z} \right)^2 \right] + g \cdot \eta = 0 \qquad \text{Equation 3.5}$$

where g is the acceleration of gravity, t is time, and η is the free surface of the fluid.

The final boundary condition that must be introduced is the boundary condition of the paddle (Equation 3.6). Here it is assumed that the paddle is flat, solid and impermeable. This means that the velocity of the fluid normal to the paddle must be the

same as the velocity of the paddle. This must hold true for the fluid next to the paddle position, that is $x = X(z,t)$.

$$\frac{\partial \phi}{\partial x} = \left(1 + \frac{z}{h+l}\right) \cdot \frac{\partial X_0(t)}{\partial t} \qquad \text{Equation 3.6}$$

For the case of the piston paddle, as in the CIEMito wave flume, $l \to \infty$, therefore the paddle boundary condition is simplified to Equation 3.7.

$$\frac{\partial \phi}{\partial x} = \frac{\partial X_0(t)}{\partial t} \qquad \text{at} \quad x = X(t) \qquad \text{Equation 3.7}$$

To solve the wavemaker problem as defined by the previous boundary conditions standard perturbation techniques are used. Here it is assumed that the velocity potential, the free surface, the paddle angle, and the paddle position may be written as a power series.

$$\phi = \sum_{n=1}^{\infty} \varepsilon^n \cdot \phi_n = \varepsilon \cdot \phi_1 + \varepsilon^2 \cdot \phi_2 + \varepsilon^3 \cdot \phi_3 + O(\varepsilon^4) + \ldots \qquad \text{Equation 3.8}$$

$$\eta = \sum_{n=1}^{\infty} \varepsilon^n \cdot \eta_n = \varepsilon \cdot \eta_1 + \varepsilon^2 \cdot \eta_2 + \varepsilon^3 \cdot \eta_3 + O(\varepsilon^4) + \ldots \qquad \text{Equation 3.9}$$

$$\theta = \sum_{n=1}^{\infty} \varepsilon^n \cdot \theta_n = \varepsilon \cdot \theta_1 + \varepsilon^2 \cdot \theta_2 + \varepsilon^3 \cdot \theta_3 + O(\varepsilon^4) + \ldots \qquad \text{Equation 3.10}$$

$$X_0 = \sum_{n=1}^{\infty} \varepsilon^n \cdot X_{0n} = \varepsilon \cdot X_{01} + \varepsilon^2 \cdot X_{02} + \varepsilon^3 \cdot X_{03} + O(\varepsilon^4) + \ldots \qquad \text{Equation 3.11}$$

where ε is the perturbation parameter, which is proportional to the wave steepness, H/L. This way ϕ_1, η_1, θ_1, and X_{01} will give the solution to the first order problem, ϕ_2, η_2, θ_2, and X_{02} will give the solution to the second order problem, and so on.

To obtain the first and second order approximation of the Laplace equation and the bottom boundary condition the velocity potential given in Equation 3.8 is substituted for ϕ into the given Laplace equation (Equation 3.2) and the bottom boundary condition (Equation 3.3), and retaining only the terms up to O(ε^2). The resulting first and second order approximations of the Laplace equation are given by Equation 3.12 and Equation 3.13, respectively, and they must hold true for the entire fluid domain.

1st Order: $$\frac{\partial^2 \phi_1}{\partial x^2} + \frac{\partial^2 \phi_1}{\partial z^2} = 0 \qquad \text{Equation 3.12}$$

2nd Order: $$\frac{\partial^2 \phi_2}{\partial x^2} + \frac{\partial^2 \phi_2}{\partial z^2} = 0 \qquad \text{Equation 3.13}$$

The resulting first and second order approximations of the bottom boundary condition are given by Equation 3.14 and Equation 3.15, respectively, and they should hold true for $z = -h$.

1st Order: $$\frac{\partial \phi_1}{\partial z} = 0 \qquad \text{Equation 3.14}$$

2nd Order: $$\frac{\partial \phi_2}{\partial z} = 0 \qquad \text{Equation 3.15}$$

To approximate both the kinematic and the dynamic free surface boundary conditions, it must be noticed that the velocity potential evaluated at $z = \eta$ can be represented as a Taylor series expansion about $z = 0$ (Equation 3.16).

$$\phi(\eta, x, t; \varepsilon) = \varepsilon \cdot \phi_1 + \varepsilon^2 \cdot \left(\phi_2 + \eta_1 \cdot \frac{\partial \phi_1}{\partial z} \right) + O\left(\varepsilon^3\right) + \ldots \qquad \text{Equation 3.16}$$

To obtain the first and second order approximations of both the kinematic and the dynamic free surface boundary conditions Equation 3.16 is substituted for ϕ and the power series definition of η (Equation 3.9) is used in the given kinematic free surface boundary condition (Equation 3.4) and the dynamic free surface boundary condition (Equation 3.5), and retaining the terms up to O(ε^2). The resulting first and second order approximations of the kinematic free surface boundary condition are given by Equation 3.17 and Equation 3.18, respectively, and they must hold for $z = 0$.

1st Order: $$\frac{\partial \eta_1}{\partial t} - \frac{\partial \phi_1}{\partial z} = 0 \qquad \text{Equation 3.17}$$

2nd Order: $$\frac{\partial \eta_2}{\partial t} + \frac{\partial \phi_1}{\partial x}\frac{\partial \eta_1}{\partial x} - \frac{\partial \phi_2}{\partial z} - \eta_1 \cdot \frac{\partial^2 \phi_1}{\partial z^2} = 0 \qquad \text{Equation 3.18}$$

The resulting first and second order approximations of the dynamic free surface boundary condition are given by Equation 3.19 and Equation 3.20, respectively, and they must hold for $z = 0$.

1st Order: $$\frac{\partial \phi_1}{\partial t} + g \cdot \eta_1 = 0 \qquad \text{Equation 3.19}$$

2nd Order: $$\frac{\partial \phi_2}{\partial t} + \eta_1 \cdot \frac{\partial^2 \phi_1}{\partial z \partial t} + \frac{1}{2} \cdot \left[\left(\frac{\partial \phi_1}{\partial x} \right)^2 + \left(\frac{\partial \phi_1}{\partial z} \right)^2 \right] + g \cdot \eta_2 = 0 \qquad \text{Equation 3.20}$$

To approximate the first and second order paddle boundary condition first the velocity potential has to be evaluated at the surface of the paddle. This is approximated by a Taylor series expansion in cylindrical coordinates about $\theta = 0$. This may also be written in Cartesian coordinates (Equation 3.21).

$$\phi(x,z,t;\varepsilon) = \varepsilon \cdot \phi_1 + \varepsilon^2 \left[\phi_2 + \theta_1 \left((l + h + z) \frac{\partial \phi_1}{\partial x} - x \cdot \frac{\partial \phi_1}{\partial z} \right) \right] + O(\varepsilon^3) + \ldots \qquad \text{Equation 3.21}$$

To obtain the first and second order approximations of the paddle boundary condition Equation 3.21 is substituted for ϕ, and the power series definition of θ (Equation 3.10) and X_0 (Equation 3.11) in the given paddle boundary condition (Equation 3.6), and retaining the terms up to O(ε^2). The resulting first and second order approximations of the paddle boundary condition are given by Equation 3.22 and Equation 3.23, respectively, and they must hold for $x = 0$.

1st Order: $$\frac{\partial \phi_1}{\partial x} = f(z) \cdot \frac{dX_{01}}{dt}$$ Equation 3.22

2nd Order: $$\frac{\partial \phi_2}{\partial x} = f(z) \cdot \frac{dX_{02}}{dt} - X_{01} \cdot \left[f(z) \cdot \frac{\partial^2 \phi_2}{\partial x^2} - \frac{1}{(l+h)} \cdot \frac{\partial \phi_1}{\partial z} \right]$$ Equation 3.23

where $f(z)$ is defined by Equation 3.24.

$$f(z) = \left(1 + \frac{1}{h+l}\right)$$ Equation 3.24

In the case of the CIEMito wave flume $f(z) = 1$, since for a piston paddle $l \to \infty$.

3.2. First Order (Linear) Wavemaker Theory

The first order solution to the wavemaker problem was first given by Bièsel and Suquet (1954) for a piston or a hinged paddle, and has since been solved by several others, such as Ursell et al. (1960), Flick and Guza (1980), Schäffer (1996) and others. Here the solution to the first order wavemaker problem is given following the solution described by Hughes (1993).

In order to find the solution to the first order wavemaker problem given by the previous boundary conditions, it is assumed that the velocity potential may be defined as following

$$\phi_1(x,z,t) = X(x) \cdot Z(z) \cdot T(t)$$ Equation 3.25

which will allow the Laplace equation to be divided into ordinary differential equations with known solutions. The final velocity potential must include all possible solutions, therefore the solutions that are found for a real, zero, and imaginary separation constant are summed. Dean and Dalrymple (1984) give the general velocity potential as Equation 3.26.

$$\phi_1(x,z,t) = \phi_{k_1} + \phi_{k_2} + \phi_{k_3} \qquad \text{Equation 3.26}$$

where ϕ_{k_1}, ϕ_{k_2}, and ϕ_{k_3} are the solution for the real, zero, and imaginary separation constant, respectively. By using the boundary conditions, and after some algebra the final combined velocity potential is found (Equation 3.27). For further details of the solution the reader is directed to Hughes (1993).

$$\phi_1(x,z,t) = A \cdot \cosh\left[k_1(h+z)\right] \cdot \sin(k_1 x - \omega t) + \\ + \cos(\omega t) \cdot \sum_{n=1}^{\infty} C_n \cdot e^{-k_{3n}x} \cdot \cos\left[k_{3n}(z+h)\right] \qquad \text{Equation 3.27}$$

The first term of Equation 3.27 defines the wave that propagates in the positive x-direction, while the second term defines a standing wave that decays exponentially in the positive x-direction. Dean and Dalrymple (1984) found that the standing wave becomes negligible at a distance of $3h$ away from the paddle.

For Equation 3.27, k, the wave number, is defined by Equation 3.28, where ω is the desired angular frequency of the wave.

$$\omega^2 = g \cdot k_1 \cdot \tanh(k_1 h) = -g \cdot k_3 \cdot \tan(k_3 h) \qquad \text{Equation 3.28}$$

There will be only one value for k_1, but there will be an infinite number of solutions for k_3, since the tangent function is periodical.

The A and C_n constants are defined by Equation 3.29 and Equation 3.30 respectively.

$$A = \frac{2 \cdot \omega \cdot S_0}{k\left[\sin\left(2k_1 h\right) + 2k_1 h\right]} \cdot \left[\sin\left(k_1 h\right) + \frac{\left(1 - \cosh\left(k_1 h\right)\right)}{k_1\left(h + l\right)}\right] \qquad \text{Equation 3.29}$$

$$C_n = -\frac{2 \cdot \omega \cdot S_0}{k_{3n}\left[\sin\left(2k_{3n} h\right) + 2k_{3n} h\right]} \cdot \left[\sin\left(k_{3n} h\right) + \frac{\cos\left(k_{3n} h\right) - 1}{k_{3n}\left(h + l\right)}\right] \qquad \text{Equation 3.30}$$

Equation 3.31 gives the complete solution to the water surface elevation generated by the paddle.

$$\eta_1(x,t) = \frac{\omega \cdot A}{g} \cdot \cosh(k_1 h) \cdot \cos\left(k_1 x - \omega t\right) + \\ + \sin\left(\omega t\right) \cdot \sum_{n=1}^{\infty} \frac{\omega \cdot C_n}{g} \cdot e^{-k_{3n} x} \cdot \cos\left(k_{3n} h\right) \qquad \text{Equation 3.31}$$

The second term of the water surface elevation equation will decay away from the paddle, so the water surface elevation away from the paddle, where it will most usually be of interest, may be simplified to Equation 3.32.

$$\eta_1(x,t) = \frac{H}{2} \cdot \cos\left(k_1 h - \omega t\right) \qquad \text{Equation 3.32}$$

where H is the desired wave height of the generated wave, and is defined by Equation 3.33.

$$H = \frac{2 \cdot \omega \cdot A}{g} \cdot \cosh\left(k_1 h\right) \qquad \text{Equation 3.33}$$

The paddle motion required to generate the described waves is given by Equation 3.34.

$$X_{01}(t) = \frac{S_0}{2} \cdot \sin(\omega t) \qquad \text{Equation 3.34}$$

where S_0 is the paddle stroke at $z = 0$, and $S_0/2$ is the stroke amplitude.

So, the final transfer function for first order wavemaker theory between the paddle stroke, S_0, and the first order wave generated, with a wave height, H, and a wave period, T, far from the paddle, is given by Equation 3.35 for the general situation (Figure 3.1)

$$\frac{H}{S_0} = \frac{4 \cdot \sinh(k_1 h)}{\sinh(2k_1 h) + 2k_1 h} \cdot \left[\sinh(k_1 h) + \frac{1 - \cosh(k_1 h)}{k(h + l)} \right] \qquad \text{Equation 3.35}$$

In the case of a piston paddle, such as the CIEMito wave flume, the transfer function given is simplified to Equation 3.36.

$$\frac{H}{S_0} = \frac{4 \cdot \sinh^2(k_1 h)}{\sinh(2k_1 h) + 2k_1 h} \qquad \text{Equation 3.36}$$

The first order wavemaker theory was adapted to the CIEMito wave flume. Figure 3.2. shows a flow chart of the application of this theory to obtain the necessary wave paddle motion to generate regular waves with desired characteristics. As an input the desired wave height, H, the wave period, T, the water depth, h, the gamma factor, which is used to take into account the wave flume inefficiencies, the maximum paddle displacement, S_{max}, the maximum relative wave height before breaking, H/h_{max}, the maximum wave steepness before breaking, H/L_{max}, the frequency with which the paddle position is given, f, and finally either the duration of the time series, t, or the number of waves that have to be generated, N.

From the input several wave parameters must be calculated, and other relationships that can characterize the wave being generated. The wave parameters are the wavelength, L, the wave number, k, and the wave angular frequency, ω, found from linear wave theory. The characterizing relationships are H/gT^2 and h/gT^2, from which

the wave type and the applicable wave theory can be determined, and the wave steepness, H/L, and the relative wave height, H/h, to ensure breaking does not occur.

Next the transfer function (Equation 3.36) may be used to find the required paddle stroke, S_0, and from this the paddle displacement time series, $X(t)$, (Equation 3.34). An error file can be generated to warn if the paddle stroke, wave steepness, or relative wave height are larger than allowable. A general information file will hold the error information, the wave type, and the applicable wave theory.

The final output will give the general information file, the paddle displacement time series at the desired frequency, and a plot of the paddle motion. A similar routine was written in Matlab, and may be found in Appendix A.

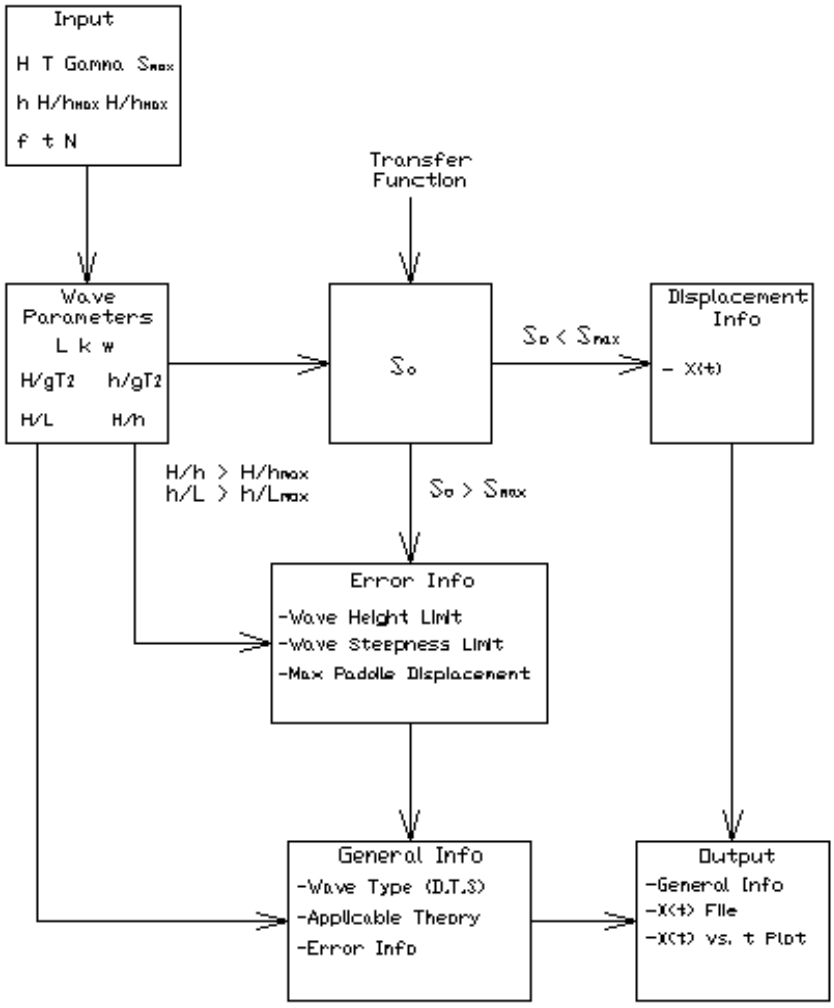

Figure 3.2. Flow chart of the application of the first order wavemaker theory.

3.3. SECOND ORDER WAVEMAKER THEORY BY MADSEN (1971)

The linear wavemaker theory works well. Still, it was found that under certain conditions, especially when generating long waves, the wave generated does not have a permanent form, as described by the theory. Instead the wave changes shape as it propagates. This is due to the fact that the paddle will not only produce the desired primary wave, but it will also produce one, or more, unwanted secondary waves which propagate at a slower speed that the primary wave (Goda, 1967). The second order wavemaker theory began being developed to solve this issue.

Finding a complete analytical solution to the second order wavemaker problem is not a simple mathematical problem. Fontanet (1961) found a complete second order solution to the waves produced by a sinusoidally moving plane wavemaker, but it was done in Lagrangian coordinates. This made it very complicated to use.

Madsen (1971) developed a simpler, and easier to use solution to the problem. He developed an approximate second order wavemaker theory to generate relatively long second order Stokes waves that would not change shape as they propagated. Also, he gave a simple analytical solution to the paddle motion required to do so.

To find the approximate solution to the second order wavemaker problem, Madsen assumed that the velocity potential could be defined as Equation 3.37.

$$\phi_2 = \phi_{21} + \phi_{22} \qquad \text{Equation 3.37}$$

where ϕ_{21} will be the solution far from the paddle, and ϕ_{22} will be the solution close to the paddle. By substituting the value of ϕ_2 given by Equation 3.37 into the previously given boundary conditions for the second order wavemaker problem two sets of boundary conditions are created, one to solve for ϕ_{21}, and the other to solve for ϕ_{22}.

To find the solution far from the paddle, ϕ_{21}, the set of boundary conditions is given by the Laplace equation (Equation 3.38), the bottom boundary condition (Equation 3.39), and the homogenous free surface boundary conditions (Equation 3.40), which is obtained by combining the kinematic and the dynamic free surface boundary conditions. Here the paddle boundary condition is not taken into consideration.

$$\frac{\partial^2 \phi_{21}}{\partial x^2} + \frac{\partial^2 \phi_{21}}{\partial z^2} = 0 \qquad \text{at entire fluid domain} \qquad \text{Equation 3.38}$$

$$\frac{\partial \phi_{21}}{\partial z} = 0 \qquad \text{at } z = -h \qquad \text{Equation 3.39}$$

$$\frac{\partial^2 \phi_{21}}{\partial t^2} + g \cdot \frac{\partial \phi_{21}}{\partial z} = -\eta_1 \left(g \cdot \frac{\partial^2 \phi_1}{\partial z^2} + \frac{\partial^3 \phi_1}{\partial z \partial t^2} \right) - 2\left(\frac{\partial \phi_1}{\partial x} \cdot \frac{\partial^2 \phi_1}{\partial x \partial t} + \frac{\partial \phi_1}{\partial z} \cdot \frac{\partial^2 \phi_1}{\partial z \partial t} \right) \quad \text{at } z = 0 \qquad \text{Equation 3.40}$$

To find the solution close to the paddle, ϕ_{22}, the set of boundary conditions is given by the Laplace equation (Equation 3.41), the bottom boundary condition (Equation 3.42), the homogenous free surface boundary conditions (Equation 3.43), which is obtained by combining the kinematic and the dynamic free surface boundary conditions, and the paddle boundary condition (Equation 3.44 and Equation 3.45).

$$\frac{\partial^2 \phi_{22}}{\partial x^2} + \frac{\partial^2 \phi_{22}}{\partial z^2} = 0 \qquad \text{at entire fluid domain} \qquad \text{Equation 3.41}$$

$$\frac{\partial \phi_{22}}{\partial z} = 0 \qquad \text{at } z = -h \qquad \text{Equation 3.42}$$

$$\frac{\partial^2 \phi_{22}}{\partial t^2} + g \cdot \frac{\partial \phi_{22}}{\partial z} = 0 \qquad \text{at } z = 0 \qquad \text{Equation 3.43}$$

$$\frac{\partial \phi_{22}}{\partial x} = -\frac{\partial \phi_{21}}{\partial x} + f(z) \cdot \frac{dX_{02}}{dt} - X_{01}\left[f(z) \cdot \frac{\partial^2 \phi_1}{\partial x^2} - \frac{1}{l+h} \cdot \frac{\partial \phi_1}{\partial z} \right] \text{ at } x = 0 \qquad \text{Equation 3.44}$$

where $f(z)$ is defined by Equation 3.45.

$$f(z) = 1 + \frac{z}{h + l}$$ Equation 3.45

Again, in the case of the CIEMito wave flume $f(z) = 1$, since for a piston paddle $l \to \infty$.

To find the solution for the velocity potential away from the paddle, ϕ_{21}, the standing wave summation term of the first order solution, ϕ_1, is neglected, simplifying the problem. This simplification may be done since the standing wave summation term will decay exponentially away form the paddle. From this the velocity potential away from the paddle may be found (Equation 3.46).

$$\phi_{21}(x,z,t) = \frac{3 \cdot \omega \cdot H}{32} \cdot \frac{\cosh\left[2k(h+z)\right]}{\sinh^4(kh)} \cdot \sin\left[2(kx - \omega t)\right]$$ Equation 3.46

To find the solution for the velocity potential close to the paddle, ϕ_{22}, the same simplification is done by neglecting the standing wave summation term of the first order solution, ϕ_1. This is only a reasonable assumption to make if the waves being generated are of relatively long period ($h/L < 0.1$). From this assumption the velocity potential close to the paddle may be found (Equation 3.47).

$$\frac{\partial \phi_{22}}{\partial x} = \left[1 - \frac{h}{2(h+l)}\right] \cdot \frac{dX_{02}}{dt} + \frac{\omega \cdot H^2}{16h}\left[\frac{2}{m_1} - \frac{3 \cdot \cosh(kh)}{\sinh^3(kh)}\right] \cdot \cos(2\omega t)$$ Equation 3.47

where m_1 is the relationship between the wave height and the paddle stroke found from the first order wavemaker theory (Equation 3.48).

$$m_1 = \frac{H}{S_0}$$ Equation 3.48

The required paddle movement to suppress the appearance of the unwanted second order waves would be found by adding X_{01} and X_{02}, such that the second order paddle movement, X_{02}, would give $\partial \phi_{22} / \partial x = 0$ (Equation 3.49).

$$X_0(t) = X_{01} + X_{02}$$ Equation 3.49

The second order paddle movement required to obtain $\partial\phi_{22}/\partial x = 0$ is given by Equation 3.50.

$$X_{02}(t) = \frac{H^2}{32h\left[1 - \frac{h}{2(h+l)}\right]} \cdot \left[\frac{3\cdot\cosh(kh)}{\sinh^3(kh)} - \frac{2}{m_1}\right] \cdot \sin(2\omega t)$$ Equation 3.50

This may be simplified for the case of a piston paddle, such as CIEMito to Equation 3.51.

$$X_{02}(t) = \frac{H^2}{32h} \cdot \left[\frac{3\cdot\cosh(kh)}{\sinh^3(kh)} - \frac{2}{m_1}\right] \cdot \sin(2\omega t)$$ Equation 3.51

Therefore the final paddle motion required to suppress the appearance of the unwanted second order waves is given by Equation 3.52.

$$X_0(t) = \frac{H}{2m_1} \cdot \sin(\omega t) + \\ + \frac{H^2}{32h\left[1 - \frac{h}{2(h+l)}\right]} \cdot \left[\frac{3\cdot\cosh(kh)}{\sinh^3(kh)} - \frac{2}{m_1}\right] \cdot \sin(2\omega t)$$ Equation 3.52

For the CIEMito wave flume the final paddle motion is simplified to Equation 3.53.

$$X_0(t) = \frac{H}{2m_1} \cdot \sin(\omega t) + \frac{H^2}{32h}\left[\frac{3\cdot\cosh(kh)}{\sinh^3(kh)} - \frac{2}{m_1}\right]$$ Equation 3.53

Madsen limited the application of this approximate second order wavemaker theory to waves that complied with the condition given by Equation 3.54.

$$\frac{H \cdot L^2}{h^3} < \frac{8 \cdot \pi^2}{3}$$ Equation 3.54

Madsen's second order wavemaker theory was adapted to the CIEMito wave flume. Figure 3.3 shows a flow chart of the application of this theory to obtain the necessary wave paddle motion to generate regular waves with desired characteristics. As an input the desired wave height, H, the wave period, T, the water depth, h, the gamma factor, which is used to take into account the wave flume inefficiencies, the maximum paddle displacement, $S_{\max}$, the maximum relative wave height before breaking, $H/h_{\max}$, the maximum wave steepness before breaking, $H/L_{\max}$, the frequency with which the paddle position is given, f, and finally either the duration of the time series, t, or the number of waves that have to be generated, N.

From the input several wave parameters must be calculated, and other relationships that can characterize the wave being generated. The wave parameters are the wavelength, L, the wave number, k, and the wave angular frequency, ω, found from linear wave theory. The characterizing relationships are H/gT^2 and h/gT^2, from which the wave type and the applicable wave theory can be determined, the wave steepness, H/L, and the relative wave height, H/h, to ensure breaking does not occur, and HL^2/h^3 to find if Madsen's theory is applicable.

Next the first order paddle stroke, S_0, and wave height to paddle stroke ratio, m_1, may be found (Equation 3.36 and Equation 3.49). From this the first order paddle motion, $X_{01}(t)$, (Equation 3.34), the second order paddle motion, $X_{02}(t)$, (Equation 3.51), and the resulting paddle motion, $X_0(t)$, (Equation 3.53), may be found. An error file can be generated to warn if the paddle stroke, wave steepness, or relative wave height are larger than allowable, and if the criteria for the applicability of Madsen's second order wavemaker theory is not met. A general information file will hold the error information, the wave type, and the applicable wave theory.

The final output will give the general information file, the paddle displacement time series at the desired frequency, and a plot of the two components of the paddle motion and the resulting paddle motion. A similar routine was written in Matlab, and may be found in Appendix B.

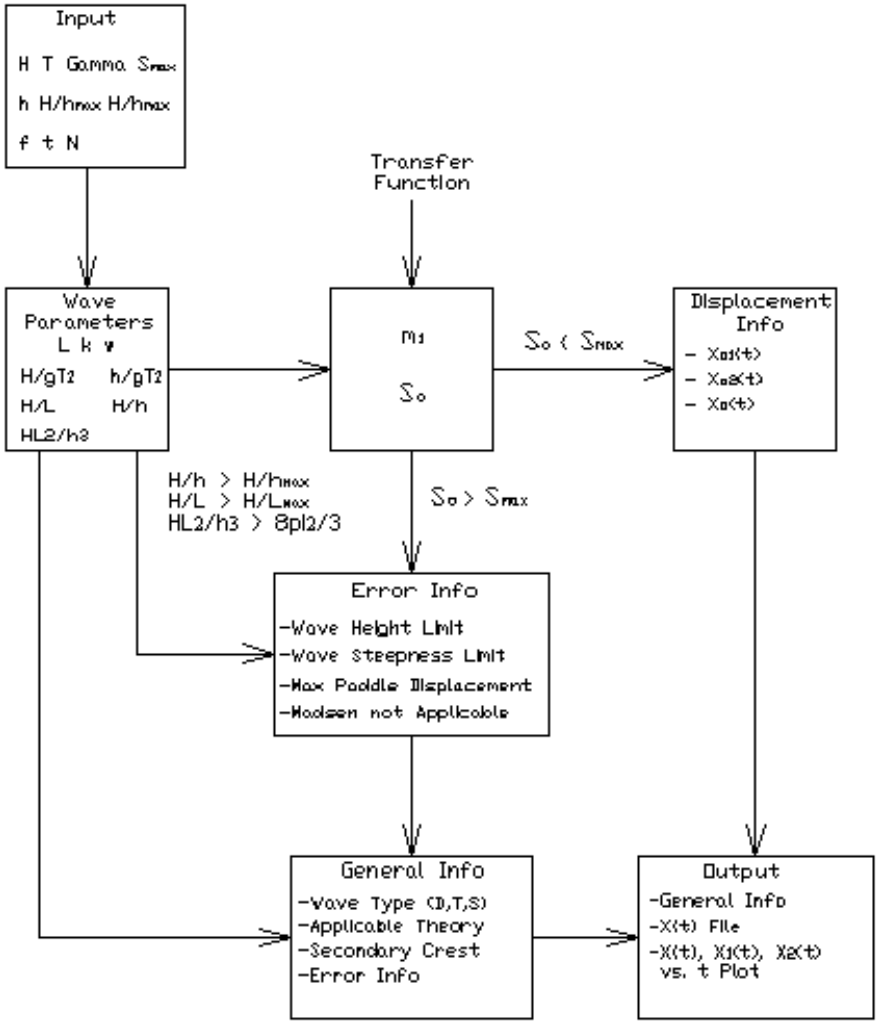

Figure 3.3. Flow chart of the application of Madsen's second order wavemaker theory.

3.4. SECOND ORDER WAVEMAKER THEORY BY FLICK AND GUZA (1980)

Flick and Guza (1980) gave an approximate second order solution to wave generated by a paddle hinged at or below the channel bottom, to a piston paddle. In their solution they include the standing wave term of the first order solution, except for the free surface boundary condition near the paddle.

This theory could not be applied to the CIEMito wave flume for two reasons. The first is that the coefficients of the standing wave term of the first order solution are solved for numerically, and an analytical expression is not given. Second, the theory does not

address the required paddle motion to suppress the appearance of unwanted secondary waves, it only describes the waves generated by a first order paddle motion.

3.5. SECOND ORDER WAVEMAKER THEORY BY HUDSPETH AND SULISZ (1991)

Hudspeth and Sulisz (1991) gave the complete solution to second order to the waves generated by a doubly articulated plane wavemaker of variable draught with a sinusoidal motion. This wavemaker configuration may be simplified to be a simpler piston paddle wavemaker, such as the one of the CIEMito wave flume. For the second order solution they include the standing wave terms of the first order solution, which was neglected in previous solutions, in all the boundary conditions, making it a complete solution. In order to satisfy all the boundary conditions the second order velocity potential is a linear combination of three time dependent velocity potentials, and two time independent velocity potentials.

Although Hudspeth and Sulisz (1991) give the complete solution to the waves generated by a piston paddle, or a hinged paddle of variable draught, it was not possible to apply this theory to the CIEMito wave flume for the purposes of this study. In order to obtain this solution Hudspeth and Sulisz (1991) use a sinusoidal motion of the paddle. The waves generated by this paddle motion include unwanted secondary waves. In their work they do not give the necessary paddle motion that would be required to suppress the appearance of the unwanted secondary waves.

3.6. SECOND ORDER WAVEMAKER THEORY BY SCHÄFFER (1996)

Schäffer (1996) derives the complete second order wavemaker theory, including superharmonics (summation frequencies), and subharmonics (difference frequencies) for a piston and a hinged type paddle. Here, the second order motion of the paddle required to obtain a constant wave profile along the wave flume, by preventing the generation of the unwanted secondary waves, is given. Through experiments with a piston paddle the

theory was tested and showed that by using this wavemaker theory a constant wave profile could be obtained.

Schäffer (1996) separates the second order velocity potential into three contributors, as shown in Equation 3.55.

$$\phi_2 = \phi_{21} + \phi_{22} + \phi_{23} \qquad \text{Equation 3.55}$$

where ϕ_{21} is the velocity potential for the bound waves, ϕ_{22} is the velocity potential for the free wave caused by the wavemaker motion and due to ϕ_{21} mismatching the boundary conditions near the wavemaker, and ϕ_{23} is the velocity potential for the free waves caused by the second order wavemaker motion. By finding a second order paddle motion such that $\phi_{22} + \phi_{23} = 0$, then the unwanted secondary waves will be suppressed.

The solution given by Schäffer (1996) to the paddle motion required to suppress the appearance of the unwanted secondary waves is complete, and every variable has been properly defined. Also, the theory includes piston paddles, like the one of the CIEMito wave flume. Still, programming this theory to find the required paddle motion to generate a desired wave condition without generating unwanted secondary waves is a challenge. This prevented the application of this theory to the CIEMito wave flume.

3.7. STREAM FUNCTION WAVEMAKER THEORY BY ZHANG AND SCHÄFFER (2006)

Zhang and Schäffer (2006) developed another wavemaker theory based on Stream Function wave theory. Stream Function wave theory uses the stream function, Ψ, instead of the velocity potential function, ϕ, to describe the waves. Through experimentations Zhang and Schäffer show how this wavemaker theory surpasses the effectiveness of second order Stokes wavemaker theory in the generation of relatively shallow water waves with constant shape. Also, for non-shallow water waves with moderate nonlinearity, the developed wavemaker theory proved superior than the second order Stokes wavemaker theories. The theory did fail to work for highly nonlinear deep-water waves.

The experiments done by Zhang and Schäffer to test their new wavemaker theory were done in a wave flume similar to the CIEMito wave flume, small scale with a piston paddle wavemaker. Since the results found by Zhang and Schäffer (2006) showed that their wavemaker theory could be a good solution to suppress the appearance of unwanted secondary waves, and since it is one of the most modern theories available, the application of this theory to the CIEMito wave flume was attempted. Still Zhang and Schäffer (2006) fail to properly define every variable, and do not give an expression for the motion required by the paddle to generate the waves. For this reason, applying the theory to the CIEMito wave flume was not possible.

4. MODELING TOOLS

As stated in Section 2.2, under certain conditions the waves generated in a wave flume may following first order wavemaker theory contain unwanted secondary waves when. Second order wavemaker theories have been developed to solve this issue, when the study requires more precise wave generation. By applying these wavemaker theories to the CIEMito wave flume, and testing different wave conditions we may find how each theory affects the waves generated in the wave flume, under what conditions the unwanted secondary waves are generated, and if the second order wavemaker theories help prevent the appearance of the unwanted waves.

It was not possible to use wavemaker theories other than the linear wavemaker theory to generate waves in the CIEMito wave flume. Because of this it was decided to use a numerical model to simulate some of these conditions. Recently it has been recognized that wave flumes may be modeled numerically, creating what is known as a numerical wave flume, which may be used in the same ways traditional wave flumes are utilized. The model utilized is a PFEM numerical model developed at the Centre Internacional de Mètodes Numèrics en l'Enginyeria (CIMNE) in Barcelona, and it will be used to represent the CIEMito wave flume.

In this chapter the history and the characteristics of the CIEMito wave flume are discussed. Then the properties of the numerical model used to model the wave generation in the CIEMito wave flume will be described.

4.1. THE CIEMITO WAVE FLUME

The Laboratori d'Enginyeria Marítima (LIM), located at the Universitat Politècnica de Catalunya (UPC), is a non-profit research center dedicated to studying and generating technology in the field of maritime engineering and marine sciences, and to the education of professionals in these fields. Since 1993 LIM counted with the CIEM wave flume to perform experiments for several different fields, such as coastal and harbor engineering. Still, since the CIEM wave flume is a large-scale facility, it is expensive and very complex to run tests in it.

To complement the CIEM wave flume, the CIEMito wave flume was designed and developed at LIM, and in 2009 it was inaugurated. The CIEMito wave flume is the small-scale wave flume of LIM, and it was built with the objective of having a quality wave flume to support the activities performed at LIM. Since CIEMito is a small-scale wave flume it is easier to operate, since the set up of experiments is much simpler, it allows tests to be performed faster, and the costs of running the wave flume are lowered. Also, because of all of this it is possible to use the wave flume for education purposes, such as class laboratory sessions.

The CIEMito wave flume consists of a metal frames and tempered glass panels. It has a length of 18 m, a width of 0.38 m, and a height of 0.58 m. The maximum water depth is of 0.36 m. The wave generation is performed by a piston paddle, which is moved by a linear actuator with a 1 m maximum paddle stroke, and a speed of response of 1.6 m/s. It has a 0.20 m diameter well at each end that serve for the filling and emptying of the flume, and for the current generating system. Figure 4.1 shows a picture of the CIEMito wave flume, and Figure 4.2 shows an image of the piston paddle of the wave flume.

Figure 4.1. Photograph of the CIEMito wave flume of the Laboratori d'Enginyeria Marítima (LIM).

Figure 4.2. Photograph of the piston paddle of the CIEMito wave flume (CIEMLAB, 2010).

4.2. THE PFEM NUMERICAL WAVE FLUME

The Particle Finite Element Method, PFEM, numerical model is a type of Lagrangian flow formulation developed at the Centre Internacional de Mètodes Numèrics en l'Enginyeria (CIMNE) in Barcelona. The model is based on the Navier-Stokes equations, and it is based on a non-fixed mesh method. The details of the PFEM numerical model are further discussed in the work of Oliveira *et al.* (2009). The model was developed to solve free surface flow problems that include large free surface motion, and interaction between the fluid and rigid bodies.

Oliveira et al. (2009) showed that the PFEM numerical wave flume was able to simulate any number of different types of wavemaker paddles, including the piston paddle, as in the CIEMito wave flume. By using the models ability to simulate interaction between the fluid and rigid bodies the wavemaker paddle could be simulated by a rigid body at one end of the wave flume. This wavemaker paddle could be given the motion found by utilizing a wavemaker theory and its transfer function. It was found that

the waves generated using the PFEM numerical flume were the same as those generated in the physical flume, when using the motion of the physical wave paddle in the numerical model. Also, since the model is designed to simulate large motion of the free surface, it is possible to simulate very steep waves without problems. It was also found that the unwanted secondary waves that are generated in the physical flumes when using first order wavemaker theory were also generated in the PFEM numerical flume, and it was further suggested that this model could be used to experiment with second order wavemaker theories to find if these theories could suppress the appearance of these unwanted waves, which is the aim of this study.

The use of numerical wave flumes, such as the PFEM numerical wave flume, brings advantages to the use of a physical wave flume such as CIEMito, since it is much more flexible. The numerical wave flumes are not limited by the infrastructure in place. Several types of wavemaker paddles can be simulated, and the size of the wave flume could even be the actual prototype size. Also, the maximum paddle stroke or the actuator velocity does not limit the wave paddle motion; therefore the maximum wave height to be generated is not limited by these issues. Still, the numerical model takes a large computer capacity, which can limit the duration of a simulation, or the number of simulations to be performed. For this study, the PFEM numerical wave flume was used to simulate the CIEMito wave flume, using its dimensions and paddle type.

Figure 4.3 shows an image of a simulation of the CIEMito wave flume in the PFEM numerical wave flume.

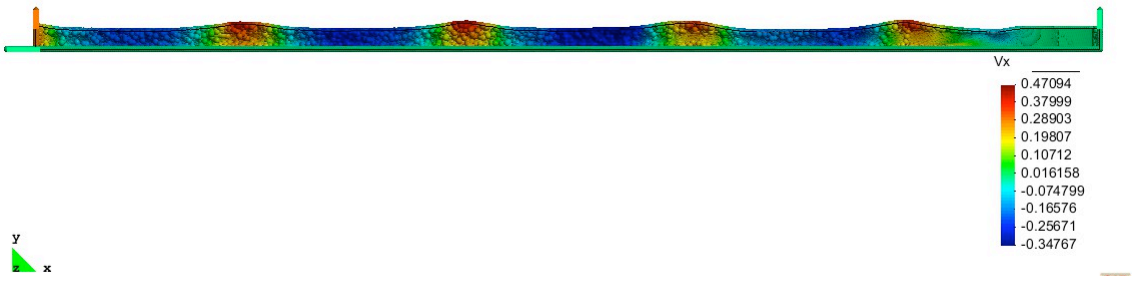

Figure 4.3. Image of the PFEM numerical wave flume simulation of the CIEMito wave flume.

5. FIRST ORDER WAVE GENERATION EXPERIMENT

As discussed in Section 2.2, when generating waves with a low relative water depth, h/L, and/or high wave steepness, H/L, by using first order wavemaker theory unwanted secondary waves may be generated along with the desired waves. One of the objectives of this study was to find under which conditions this occurs, and to what degree in the CIEMito wave flume. A set of experiments was performed in the CIEMito wave flume, and from the data obtained the problematic conditions could be identified.

Another objective was to find if, by using second order wavemaker theories, the generation of the unwanted secondary waves could be suppressed in the CIEMito wave flume. Unfortunately, due to issues with the wave flume only first order waves could be generated in it. Recently it has been recognized that wave flumes may be modeled numerically, creating what is known as a numerical wave flume. In order to test the results of second order wavemaker theories the PFEM numerical model was used to simulate the CIEMito wave flume. First it was important to ensure that the PFEM numerical wave flume produced results that coincided with the ones obtained from the actual CIEMito wave flume. For this reason the wave conditions that were chosen to be tested using second order wavemaker theory were first simulated in the PFEM numerical wave flume. From this the results of the CIEMito wave flume and the PFEM numerical wave flume could be compared, ensuring that the results of the second order wavemaker theory simulations will accurately represent what would happen in the CIEMito wave flume.

In this chapter both the physical and the numerical wave generation experiments will be discussed. First the experiment set-up is described, specifying what wave conditions were tested, the paddle movement used, and how the data was recorded. Then the methods used to treat analyze the data will be discussed. Finally the results found from these experiments will be given. After this a comparison of the results of the physical wave generation experiment and the numerical wave generation simulation is done.

5.1. PHYSICAL WAVE GENERATION

In this section all the details of the physical wave generation experiment are given, from the experiment set-up, to the data analysis, and finally the results.

5.1.1. EXPERIMENT SET-UP

In this section all the considerations taken for the first order physical wave generation experiment will be discussed. First, the selection of the wave conditions to be tested. Next, the required paddle motion to achieve these wave conditions, and how it was obtained. Finally, the means used to record and obtain the data from the experiments.

5.1.1.1. Wave Conditions

The experiment conditions are based on other experiments that have been done on the subject, specifically those done by Zhang and Schäffer (1996), Schäffer (2006), and Calabrese *et al*. (2009). This way, the results may be compared with the past experiments.

As in the experiments which served as a basis to the performed experiments, several wave periods and wave heights were chosen to obtain different non-linearity of the waves, and different relative water depth. The relative water depth is defined as h/L_0, where h is the water depth, and L_0 is the wavelength in deep water according to linear wave theory (Equation 5.1). This way different wave conditions are tested, to see when the first order wavemaker theory produces unwanted secondary waves.

$$L_0 = \left(\frac{g}{2\pi}\right) \cdot T^2 \qquad \text{Equation 5.1}$$

where, g is the acceleration of gravity, and T is the wave period.

For the experiment two sets of wave conditions were selected. The first set of conditions would be performed at a water depth of 0.32 m. This is not the maximum

working water depth of the wave flume, 0.36 m, but was taken to be the maximum safe water depth. The second set of wave conditions would be performed at a water depth of 0.25 m. The water depth for the first set of conditions was selected to be the maximum possible so that larger waves, which are more readily viewable, may be used to obtain the same relative water depth. The water depth for the second set of conditions was selected since this is the actual water depth used by Calebrese *et al*. (2008). Since this is a water depth that could be used in the CIEMito wave flume, and these experimental conditions have become the "ad hoc" conditions for the subject, it was decided that this water depth would be used.

The limitations of the CIEMito wave flume had to be taken into consideration when deciding what wave conditions would be tested. The piston wavemaker must be able to create the required waves, and the waves created must be stable and not break. Since this was not an experiment testing the wave height limits of the flume the waves produced were not the maximum attainable in the wave flume.

First, the maximum wave height without breaking was taken into consideration. The Coastal Engineering Manual (2006) states that the maximum ratio between the wave height and the water depth, H/h, is 0.78 before breaking occurs. However, Nelson (1994) found that for shallow water waves the maximum wave height to water depth ratio for shallow water waves is 0.55. For the experiments the maximum wave height to water depth ratio, H/h, used was 0.5. This ensured there was no wave breaking due to insufficient water depth.

Second, the maximum wave steepness had to be considered. Following the Coastal Engineering Manual (2006) the wave steepness was limited to 0.141, this way breaking due to steepness was prevented.

Finally, the wave paddle capacity was considered. The waves tested could not be so large that the wave paddle would be unable to create them. The maximum paddle stroke of the CIEMito wave flume is of 1 m (CIEMLAB, 2010). Still, a safer maximum paddle stroke was selected to be 0.27 m, therefore the waves must not require a larger paddle stroke than this.

As stated, the experimental set-up was based on past experiments, still, since the equipment used in these laboratories did not have the same dimensions as the CIEMito wave flume, scaling was done to fit the conditions to the CIEMito wave flume.

To scale the conditions from these experiments the relative water depth, and the ratio between water depths, the water depth in the CIEMito wave flume to the water depth in the other experiments, were used.

First, the wave height, H, was scaled using the water depth ratio as the scaling factor (Equation 5.2).

$$H_{CIEMito} = H_{other} \cdot \left(\frac{h_{CIEMito}}{h_{other}} \right) \qquad \text{Equation 5.2}$$

where $H_{CIEMito}$ and $h_{CIEMito}$ are the wave height and water depth for the test done in the CIEMito wave flume, respectively, and H_{other} and h_{other} are the wave height and water depth of the base experiments, respectively.

Second, to find the scaled wave period the relative water depth was kept equal between the CIEMito test and the other experiments. Since the relative water depth is a unitless value, it should remain equal. From this the wavelength in deep water of the CIEMito test was found, and since the wavelength in deep water is only dependant on the wave period, the wave period of the CIEMito test may be obtained (Equation 5.3).

$$L_{0-CIEMito} = \frac{h_{CIEMito}}{\left(h/L_0\right)_{other}} \qquad \text{Equation 5.3}$$

where $L_{0-CIEMito}$ and $h_{CIEMito}$ are the deep-water wavelength and water depth of the CIEMito experiment, respectively, and $(h/L_0)_{other}$ is the relative water depth of the base experiment.

The wave heights and wave periods found for the CIEMito scale were then rounded to more manageable numbers; so, the final experimental conditions vary slightly from those of the other experiments.

From this 50 wave conditions were obtained, but from these only 24 were selected as the first set of wave conditions, Set 1, to be tested in 0.32 m water depth. Since some of these wave conditions exceeded some of the wave flume limitations, as set above, these were not done. Also, some conditions were repeated, or very similar to one another, therefore it was unnecessary to perform them twice. Amongst the 24 wave conditions selected were the 12 wave conditions given in Calabrese *et al*. (2009), and a mix of conditions from Zhang and Schäffer (1996), and Schäffer (2006).

To the first set of wave conditions to be used in the experiments, Set 1, a second set of wave conditions were selected, Set 2. This second set of wave conditions are the 12 exact wave conditions given by Calabrese *et al*. (2009), performed at a water depth of 0.25 m, and one other wave condition. For Set 2 no scaling was necessary.

The wave conditions presented by Calabrese *et al.* (2009) were first used by Goda (1997), and have since become standard tests for the subject (Calabrese *et al*., 2009). For this reason the majority of the selected wave conditions are based on these experiments.

A summary of the final 24 wave conditions of Set 1, and the 13 wave conditions of Set 2, used for the wave generation experiments is given in Table 5.1 and Table 5.2, respectively. Here the conditions highlighted in grey are those conditions presented by Calabrese *et al*. (2009). In both tables T is the wave period in seconds, H is the expected wave height in meters, L_0 is the deep-water wavelength (Equation 5.1), h/L_0 is the relative water depth, H/L_0 is the wave steepness, and N is the number of waves to be generated.

Table 5.1. Summary of Set 1, wave conditions selected for wave generation experiment with h= 0.32 m.

Case	T (s)	H (m)	L_0 (m)	h/L_0	H/L_0	N
1	2.00	0.16	6.245	0.0512	0.0256	10
2	2.00	0.12	6.245	0.0512	0.0192	10
3	1.90	0.10	5.636	0.0568	0.0177	10
4	1.90	0.06	5.636	0.0568	0.0106	10
5	1.90	0.03	5.636	0.0568	0.0053	10
6	1.70	0.10	4.512	0.0709	0.0222	10
7	1.70	0.06	4.512	0.0709	0.0133	10
8	1.70	0.03	4.512	0.0709	0.0066	10
9	1.40	0.16	3.060	0.1046	0.0523	10
10	1.40	0.10	3.060	0.1046	0.0327	10
11	1.40	0.06	3.060	0.1046	0.0196	10
12	1.40	0.03	3.060	0.1046	0.0098	10
13	1.25	0.16	2.440	0.1312	0.0656	10
14	1.25	0.12	2.440	0.1312	0.0492	10
15	1.10	0.10	1.889	0.1694	0.0529	10
16	1.10	0.06	1.889	0.1694	0.0318	10
17	1.10	0.03	1.889	0.1694	0.0159	10
18	1.00	0.10	1.561	0.2050	0.0640	10
19	1.00	0.07	1.561	0.2050	0.0448	10
20	0.80	0.10	0.999	0.3202	0.1001	20
21	0.80	0.08	0.999	0.3202	0.0801	20
22	0.70	0.06	0.765	0.4183	0.0784	20
23	0.70	0.05	0.765	0.4183	0.0654	20
24	0.50	0.04	0.390	0.8198	0.1025	20

Table 5.2. Summary of Set 2, wave conditions selected for wave generation experiment with h= 0.25 m.

Case	T (s)	H (m)	L_0 (m)	h/L_0	H/L_0	N
25	1.70	0.075	4.512	0.0554	0.0166	20
26	1.70	0.050	4.512	0.0554	0.0111	20
27	1.70	0.025	4.512	0.0554	0.0055	20
28	1.50	0.075	3.513	0.0712	0.0213	20
29	1.50	0.050	3.513	0.0712	0.0142	20
30	1.50	0.025	3.513	0.0712	0.0071	20
31	1.20	0.075	2.248	0.1112	0.0334	20
32	1.20	0.050	2.248	0.1112	0.0222	20
33	1.20	0.025	2.248	0.1112	0.0111	20
34	1.00	0.075	1.561	0.1601	0.0480	20
35	1.00	0.050	1.561	0.1601	0.0320	20
36	1.00	0.025	1.561	0.1601	0.0160	20
37	1.70	0.12	4.512	0.0554	0.0266	20

The number of generated waves should allow for the length of the wave flume to be filled by waves. This way the decay of the waves with shorter period will not cause the generated waves to dissipate before reaching the end of the flume. For this reason for case 1 through case 19 there should be 10 waves generated, and for the other cases 20 waves. This should provide enough information to perform the analysis of the generated waves.

Figure 5.1 and Figure 5.2 show the different non-linearity and the applicable wave theories of the wave conditions in Set 1 and Set 2, respectively. The image in the background of the graphs in Figure 5.1 and Figure 5.2 is taken from the Coastal Engineering Manual (2006), and shows the ranges of suitability for various wave theories according to Le Méhauté (1976). Here we can see how the wave conditions spread over several wave theories, from Stoke's 2^{nd} and 3^{rd} Order, and one close to 4^{th} Order, and Stream Theory. Also, they spread over several relative water depths, making some closer to shallow-water waves, and others closer to the deep-water waves. There is one case that is actually a deep-water wave. Producing actual linear waves is not possible since it would require extremely small wave heights with long periods, which the wavemaker is not able to produce.

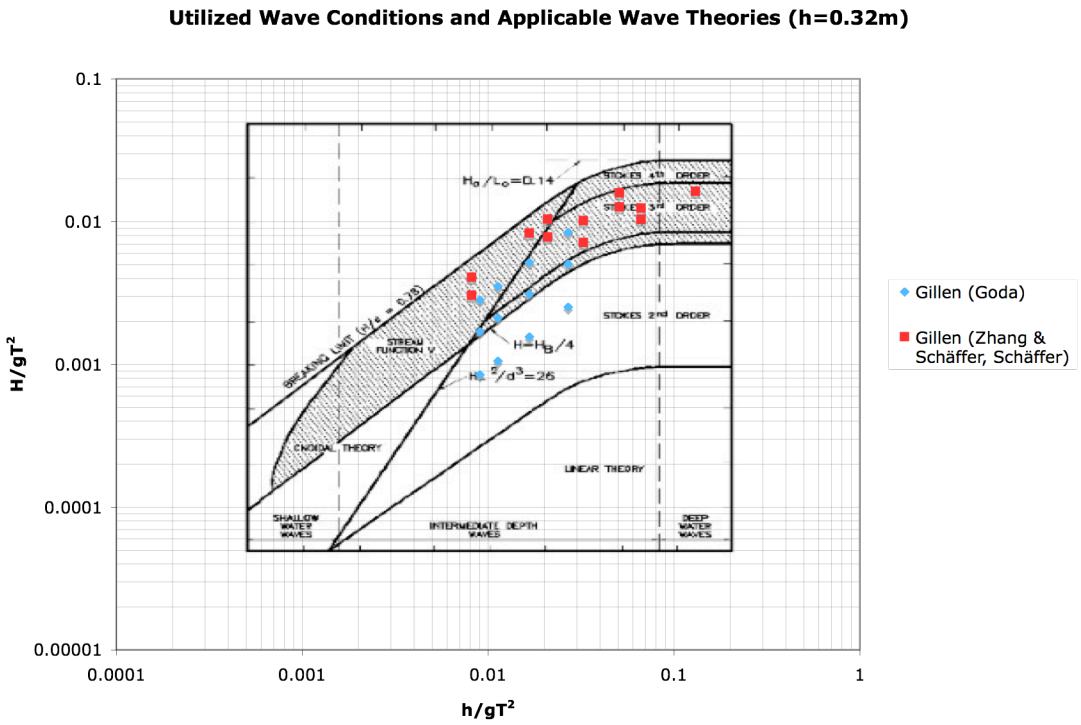

Figure 5.1. Applicable wave theories to Set 1 wave conditions in h=0.32m according to Le Méhauté (1976) (CEM, 2006).

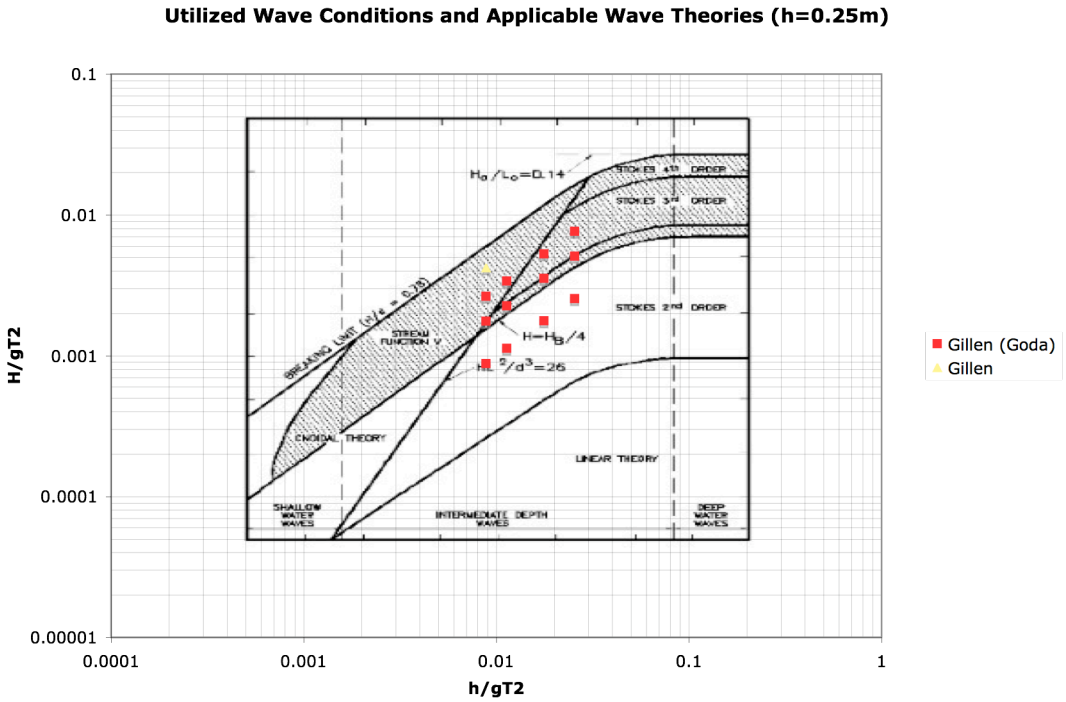

Figure 5.2. Applicable wave theories to Set 2 wave conditions in h=0.25m according to Le Méhauté (1976) (CEM, 2006).

Figure 5.3 shows the paddle and wave flume capacity curves under the described limits, a maximum wave height to depth ratio of 0.5, a maximum paddle stroke of 27 cm, and a maximum wave steepness of 0.141, with the wave conditions of Set 1, water depth of 0.32 m. Figure 5.4 shows the same as Figure 5.3, but for the wave conditions of Set 2, water depth of 0.25 m. These are not the actual paddle and wave flume limits, since, because this is not an experiment testing the limits of the paddle and wave flume, more conservative limits have been used.

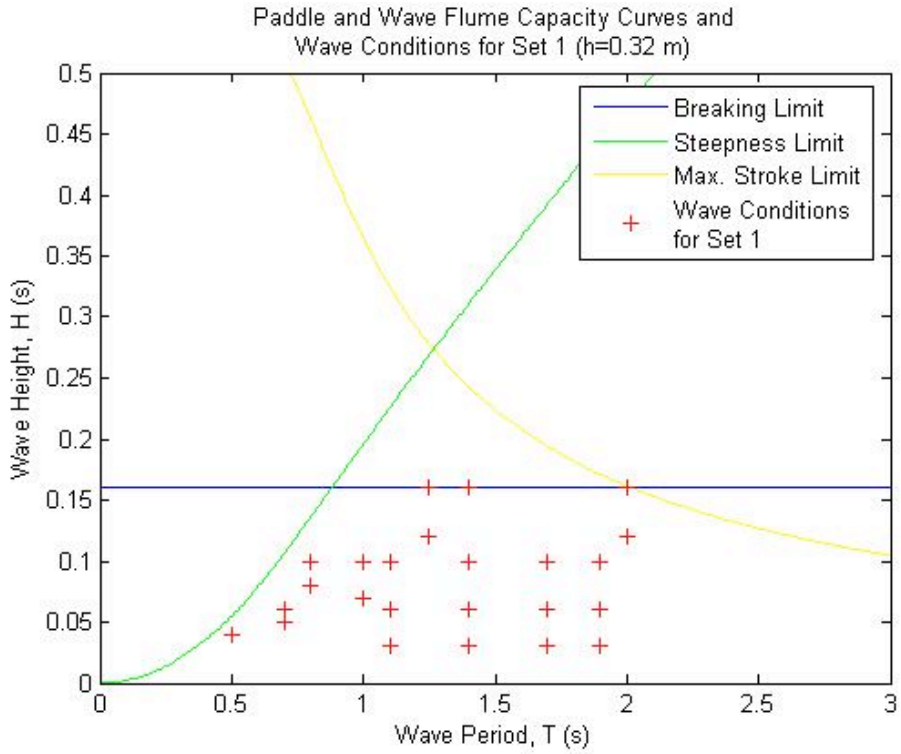

Figure 5.3. Paddle and wave flume capacity curves with the wave conditions of Set 1.

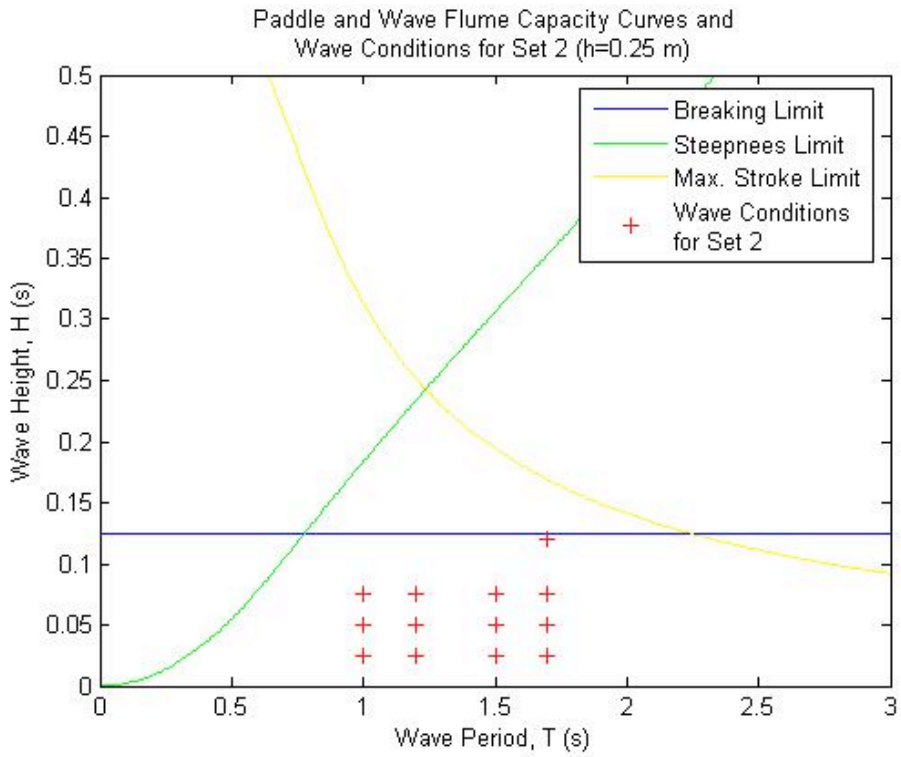

Figure 5.4. Paddle and wave flume capacity curves with the wave conditions of Set 2.

5.1.1.2. Paddle Motion

In order to obtain the motion of the piston paddle, the generation software developed at LIM was used. This software follows the linear wavemaker theory, as discussed in Section 3.2. The routine described in Section 3.2, which may be found in Appendix A, was also developed to find the required paddle motion to create the desired regular wave conditions, amongst other information, following the linear wavemaker theory.

Figure 5.5 shows a graph with the position of the piston paddle with respect to time for Case 1, which has a wave height, H, of 0.16 m, and a wave period, T, of 2.0 s. It is seen that the paddle motion is completely sinusoidal, following the linear wavemaker theory (Equation 5.4).

$$X(t) = \frac{S}{2} \cdot \sin(\omega t) \qquad \text{Equation 5.4}$$

where $X(t)$ is the position of the paddle at a given time t, S is the wave board stroke at the water surface level, which is given by the transfer function, and ω is the wave angular frequency.

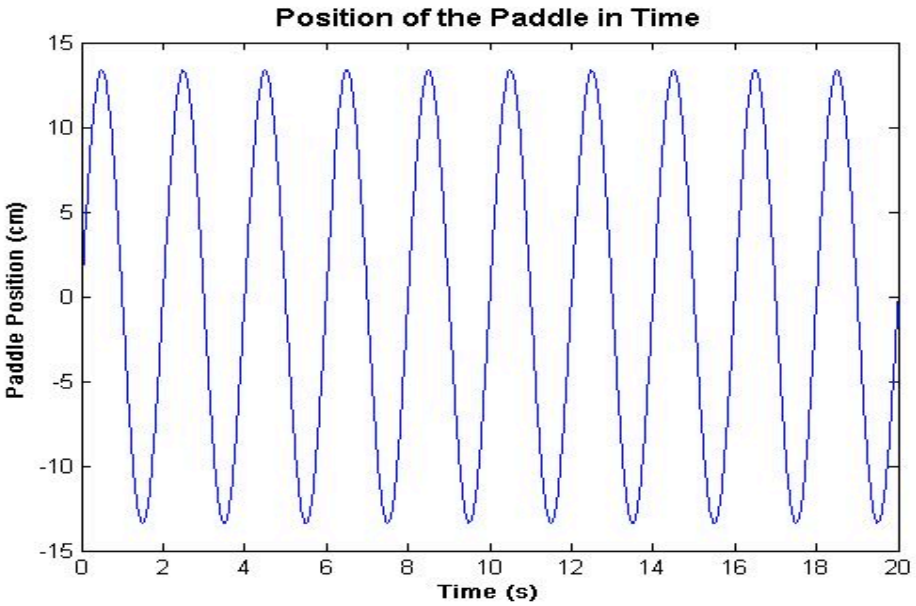

Figure 5.5. Time series of the paddle displacement for the generation of Case 1, H=0.16 m, T=2.0 s.

To the paddle displacement shown in Figure 5.5 a ramp must be added at the beginning and at the end of the time series. The ramp is a gradual increase of the paddle movement, usually over one or two wave periods, to the final amplitude of the paddle displacement. This way there is a gentle start and stop of the paddle movement to prevent damage to the wavemaker system due to sudden starts and/or stops. During the experiments the ramp used was either one or two wave periods.

5.1.1.3. Wave Gauges

To record the surface elevation during the experiments, eight HR Wallingford wave gauges were positioned throughout the wave flume. The position of the wave gauges were also taken form the past experiments that were taken as a base for these experiments. Since the specific location of the wave gauges in the tests described by Calabrese et al. (2009), only the positions of the tests described by Zhang and Schäffer

(1996), and Schäffer (2006) were used. The position of the wave gauges were also scaled to the CIEMito wave flume dimensions using the water depth ratios as a scaling factor (Equation 5.5).

$$X_{WG-CIEMito} = X_{WG-other} \cdot \left(\frac{h_{CIEMito}}{h_{other}} \right) \qquad \text{Equation 5.5}$$

where $X_{WG-CIEMito}$ and $h_{CIEMito}$ are the distance of the wave gauge from the mean paddle position and the water depth of the CIEMito experiment, respectively, and $X_{WG-other}$ and h_{other} are the distance of the wave gauge from the mean paddle position and the water depth of the base experiment, respectively.

From this seven wave gauge positions were obtained, at 0.5 m, 1.0 m, 1.8 m, 2.0 m 3.5 m, 4.0 m, and 7.0 m from the mean paddle position, but not all could be placed where it was wanted. The first wave gauge was to be placed too close to the mean paddle position (0.5 m), and the configuration of the CIEMito wave flume made it impossible to place it there. Also, it is best to not place a wave gauge inside a distance of three times the water depth since the linear wavemaker theory produces standing waves close to the paddle, which decay sufficiently after this distance to become negligible. Another two wave gauges were to be set very close to each other (1.8 m and 2.0 m), so it was decided to use only one of these (2.0 m). Also, only two wave gauges could be placed four meters from the mean paddle position, since the other wave gauges lacked the cable length necessary to place them there. Because of this, the wave gauge that was supposed to be placed 3.5 m from the mean paddle position was instead placed at 4.5 m from the mean paddle position. This way the distance of 0.5 m between the consecutive wave gauges would be maintained.

Since there were still three unused wave gauges it was decided to place two of them further from the mean paddle position, where no wages gauges were placed, and the last wave gauge was placed 6.0 m from the mean paddle position, to have a higher resolution close to the paddle. The final position of the wave gauges is summarized in Table 5.3. The position is given in meters away from the mean paddle position.

Table 5.3. Final position of the wave gauges with respect to the mean paddle position.

Wave Gauge	Position (m)
WG0	1.0
WG1	2.0
WG2	4.0
WG3	4.5
WG4	6.0
WG5	7.0
WG6	9.0
WG7	10.0

By having these wave gauge positions there should be no problem obtaining enough information to perform the desired analyses. As discussed in Section 2.2 the secondary wave travels at a different speed than the primary wave. For this reason sometimes the primary peak and the secondary peak are at different places, so the secondary peak is visible, and sometimes the primary peak and secondary peak coincide, therefore the secondary peak is not visible. By having this array of wave gauges both situations should be obtainable. Also, if there are any changes in the wave as it moves through the wave flume they should be noticeable. A problem may rise with the wave gauges furthest away from the paddle, since they may receive the reflected waves before sufficient clean data is obtained, but this will be assessed in the data analysis.

The wave gauges consist of an electrical circuit with a pair of stainless steel wires that are partially submerged in the water, and the water closes the circuit. Depending on the amount of the stiff wire that is submerged the resistance of the circuit will change. The current is converted to voltage, which will change when the resistance increases or decreases because of the water level variations. To correctly relate this voltage to a water level the wave gauges need to be calibrated before the experiments are run. To do this, the wave gauges are first placed at a position to obtain a voltage signal. Next they are raised or lowered by a known distance, in this case 12 cm, this way the voltage change is related to a water level change. To facilitate the calibration the wave gauges are attached to a calibrated stem, which has very accurately distanced holes along its length. In this

case each hole is 3 cm apart, so by moving the wave gauge 4 holes up or down, the required distance change of 12 cm is obtained. Figure 5.6 shows a picture of one of the used wave gauges attached to the calibrated stem in the CIEMito wave flume.

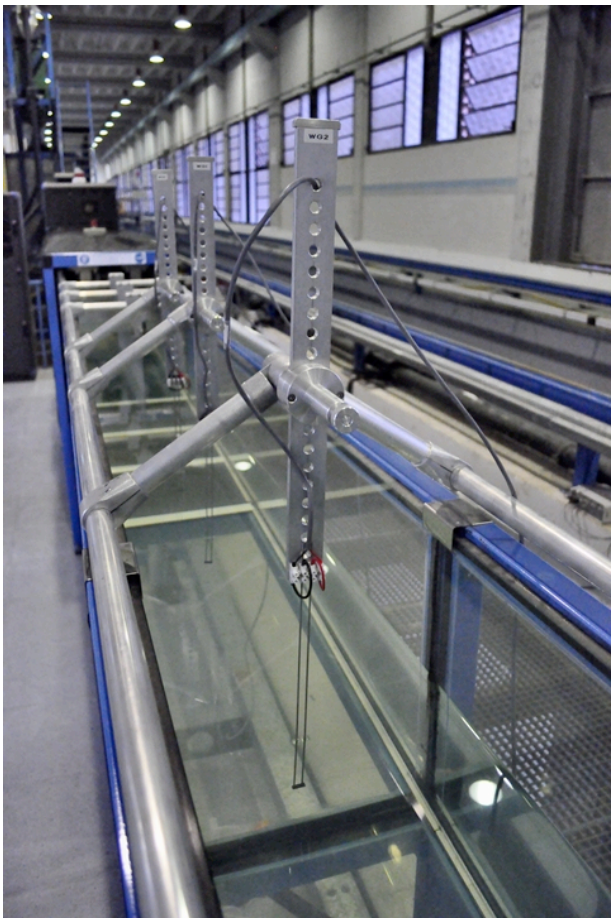

Figure 5.6. A CIEMito wave gauge and the calibrated stem (CIEMLAB, 2010).

The sampling frequency of the wave gauges was set to 100 Hz. Since the duration of each time series is short, there would be no problem of having too much data by using a high sampling frequency. For this reason a high sampling frequency was used. The accuracy of the wave gauges is of ±0.1 mm.

5.1.1.4. Video Recording

As another method of recording the experiments a video camera was used to record the generated waves. The camera was placed on a tripod and took video of the

area around wave gauge WG4 and WG5. In some cases where something unusual was seen, or just to get a different perspective, another angle was used.

By having video footage of the experiments, images of the unwanted secondary waves may be obtained. This could facilitate the visualization of the phenomena being studied. Still, the video footage of the experiments will only serve as a secondary means to show the presence of the secondary waves, since they may not always be easily viewable, as could be the case with small wave heights or small secondary waves. The primary method of showing the presence of the unwanted waves will be through the analysis of the surface elevation data obtained from the wave gauges.

5.1.2. DATA ANALYSIS

After performing the wave generation experiments in the CIEMito wave flume the resulting data must be treated and analyzed in a certain way to obtain the desired information from it. In this section the considerations taken in analyzing the data obtained from the wave generation experiments will be discussed. First, how the data is transformed from voltage to free water elevation is described. Then, how the selection of the free water elevation time series was done, and how it was treated before it was analyzed. Then, how the treated time series was analyzed to obtain the generated wave height, and the different spectral analyses. Finally, it will be discussed how the video data recorded during the experiment was dealt with.

5.1.2.1. Transformation of Raw Data

The data collected by the wave gauges during the wave generation experiment is a time series of voltage. In order to make it useful the data must first be transformed from a voltage time series, to a free water elevation time series. To do this, the data obtained from the wave gauge calibration, discussed in Section 5.1.1.3, is used to relate the voltage to a free water elevation for each wave gauge.

5.1.2.2. Selection of Utilized Time Series

The entire free water elevation time series obtained from the experiments cannot be used for the analysis. Three things must be taken into consideration, the waves generated during ramp of the wavemaker motion, the dissipation of waves as they propagate through the wave flume, and the effects due to the reflection of waves from the end of the wave flume. This means that the utilized free water elevation time series is much shorter than the original time series obtained.

Figure 5.7 shows the complete free water elevation time series for Case 2, with an expected wave height, H, of 0.10 m, and a wave period, T, of 2.0 s, as recorded by wave gauge WG1. In this figure it is seen that the first wave of the series is significantly smaller than the rest, since it was generated during the ramp of the wavemaker motion. It may also be seen that near the end of the generated waves there is a sudden increase in the wave height (circled). This is the effect of the wave reflection from the end of the wave flume.

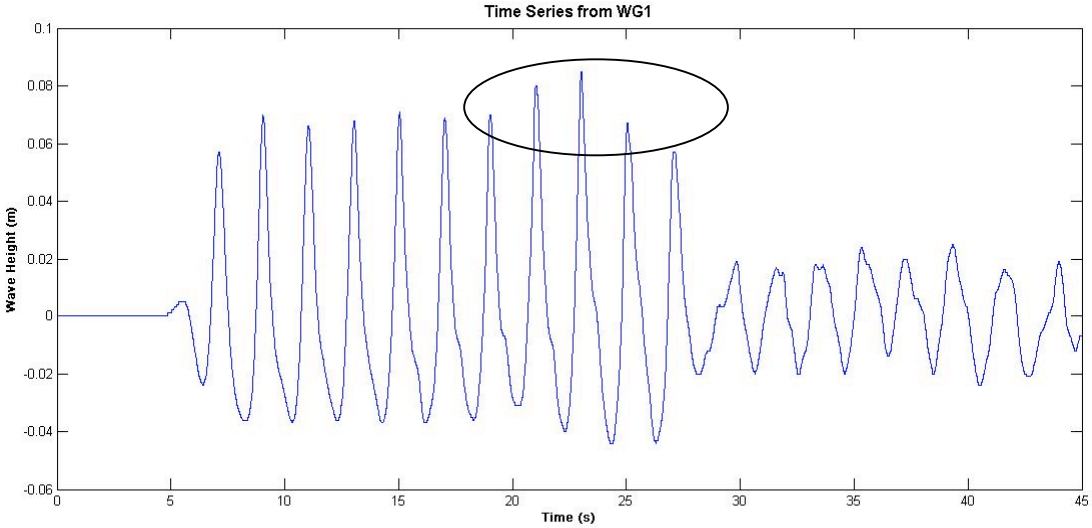

Figure 5.7. Complete free water elevation time series for Case 2, H= 0.10 m, T= 2.0 s, at WG1.

As discussed in Section 5.1.1.2, at the beginning and at the end of the paddle motion a ramp in the motion of the wavemaker is used to prevent damaging the wavemaker system due to sudden starts and/or stops. This means that at the beginning of

each time series there is at least one ramp wave. The ramp wave is a wave generated during the ramp in the motion of the wavemaker. The ramp wave is smaller than the desired waves because the wavemaker has yet to reach the desired paddle motion. Since using this section of the time series would give incorrect results it must be removed from the beginning of the time series.

In order to remove the ramp wave from the beginning of the free water elevation time series, the beginning of the utilized time series will be the second or the third zero up crossing, depending on weather one or two wave periods were used as a ramp, respectively. This way the ramp wave, or ramp waves, will not be a part of the utilized time series.

Another thing that had to be considered at the beginning of the free water elevation time series was the dissipation of waves as they propagate along the wave flume. As a wave propagates it will loose energy due to friction and dissipate. Depending on the characteristics of the wave, the position of the wave gauges may be considered a long or short distance for the wave to propagate. In order to quantify this we may use the relative distance of the wave gauge, which is defined as X_{WG}/L, where X_{WG} is the distance of the wave gauge to the mean position of the paddle, and L is the wavelength. If the relative distance of the wave gauge is large, then there will be some wave dissipation.

Figure 5.8 shows the original free wave time series for Case 20, with a wave height, H, of 0.10 m, and a wave period, T, of 0.8 s, as recorded by wave gauge WG5. For Case 20 the ramp used was of two wave periods. The relative distance for wave gauge WG5 and this wave condition is of 7.23, which is enough for some wave dissipation to occur. From this figure it may be seen that there are more than just the two ramp waves with a significantly smaller wave height than the expected wave height.

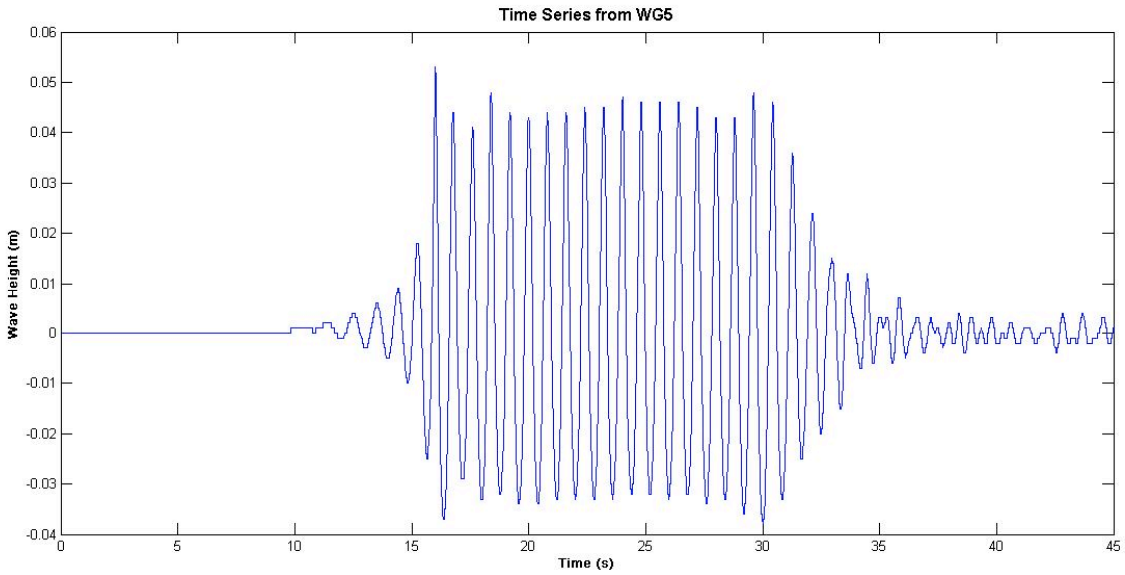

Figure 5.8. Complete free water elevation time series for Case 20, H= 0.10 m, T= 0.8 s, at WG5.

The problem of wave dissipation varied from case to case. Also, for a particular case, depending on which wave gauge is taken into consideration, the number of dissipated waves will change. This is due to the fact that the wave gauges closer to the paddle allow less distance for the waves to dissipate than those further away. For this reason, in order to obtain the utilized free water elevation time series, it was necessary to use inspection to decide how many waves needed to be neglected from the beginning of the time series for each case and wave gauge.

The final consideration to the selection of the time series to be analyzed was reflection. Even though the CIEMito wave flume is equipped with an absorption system to reduce wave reflection, it is not a perfect system; therefore some wave energy is reflected. If the part of the time series that contains the reflected waves is taken into consideration it could alter the results, so this final part of the time series, where the reflection may affect the results, must be discarded as well.

Since the wave gauges are placed at a different distance from the end of the wave flume, the reflection will take different times to reach each one. This means that the wave gauges closest to the end of the wave flume will have less time between the wave arrival and the reflected wave arrival, and therefore less undisturbed data than the ones closer to the paddle. The time period between the wave first being registered by the wave

gauge and the time its reflection reaches the wave gauge is determined by the celerity of the wave, and the distance between the wave gauge and the end of the wave flume. Equation 5.6 shows how the time of arrival of the reflected wave for a particular wave gauge was obtained.

$$\Delta t_{WG} = 2 \cdot \frac{\Delta x_{WG}}{c} \qquad \text{or} \qquad \Delta t_{WG} = 2 \cdot \frac{L}{T} \cdot \Delta x_{WG} \qquad \text{Equation 5.6}$$

where Δt_{WG} is the time of arrival of the reflected wave to a wave gauge, Δx_{WG} is the distance from the wave gauge to the end of the wave flume, c is the wave celerity, L is the wavelength, and T is the wave period.

The first wave that is recorded at a wave gauge may not necessarily reflect back to the wave gauge since, as stated before, some of the waves dissipate as they propagate along the wave flume. For this reason, if a wave has a height smaller then 1 cm when recorded at wave gauge WG7, which is located closest to the end of the wave flume, it was assumed that the wave would dissipate before reflecting, and would therefore not be taken into consideration for the time of arrival of the reflected wave to a wave gauge.

If the time of arrival of the reflected wave allowed for the utilized free water elevation time series to be longer than five wave periods, then the utilized time series would be limited to only five wave periods. However, sometimes the time of arrival of the reflected wave is less than this, causing the undisturbed time series to be shorter than five wave periods. Also, in some cases there is no undisturbed time series, since the ramp wave will have reflected and reached the wave gauge before the desired waves arrive to the wave gauge, or the undisturbed time series is very short and does not provide enough data for a proper analysis to be performed. This is mostly the case for wave conditions with high wave period (high wave celerity), which have a shorter time of arrival of the reflected wave. Wave gauges WG6 and WG7 presented this issue the most, since they are located the closest to the end of the wave flume.

Figure 5.9 shows the final utilized free water elevation time series for Case 2, as recorded by wave gauge WG1. Here, close to five wave periods are utilized. No ramp

waves or dissipated waves are included at the beginning of the time series. Also, at the end of the time series no effects of reflected waves are included.

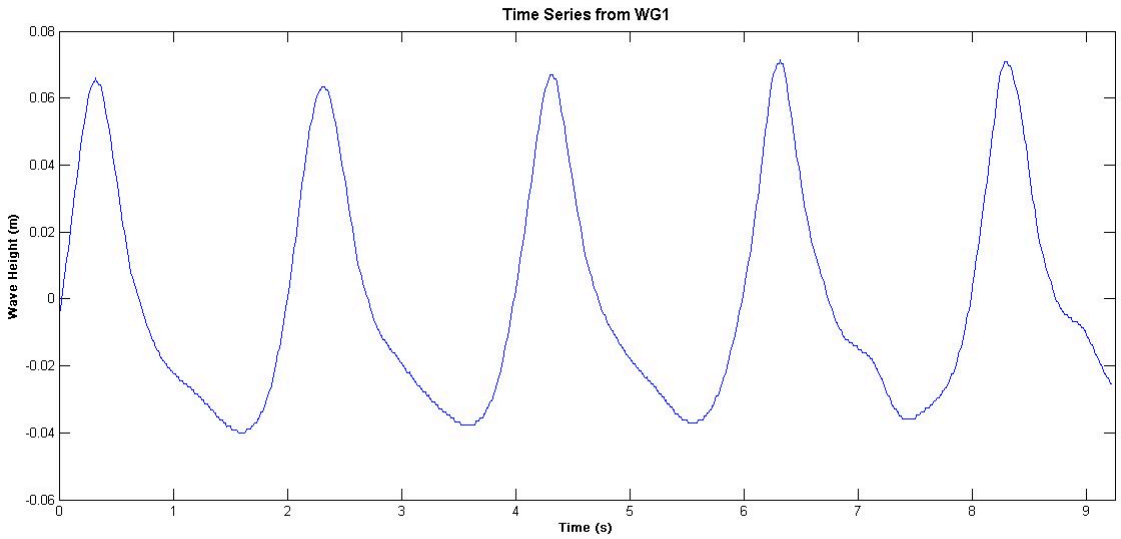

Figure 5.9. Utilized time series for Case 2, H= 0.10 m, T= 2.0 s, at WG1.

5.1.2.3. Normalization of the Data

The second step in the analysis of the data was to normalize the data, in order to remove any possible existing linear trends. The linear trends could be caused by the slow increase of water level due to the push from the generated waves, known as wave set up. In this case, since only ten to twenty waves were generated per time series, the effect of water level increase due to the waves should be small. Still, it is preferable to remove any trends that may alter the results of the time series analysis.

To remove a linear trend first the original time series must be fitted to a line defined by $y = a \cdot x + b$. Then the trend is removed from the original free water elevation time series, η, to obtain the normalized time series, η' (Equation 5.7).

$$\eta' = \eta - y \qquad \text{Equation 5.7}$$

Once the undisturbed time series is normalized, the analysis of the data can be performed.

5.1.2.4. Generated Wave Height

To obtain the actual wave height of the waves that were generated the free water elevation time series, which has been selected from the original time series and normalized, was analyzed according to the zero up crossing method. The time series is divided into five, or less, waves. According to the zero up crossing method, a wave starts when the water elevation crosses the zero level while increasing, and ends when the water elevation does this again. From this the wave height of each wave is determined as the distance between the maximum and minimum water elevation in the wave. If the utilized time series for a given wave gauge was too short to provide information about wave height, then it was not taken into consideration.

The average wave height at each sensor was found by averaging the heights of every wave within the time series recorded at that sensor (Equation 5.8). From the average wave height at each sensor we may find if there is a change in the generated wave height as the wave propagates along the wave flume, and if there is a trend to this.

$$\overline{H}_{WG} = \frac{\sum_{i=1}^{N} H_i}{N} \qquad \text{Equation 5.8}$$

where $\overline{H}_{WG}$ is the average wave height for a given wave gauge, H_i is the wave height of each individual waves in a time series recorded by that wave gauge, and N is the total number of waves in the time series.

The total average wave height is then found by averaging the average wave height at each sensor (Equation 5.9). In this case the total average wave height will be considered as the generated wave height for each case ran in the wave flume. This generated wave height may be compared to the expected wave height, the wave height that was specified, to see if there is a difference between these, and if there is a trend to

this. To quantify this the wave height ratio, $H_{gen}/H_{\exp}$, which is the ratio of the generated wave height, H_{gen}, to the expected wave height, $H_{\exp}$, was found.

$$H_{gen} = \frac{\sum_{j=1}^{M} \overline{H}_{WGj}}{M} \qquad \text{Equation 5.9}$$

where H_{gen} is the generated wave height, $\overline{H}_{WGj}$ is the average wave height for a given wave gauge j, and M is the number of wave gauges that have enough data to calculate at least one wave height.

5.1.2.5. Spectral Analysis

Sometimes the unwanted secondary waves are readily seen in the free water elevation time series. Still, in other cases it is not as evident. In order to identify the presence of the unwanted secondary waves, and the degree to which it was generated, a spectral analysis of the time series was performed. Two types of frequency spectrums will be obtained. The first will be a common spectrum, where the energy of the waves are distributed over their frequencies, and the second will be a normalized spectrum, where the maximum energy will always be one.

To calculate the regular spectrum the Wave Analysis for Fatigue and Oceanography, WAFO, Matlab toolbox was used. With this application the produced spectrums are smoothed out significantly, even when using the highest resolution possible. Obtaining a high resolution may be difficult, given that the time series is very short. Still, it is important to have a good resolution in order to be able to distinguish different peak frequencies.

To try to improve the resolution of the frequency spectrums the utilized time series was repeated 100 times. It was necessary to ensure that the joints, where one time series ends and will be repeated again, were smooth, and did not include a sharp jump, or any other discrepancy that could produce an error in the resulting spectrum. The frequency spectrums obtained from this analysis were still smoothed out significantly, but

the peaks could be resolved, and therefore was deemed sufficient for the purpose of this study.

Figure 5.10 shows the spectral density plot for Case 2, as viewed by wave gauge WG1. It may be seen that the energy is distributed over several frequencies, which should not be the case since this is a regular wave. Still, the different peaks can be distinguished, making the graph useful for the analysis.

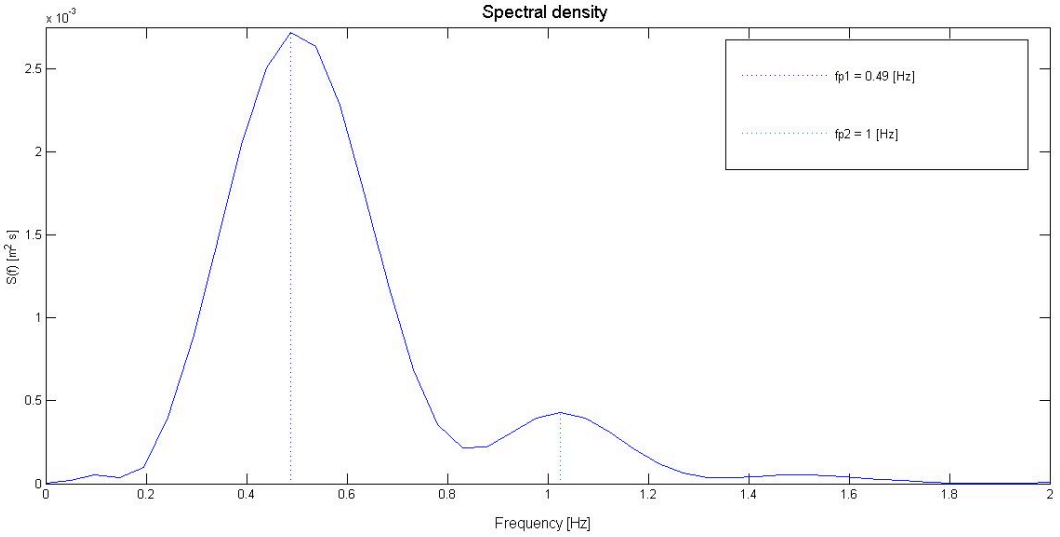

Figure 5.10. Spectral density plot of Case 2, H= 0.12 m T= 2.0 s, at WG1.

In order to enable a better comparison between the resulting spectrums from different wave conditions and between the time series of each wave gauge for a given condition, the normalized spectrums were generated. This way the maximum energy will be the same, one, for all of the spectrums, and the amount of energy found in the secondary frequencies relative to the main frequency may be obtained.

The normalized spectral density is given by $S(f)/S(f_p)$, where $S(f)$ is the spectral density, and $S(f_p)$ is the spectral density at the peak frequency, f_p. The normalized frequency is given by f/f_p, where f is the frequency, and f_p is the peak frequency.

Figure 5.11 shows a normalized spectral density plot for wave gauge Case 2, as recorded by wave gauge WG1. The normalized spectrums were limited to a frequency of $4 f_p$ since above this frequency the data could be noise from the sensors.

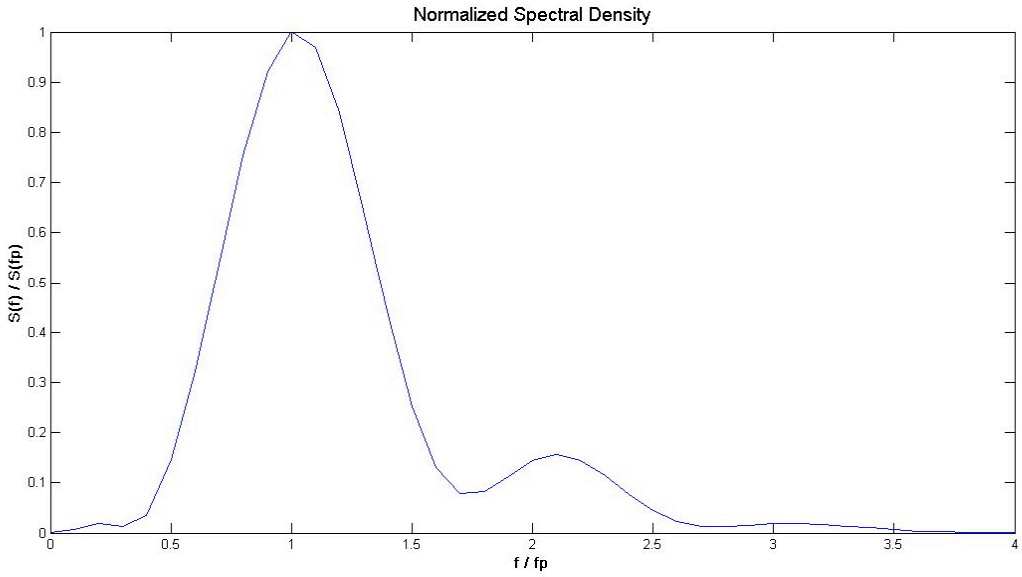

Figure 5.11. Normalized spectral density plot of Case 2, H= 0.12 m T= 2.0 s, at WG1.

5.1.2.6. Review of Film

Finally, the video that was recorded during the experimental process was reviewed and compared to the results from the data of the wave gauges to see if good images of the unwanted secondary waves were captured. From the film, still images were taken to show the actual free water elevation during a certain time that may be interesting.

5.1.3. RESULTS

In this section the results found from the first order physical wave generation experiment are given. The complete wave profile, wave height, and spectral analysis will only be given for four of the tested wave conditions, Case 2, Case 9, Case 11, and Case 14. The complete results of the remaining cases are found in Appendix C.

5.1.3.1. Wave Profile

Figure 5.12, Figure 5.13, Figure 5.14 and Figure 5.15 show the resulting free surface elevation time series at each wave gauge for Case 2, Case 9, Case 11, and Case 14, respectively. From them we may see how the wave profile evolves as the wave propagates along the wave flume. The time series for the wave gauges located furthest from the mean paddle position may be shorter due to reflection, as discussed in Section 5.1.2.2.

For Case 2, we may see that the wave profile changes significantly as the wave propagates through the wave flume. The wave profile at wave gauge WG0 shows there is a secondary crest to the right of the primary crest, at wave gauge WG2 the secondary crest is at the trough of the wave profile, and at wave gauge WG4 the secondary crest is not very well discerned. For Case 9, the wave profile does not change significantly as the wave propagates. A secondary crest may be seen at wave gauge WG0 and WG1, but it is not recognizable in the other wave gauges. For Case 11 and Case 14 the wave profile does not change as the wave propagates, and there is no discernible secondary crest.

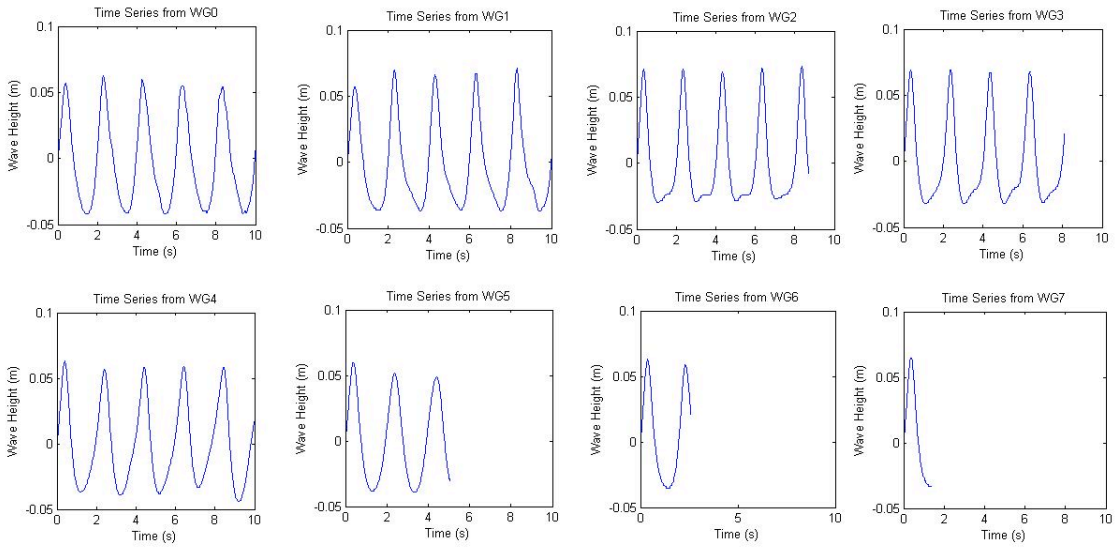

Figure 5.12. Utilized free surface elevation time series of Case 2.

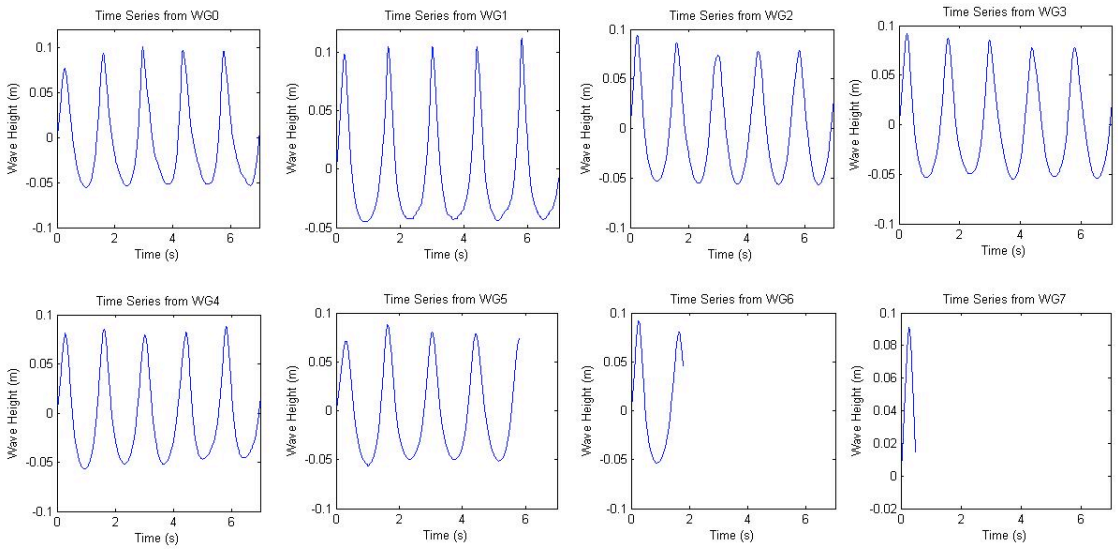

Figure 5.13. Utilized free surface elevation time series of Case 9.

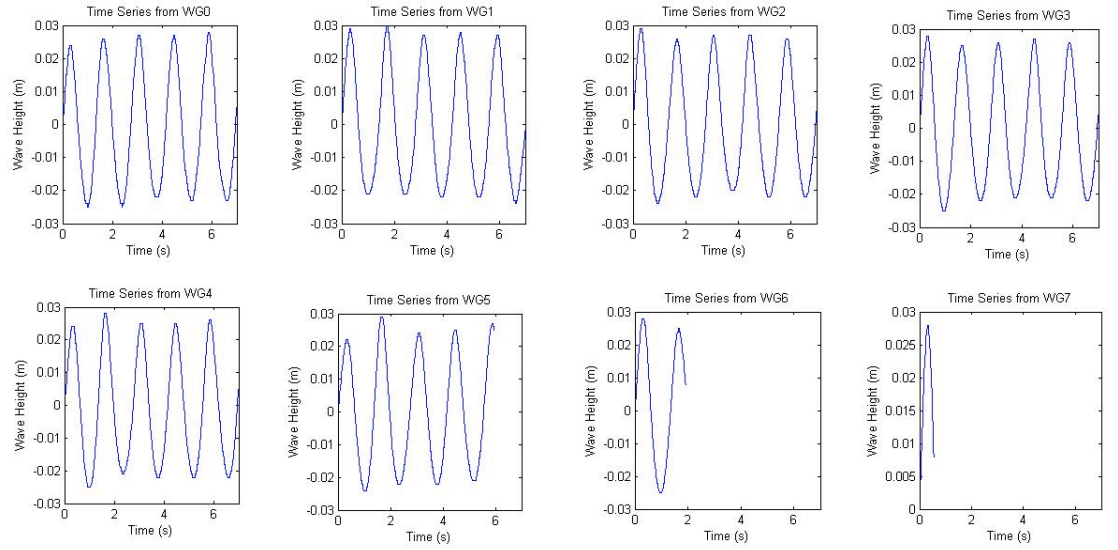

Figure 5.14. Utilized free surface elevation time series of Case 11.

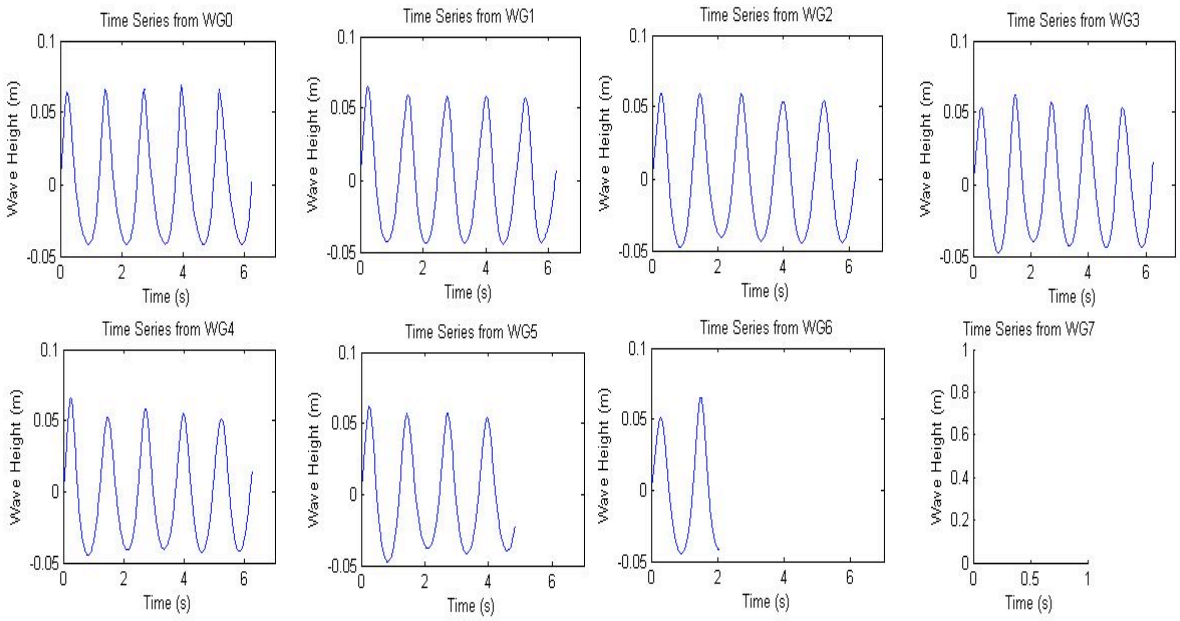

Figure 5.15. Utilized free surface elevation time series of Case 14.

5.1.3.2. Wave Height

The wave height found from the zero upcrossing method at each wave gauge, the generated wave height (the average), and the ratio between the generated wave height and the expected wave height for the wave conditions of Set 1 are summarized in Table 5.4, and for the wave conditions of Set 2 in Table 5.5. All the wave heights are given in meters.

From these tables we may see that the wave height does not remain constant as the wave travels along the wave flume, it varies. In some cases this variation is larger than other cases. Also, we find that the generated wave height differs from the expected wave height, in some cases slightly more than others. For Set 1 the average generated wave height to expected wave height ratio is 0.8286, with the maximum being 0.8740 and the minimum being 0.7110. For Set 2 the average ratio is 0.8495, with the maximum being 0.9290 and the minimum being 0.7762.

Table 5.4. Wave height recorded at each wave gauge, average, and ratio of obtained wave height to expected wave height for Set 1.

Case	WG0	WG1	WG2	WG3	WG4	WG5	WG6	WG7	Avg.	H/H_{exp}
1	0.1373	0.1543	0.1504	0.1487	0.1308	0.1213	0.1330	-	0.1394	0.8712
2	0.0994	0.1030	0.0992	0.1003	0.0972	0.0945	0.0980	-	0.0988	0.8233
3	0.0836	0.0830	0.0820	0.0810	0.0792	0.0790	0.0810	-	0.0813	0.8126
4	0.0478	0.0462	0.0460	0.0450	0.0460	0.0450	0.0460	-	0.0460	0.7667
5	0.0226	0.0220	0.0212	0.0210	0.0205	0.0210	0.0210	-	0.0213	0.7110
6	0.0858	0.0880	0.0854	0.0820	0.0824	0.0817	0.0830	0.0820	0.0838	0.8378
7	0.0478	0.0488	0.0484	0.0480	0.0478	0.0480	0.0480	0.0490	0.0482	0.8037
8	0.0232	0.0234	0.0230	0.0233	0.0230	0.0227	0.0230	0.0240	0.0232	0.7730
9	0.1462	0.1470	0.1378	0.1366	0.1338	0.1315	0.1460	-	0.1398	0.8740
10	0.0878	0.0857	0.0852	0.0844	0.0832	0.0815	0.0910	-	0.0855	0.8555
11	0.0500	0.0500	0.0490	0.0486	0.0480	0.0473	0.0530	-	0.0494	0.8235
12	0.0238	0.0238	0.0236	0.0238	0.0232	0.0228	0.0240	0.0260	0.0239	0.7958
13	0.1465	0.1322	0.1322	0.1302	0.1266	0.1300	0.1350	-	0.1332	0.8328
14	0.1082	0.1034	0.1016	0.0998	0.0988	0.1013	0.0960	-	0.1013	0.8442
15	0.0887	0.0882	0.0854	0.0852	0.0828	0.0835	0.0855	-	0.0856	0.8562
16	0.0520	0.0528	0.0514	0.0508	0.0490	0.0502	0.0500	-	0.0509	0.8481
17	0.0255	0.0262	0.0252	0.0254	0.0250	0.0250	0.0260	0.0260	0.0255	0.8512
18	0.0892	0.0878	0.0856	0.0842	0.0840	0.0818	0.0800	-	0.0847	0.8466
19	0.0630	0.0616	0.0604	0.0592	0.0586	0.0588	0.0660	-	0.0611	0.8727
20	0.0854	0.0832	0.0838	0.0814	0.0786	0.0790	0.0757	-	0.0810	0.8102
21	0.0713	0.0700	0.0684	0.0682	0.0678	0.0668	0.0680	-	0.0686	0.8579
22	0.0540	0.0522	0.0514	0.0508	0.0500	0.0498	0.0474	0.0465	0.0503	0.8377
23	0.0448	0.0448	0.0436	0.0432	0.0422	0.0424	0.0414	0.0420	0.0430	0.8610
24	0.0356	0.0340	0.0315	0.0320	0.0297	0.0292	0.0282	0.0272	0.0309	0.7737

Table 5.5. Wave height recorded at each wave gauge, average, and ratio of obtained wave height to expected wave height for Set 2.

Case	WG0	WG1	WG2	WG3	WG4	WG5	WG6	WG7	Avg.	H/H_{exp}
25	0.0656	0.0708	0.0678	0.0670	0.0640	0.0635	0.0620	-	0.0658	0.8773
26	0.0412	0.0430	0.0432	0.0428	0.0414	0.0410	0.0400	-	0.0418	0.8361
27	0.0194	0.0200	0.0200	0.0200	0.0200	0.0193	0.0185	0.0180	0.0194	0.7762
28	0.0698	0.0673	0.0644	0.0670	0.0653	0.0650	0.0620	-	0.0658	0.8774
29	0.0442	0.0438	0.0434	0.0434	0.0424	0.0422	0.0410	0.0390	0.0424	0.8486
30	0.0214	0.0225	0.0214	0.0214	0.0212	0.0207	0.0200	0.0190	0.0210	0.8385
31	0.0643	0.0625	0.0630	0.0632	0.0618	0.0604	0.0615	0.0600	0.0621	0.8278
32	0.0414	0.0410	0.0410	0.0414	0.0404	0.0398	0.0410	0.0400	0.0407	0.8150
33	0.0207	0.0205	0.0203	0.0203	0.0196	0.0194	0.0197	0.0200	0.0201	0.8021
34	0.0662	0.0653	0.0634	0.0656	0.0634	0.0634	0.0650	-	0.0646	0.8614
35	0.0444	0.0440	0.0426	0.0436	0.0424	0.0420	0.0435	-	0.0432	0.8646
36	0.0224	0.0228	0.0226	0.0224	0.0216	0.0216	0.0220	0.0225	0.0222	0.8895
37	0.1118	0.1288	0.1192	0.1140	0.1050	0.1100	0.1030	0.1000	0.1115	0.9290

Since the generated wave height differs from the expected wave height the wave theories that apply to the generated waves may differ from those that apply to the expected waves. Figure 5.16 and Figure 5.17 show the wave theories that apply to the generated waves, according to Le Méhauté (1976), for wave conditions of Set 1 and Set 2, respectively.

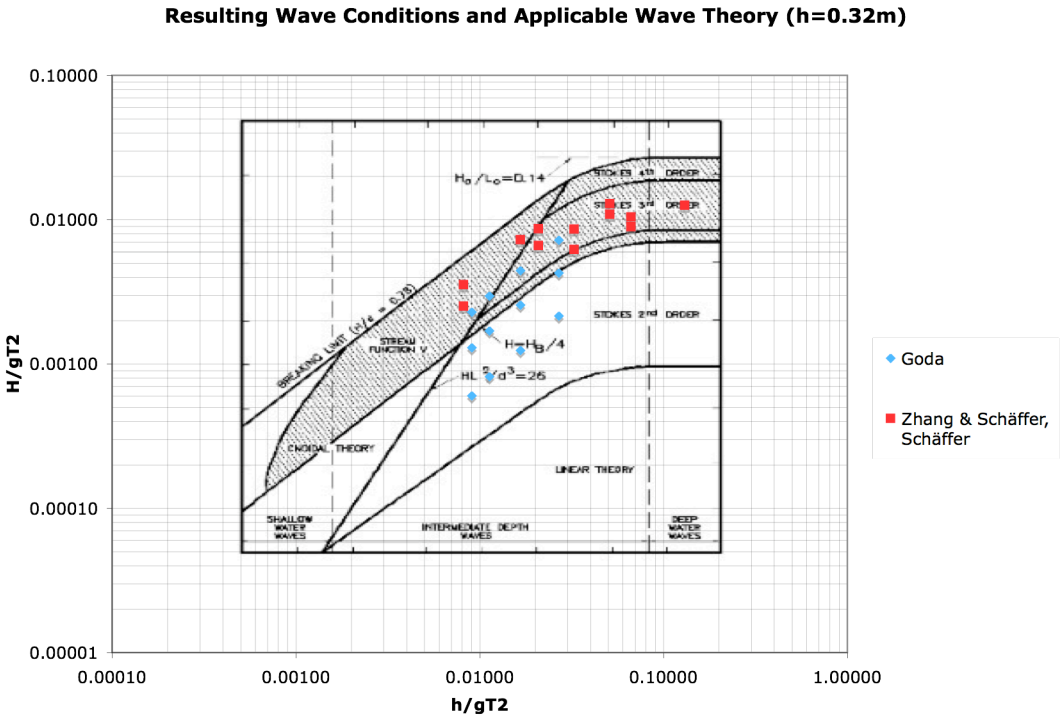

Figure 5.16. Applicable wave theories to generated waves of Set 1, in h=0.32m according to Le Méhauté (1976) (CEM, 2006).

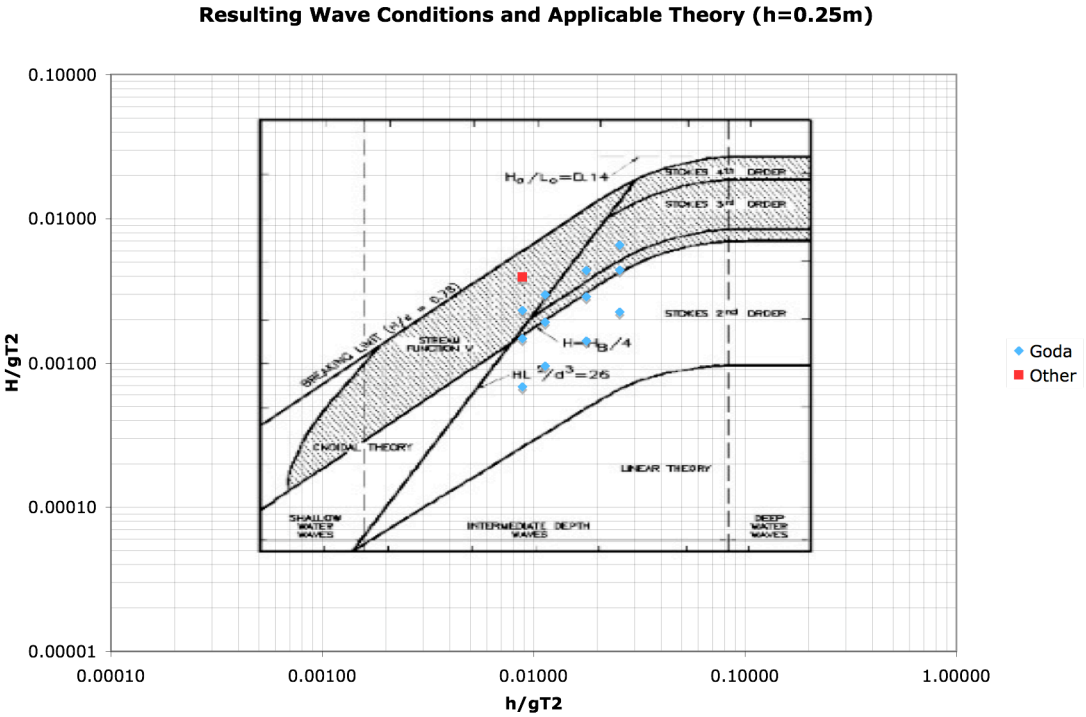

Figure 5.17. Applicable wave theories to resulting waves of Set 2, in h=0.25m according to Le Méhauté (1976) (CEM, 2006).

5.1.3.3. Harmonics

From the spectral analysis the frequency spectrums and the normalized frequency spectrums were found. Figure 5.18 and Figure 5.19, Figure 5.20 and Figure 5.21, Figure 5.22 and Figure 5.23, and Figure 5.24 and Figure 5.25 show the frequency spectrum and the normalized frequency spectrum for Case 2, Case 9, Case 11, and Case 14, respectively.

For Case 2 we find that as expected the peak frequency is about 0.5 Hz, since this is the only frequency that was to be generated. Still, we also fine a defined second peak at a frequency about twice the peak frequency, 1 Hz, and in the spectrums from wave gauge WG1, WG2, and WG3 a small third peak is also seen at a frequency about three times the peak frequency, 1.5 Hz. The normalized spectrum confirms this. The height of the second peak has a maximum of 0.2917 and an average of 0.1489. This height is gives the amount of energy found in the second peak relative to the energy in the primary peak. It may also be seen that the spectrum varies along the wave flume.

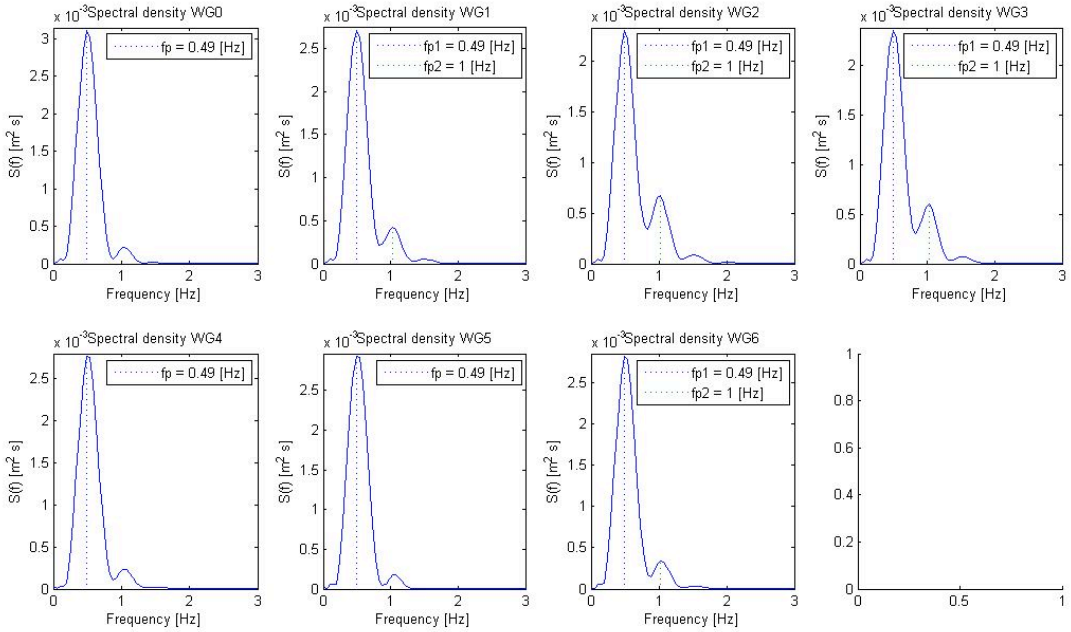

Figure 5.18. Spectral Density plot for Case 2

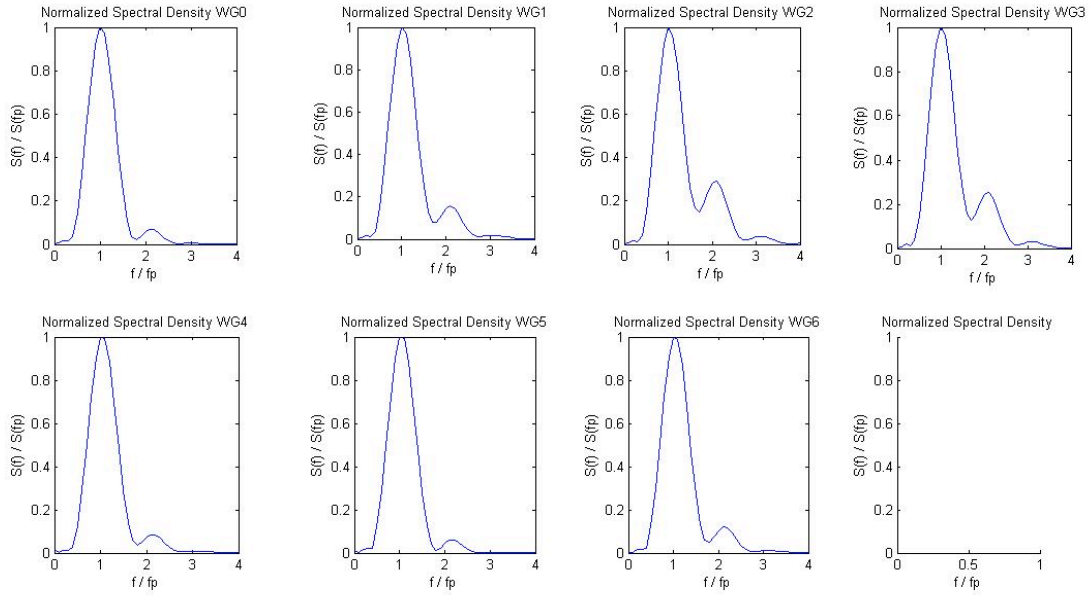

Figure 5.19. Normalized spectral density plot for Case 2.

For Case 9 we find the peak frequency at 0.73 Hz, which is close to the expected peak frequency of 0.714 Hz. Again, here we find there is a second peak at a frequency about twice the peak frequency, 1.4 Hz, and a very slight third peak may be seen at wave gauge WG1 at a frequency about three times the peak frequency, 2.1 Hz. This may also be seen in the normalized spectrum. The height of the second peak has a maximum of 0.2044 and an average of 0.1090, again in relation to the height of the primary peak.

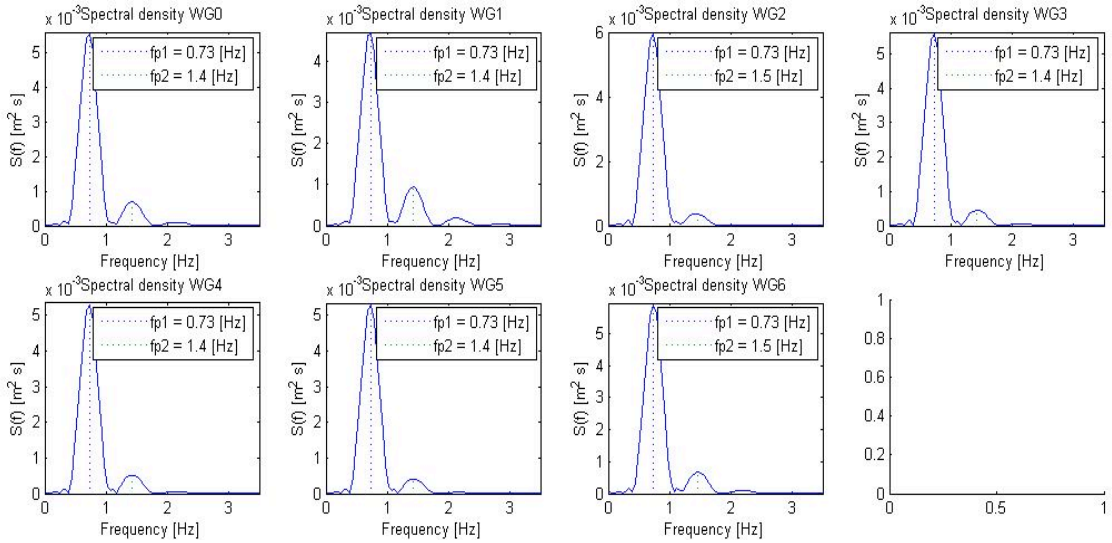

Figure 5.20. Spectral density plot for Case 9.

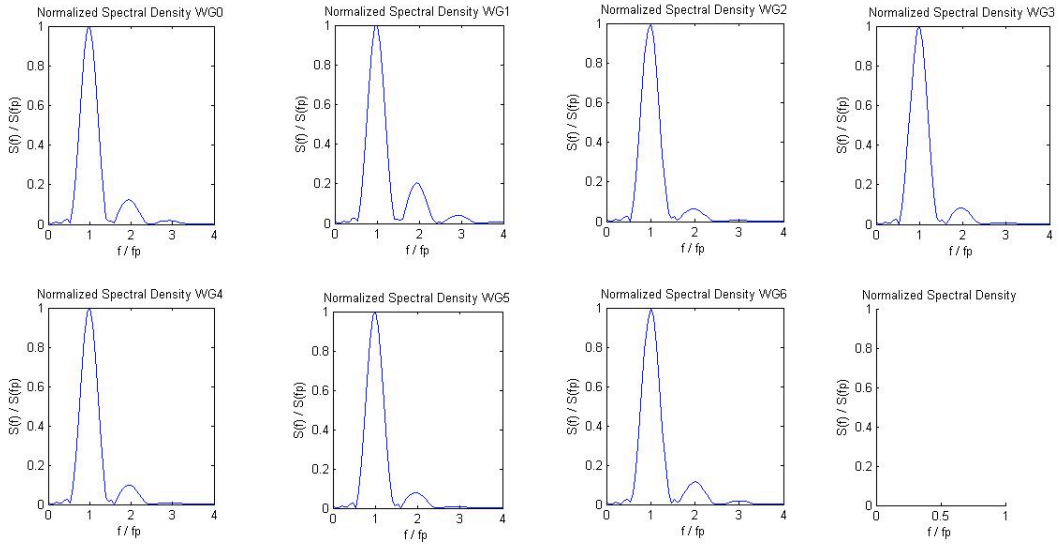

Figure 5.21. Normalized spectral density plot for Case 9.

For Case 11 we find the peak frequency at 0.73 Hz, which is close to the expected frequency 0.714 Hz. In this case there is no well-defined second peak, and the spectrum remains relatively unchanged along the wave flume.

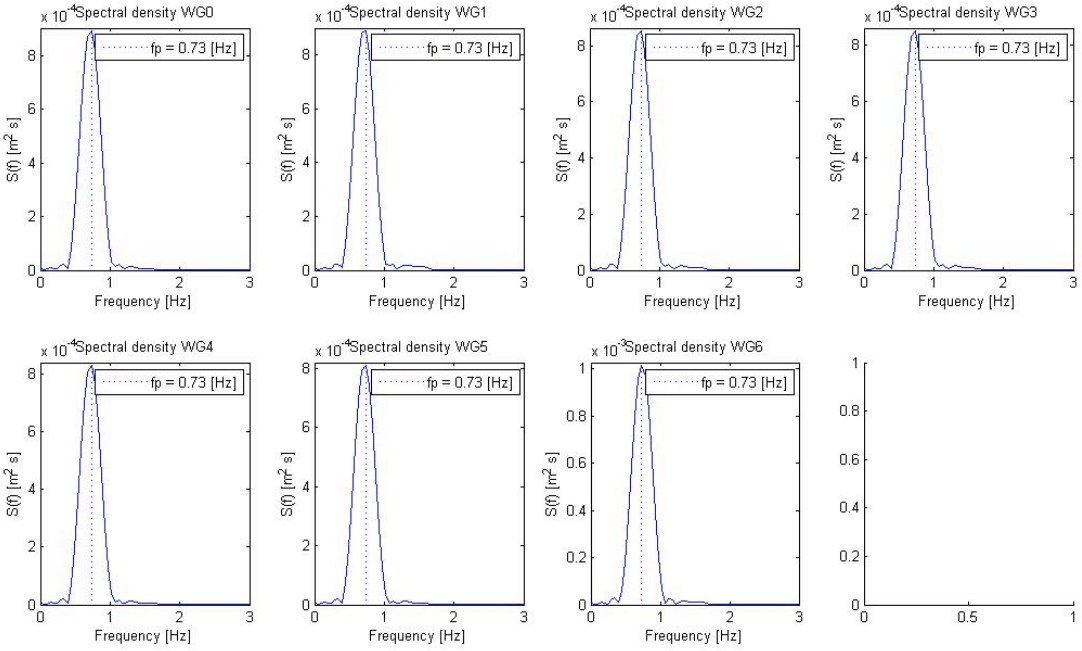

Figure 5.22. Spectral density plot for Case 11.

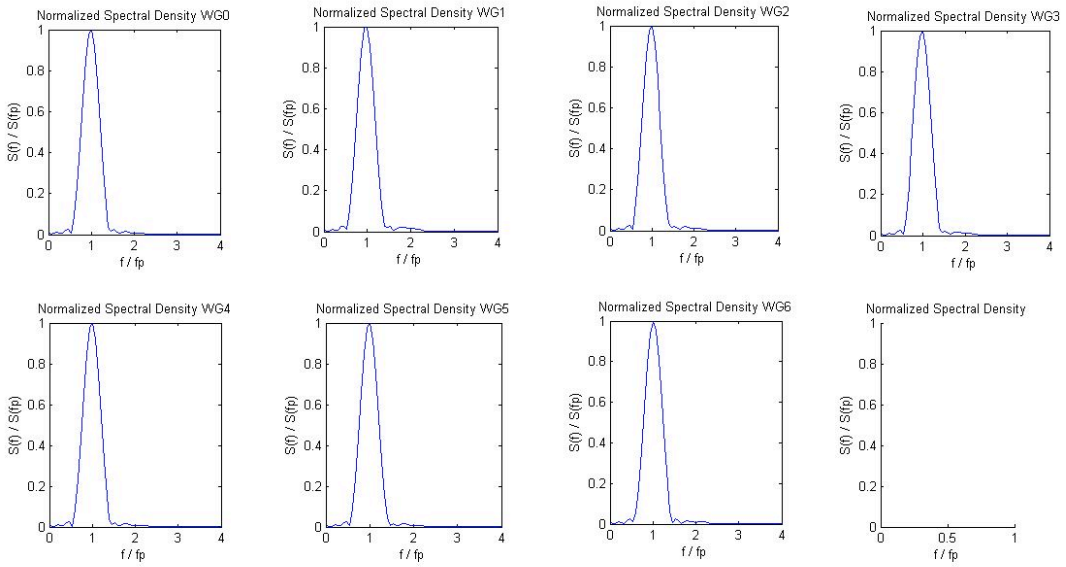

Figure 5.23. Normalized spectral density plot for Case 11.

For Case 14 the peak frequency found varied at each wave gauge, but was either 0.78 Hz or 0.83 Hz, which is close to the expected value of 0.8 Hz. Here there is also a small second peak at a frequency about twice the peak frequency, 1.6 Hz. This may also be seen in the normalized spectrum. The height of the second peak has a maximum of 0.0753 and an average of 0.0395.

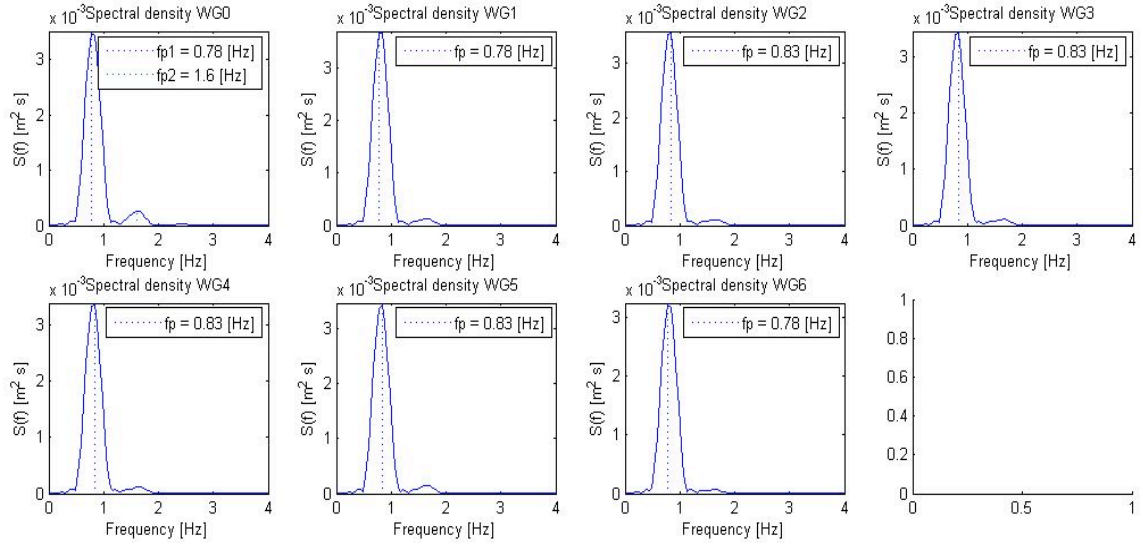

Figure 5.24. Spectral density plot for Case 14.

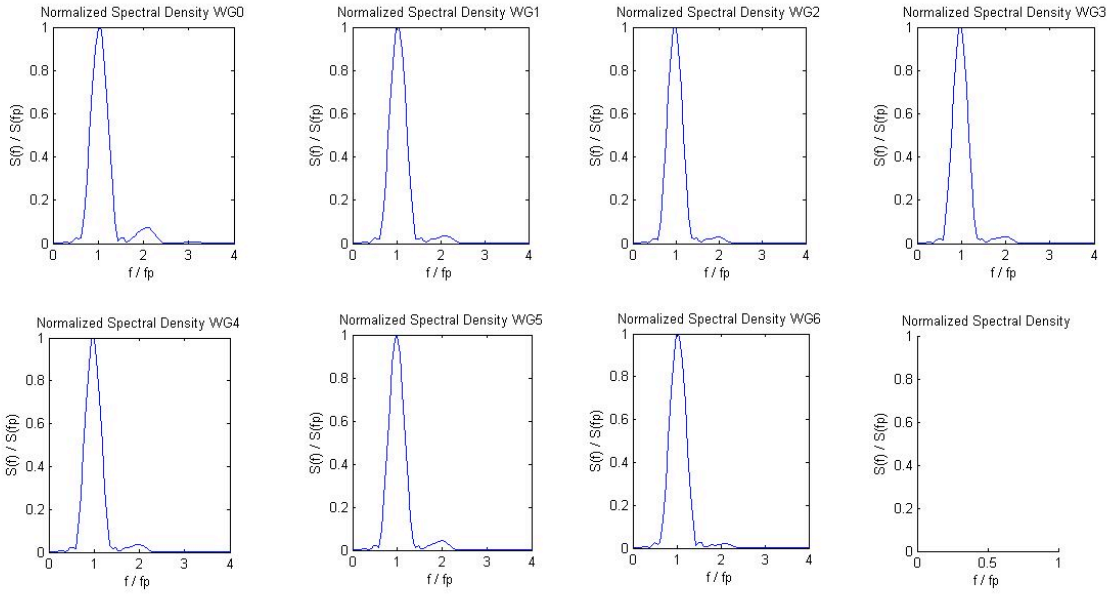

Figure 5.25. Normalized spectral density plot for Case 14.

The height of the second peak at each wave gauge, and the average of these, for each of the tested wave conditions are summarized in Table 5.6 for Set 1, and Table 5.7, for Set 2.

Table 5.6. Height of normalize secondary peak recorded at each wave gauge, and average for Set 1.

Case	WG0	WG1	WG2	WG3	WG4	WG5	WG6	WG7	Avg.
1	0.1203	0.2930	0.5119	0.4328	0.1259	0.0815	0.1997	-	0.2522
2	0.0698	0.1573	0.2917	0.2556	0.0855	0.0607	0.1216	-	0.1489
3	0.0502	0.1166	0.1561	0.1256	0.0358	0.0519	0.0965	-	0.0904
4	0.0197	0.0374	0.0553	0.0512	0.0247	0.0252	0.0459	-	0.0371
5	0.0138	0.0136	0.0158	0.0160	0.0160	0.0129	0.0249	-	0.0161
6	0.0557	0.1296	0.0552	0.0356	0.0732	0.0887	0.0567	0.0467	0.0677
7	0.0191	0.0376	0.0303	0.0217	0.0267	0.0350	0.0248	0.0191	0.0268
8	0.0093	0.0141	0.0170	0.0141	0.0117	0.0153	0.0128	0.0103	0.0131
9	0.1241	0.2044	0.0621	0.0812	0.0977	0.0787	0.1148	-	0.1090
10	0.0449	0.0489	0.0524	0.0396	0.0315	0.0308	0.0357	-	0.0405
11	0.0102	0.0200	0.0165	0.0156	0.0125	0.0103	0.0137	-	0.0141
12	0.0030	0.0086	0.0081	0.0064	0.0056	0.0051	0.0070	0.0063	0.0063
13	0.1259	0.1317	0.0679	0.0710	0.0737	0.0753	0.0489	-	0.0849
14	0.0753	0.0372	0.0310	0.0330	0.0353	0.0442	0.0208	-	0.0395
15	0.0752	0.0409	0.0237	0.0245	0.0234	0.0260	0.0250	-	0.0341
16	0.0329	0.0234	0.0087	0.0096	0.0076	0.0091	0.0062	-	0.0139
17	0.0132	0.0116	0.0045	0.0032	0.0043	0.0033	0.0055	0.0027	0.0060
18	0.0375	0.0377	0.0272	0.0195	0.0226	0.0204	0.0114	-	0.0252
19	0.0098	0.0093	0.0094	0.0104	0.0098	0.0109	0.0116	-	0.0102
20	0.0155	0.0199	0.0304	0.0213	0.0242	0.0319	0.0197	-	0.0233
21	0.0212	0.0211	0.0144	0.0175	0.0162	0.0179	0.0183	-	0.0181
22	0.0125	0.0123	0.0135	0.0105	0.0100	0.0103	0.0110	0.0122	0.0115
23	0.0049	0.0063	0.0084	0.0088	0.0094	0.0086	0.0077	0.0075	0.0077
24	0.0253	0.0230	0.0248	0.0211	0.0118	0.0212	0.0142	0.0175	0.0199

Table 5.7. Height of normalized secondary peak recorded at each wave gauge, and average for Set 2.

Case	WG0	WG1	WG2	WG3	WG4	WG5	WG6	WG7	Avg.
25	0.0611	0.1828	0.1331	0.0696	0.0393	0.0890	0.0858	-	0.0944
26	0.0255	0.0641	0.0734	0.0498	0.0183	0.0392	0.0431	-	0.0448
27	0.0101	0.0195	0.0244	0.0234	0.0097	0.0133	0.0169	0.0140	0.0164
28	0.0739	0.1168	0.0299	0.0578	0.0841	0.0512	0.0484	-	0.0660
29	0.0325	0.0531	0.0178	0.0286	0.0429	0.0250	0.0309	0.0218	0.0316
30	0.0118	0.0215	0.0094	0.0112	0.0175	0.0127	0.0140	0.0123	0.0138
31	0.0391	0.0233	0.0260	0.0311	0.0288	0.0266	0.0295	0.0223	0.0283
32	0.0138	0.0098	0.0113	0.0145	0.0134	0.0121	0.0130	0.0101	0.0123
33	0.0064	0.0034	0.0049	0.0051	0.0048	0.0041	0.0051	0.0050	0.0049
34	0.0361	0.0385	0.0212	0.0219	0.0217	0.0243	0.0280	-	0.0274
35	0.0108	0.0133	0.0083	0.0106	0.0092	0.0108	0.0120	-	0.0107
36	0.0037	0.0050	0.0034	0.0049	0.0037	0.0046	0.0038	0.0031	0.0040
37	0.1210	0.4318	0.3041	0.1773	0.0745	0.2561	0.2015	0.1542	0.2151

Since the secondary wave generation is related to the relative depth, as discussed in Section 2.2, Figure 5.26 shows how the height of the second peak varies with respect to the relative depth. We may see that as the relative depth decreases the height of the second peak, and therefore the issue with the unwanted secondary waves, increases. Also, for a given relative depth the height of the second peak is not the same for every case. For a given relative depth, the height of the second peak is larger when the wave height, and therefore the wave steepness, is larger. At a relative depth of below 0.15 the height of the second peak increases considerable. At a relative depth above 0.15 the height of the second peak does not change considerable. For all the cases with a relative depth larger than 0.16 the height of the second peak was less than 0.035.

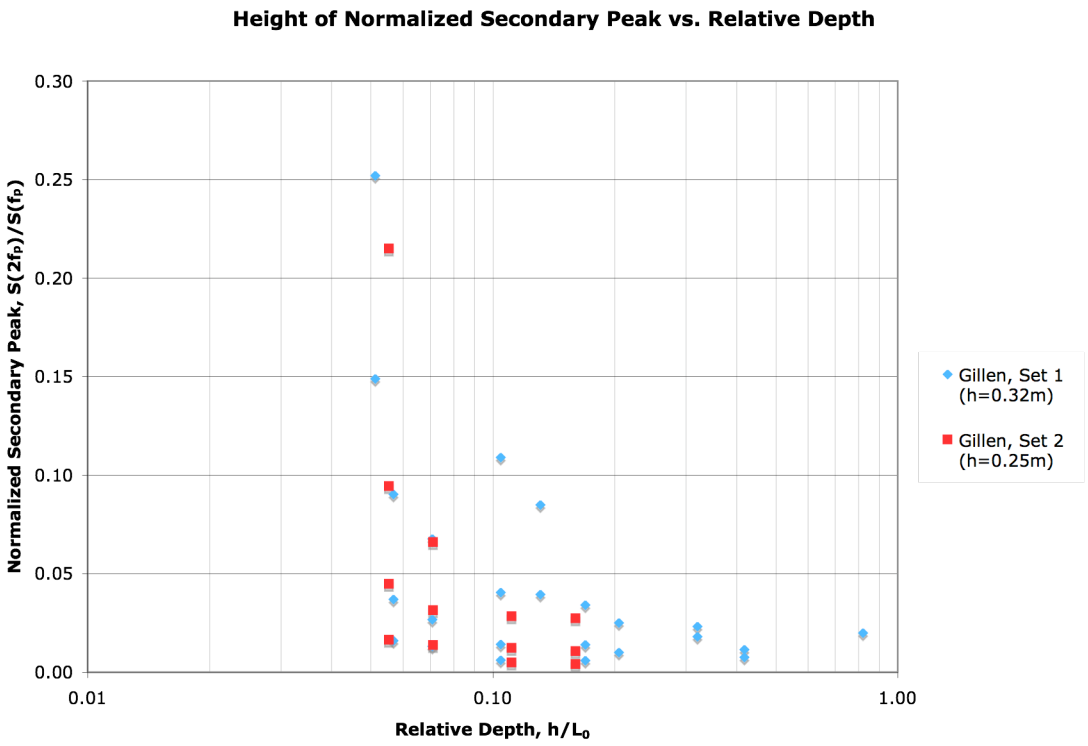

Figure 5.26. Plot of the height of the normalized secondary peak vs. the relative depth.

Figure 5.27 shows the relationship between the Ursell number, U_R, and the height of the second peak. The Ursell number is used as a measure of the nonlinearity of a wave. From this figure we may see that the height of the second peak increases exponentially as the nonlinearity of the generated wave increases.

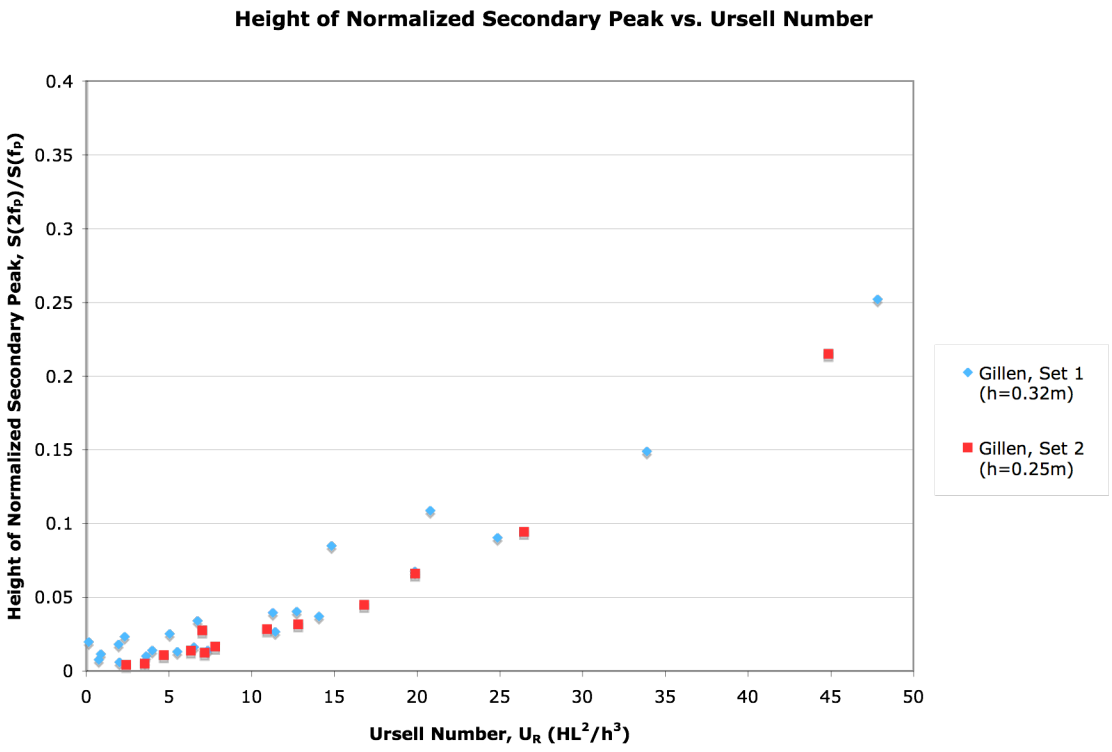

Figure 5.27. Plot of the height of the normalized secondary peak vs. the Ursell number.

5.2. NUMERICAL WAVE GENERATION

In this section al the details of the numerical wave generation simulation are given, from the simulation set-up, to the data analysis, and finally the results.

5.2.1. SIMULATION SET-UP

In this section all the considerations taken for the first order numerical wave generation simulation will be discussed. First, the selection of the wave conditions to be tested. Next, the required paddle motion to achieve these wave conditions, and how it was obtained. Finally, the means used to record and obtain the data from the simulation.

5.2.1.1. Wave Conditions

Since the CIEMito wave flume could not be used to test the second order wavemaker theory, the PFEM numerical wave flume was used to simulate the CIEMito

wave flume. In order to know if the second order wavemaker theory would reduce the appearance of the secondary unwanted waves it is necessary to have a reference result by using first order wavemaker theory. Because of this the selected wave conditions to be simulated were some of the conditions that were tested in the CIEMito wave flume, described in Section 5.1.1.1.

The simulation of different wave conditions could take some time, so it was decided to only use four of the 37 wave conditions presented in Section 5.1.1.1 to be simulated. Since, depending on the water depth the relationship between the simulated waves and the actual waves could change, it was decided to use only one water depth in the simulations, 0.32 m. The only second order wavemaker theory that was adapted to the CIEMito wave flume was Madsen's second order wavemaker theory. As discussed in Section 3.3 the applicability of the this wavemaker theory is limited to waves that meet the following criteria

$$\frac{H \cdot L^2}{h^3} < \frac{8 \cdot \pi^2}{3} \qquad \text{Equation 5.10}$$

where H is the wave height, L is the wavelength, and h is the water depth.

Not all of the wave conditions tested in the CIEMito wave flume meet the criteria given by Madsen. It was decided to use two cases where the Madsen criterion was met, and in the physical wave generation experiment had a significant generation of unwanted secondary waves. The other two cases chosen do not comply with the Madsen criterion, but have the worst contamination by the unwanted waves. The purpose of this is to find if Madsen's second order wavemaker theory will still help reduce the appearance of the unwanted waves even if the wave conditions were outside of the application range.

As seen from the results of the physical wave generation experiment, Section 5.1.3, the actual wave height generated by the CIEMito wave flume is less than the expected wave height, which is due to inefficiencies of the piston paddle. The simulated piston paddle in the PFEM numerical wave flume would not have these inefficiencies, therefore it is necessary to reduce the simulated wave height in order for the simulation to

represent what would happen in the CIEMito wave flume. It was decided to simulate a wave height that was 80% of the expected wave height.

The four wave conditions that were chosen to be simulated in the PFEM numerical wave flume are shown in Table 5.8. The conditions that do not meet the criterion given by Madsen, Case 2 and Case 9, are highlighted in grey. Here T is the wave period in seconds, H is the expected wave height in meters, H_{sim} is the simulated wave height in meters, h is the water depth in meters, L_0 is the wavelength in meters, L_0/h is the relative water depth, and N is the number of waves to be generated.

Table 5.8. Summary of wave conditions selected to be simulated with the PFEM numerical flume.

Case	T (s)	H (m)	H_{sim} (m)	h (m)	L_0 (m)	L_0/h	N
2	2.00	0.12	0.096	0.32	6.245	0.0512	10
9	1.40	0.16	0.128	0.32	3.060	0.1046	10
11	1.40	0.06	0.048	0.32	3.060	0.1046	10
14	1.25	0.12	0.096	0.32	2.440	0.1312	10

First these selected wave conditions were simulated using first order wavemaker theory to enable the comparison with the results of tests of these wave conditions in the CIEMito wave flume.

5.2.1.2. Paddle Motion

The paddle motion used for the simulation was almost the same as the paddle motion used for the physical wave generation experiment, Section 5.1.1.2. One modification to the paddle motion had to be done; the paddle motion time series used in the physical experiment was multiplied by a factor of 0.8. This would ensure that the wave height being simulated was 80% of the expected wave height, as desired.

5.2.1.3. PFEM Model Settings

The PFEM numerical wave flume was set up to simulate the CIEMito wave flume. For this the same dimensions as the CIEMito wave flume, length, height, and

width of the wave flume, were used. The absorption system at the end of the flume was simulated using a higher viscosity fluid (Oliveira *et al*., 2009b). The time step used was of 0.001 s, and the grid size used was of 0.01 m. The information of the free surface elevation was obtained for every time step at a distance from the mean paddle position equal to the distance given to the wave gauges in the CIEMito wave flume. This way the results could be compared. In addition to the free surface elevation data the position, the pressure, and the velocity of each particle were found at a time step of 0.2 s.

5.2.2. DATA ANALYSIS

The data collected from the simulation in the PFEM numerical wave flume were treated and analyzed similarly to the data of the physical wave generation experiment, Section 5.1.2, but with some variations due to the nature of the data.

The time series obtained was already a free water elevation time series. Still, being a numerical mode, sometimes the frequency of the data is more, or less, than expected. In order to ensure the free water elevation time series was given at a frequency of 100 Hz the raw time series was ran through a software that will linearly interpolate between to points if data is missing, or eliminate a data point if it has a higher frequency.

The selection of the time series followed the same considerations expressed in Section 5.1.2.2, ensuring the beginning of the time series did not consider either the ramp waves or the dissipated waves, and ending after five wave periods or when the reflection would arrive. The data was then normalized to eliminate any linear trends.

Finally, the generated wave height was calculated and the spectral analysis performed, just as discussed in Section 5.1.2.4 and Section 5.1.2.5, respectively.

5.2.3. RESULTS

In this section all the results found from the first order wave generation simulation are given.

5.2.3.1. Wave Profile

Figure 5.28, Figure 5.29, Figure 5.30 and Figure 5.31 show the resulting free surface elevation time series at each wave gauge for Case 2, Case 9, Case 11, and Case 14, respectively.

For Case 2, we may see that the wave profile changes significantly as the wave propagates through the wave flume. The wave profile at wave gauge WG1 shows there is a secondary crest to the right of the primary crest, at wave gauge WG2 the secondary crest is at the trough of the wave profile, and at wave gauge WG3 the secondary crest is to the left of the primary crest. For Case 9 a secondary crest may be seen but it is not very well defined. The wave profile also changes as the wave propagates. For Case 11 and Case 14 the wave profile does not change noticeably as the wave propagates, and there is no discernible secondary crest.

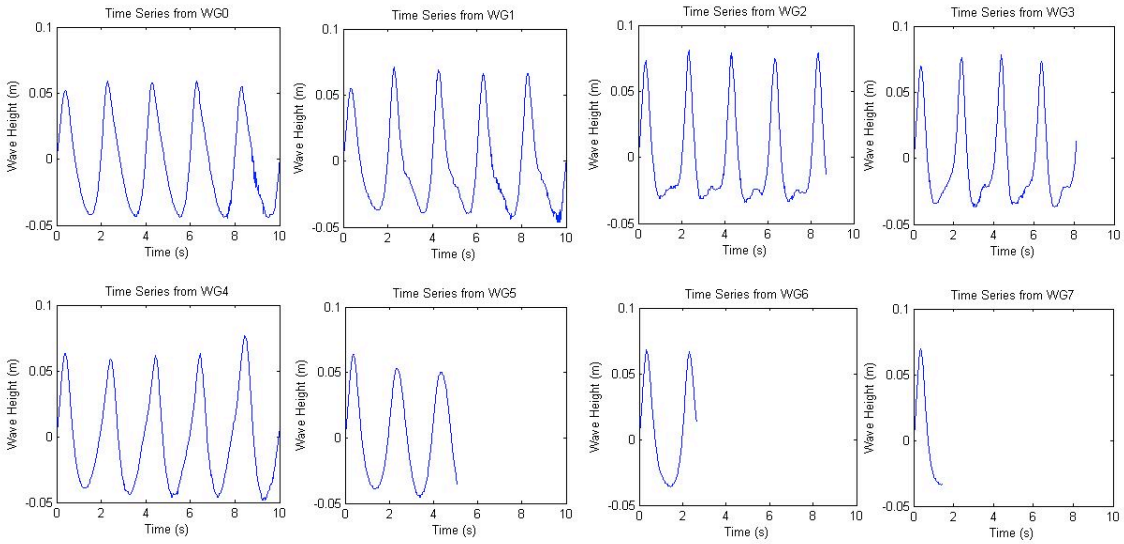

Figure 5.28. Utilized free surface elevation time series for first order simulation of Case 2.

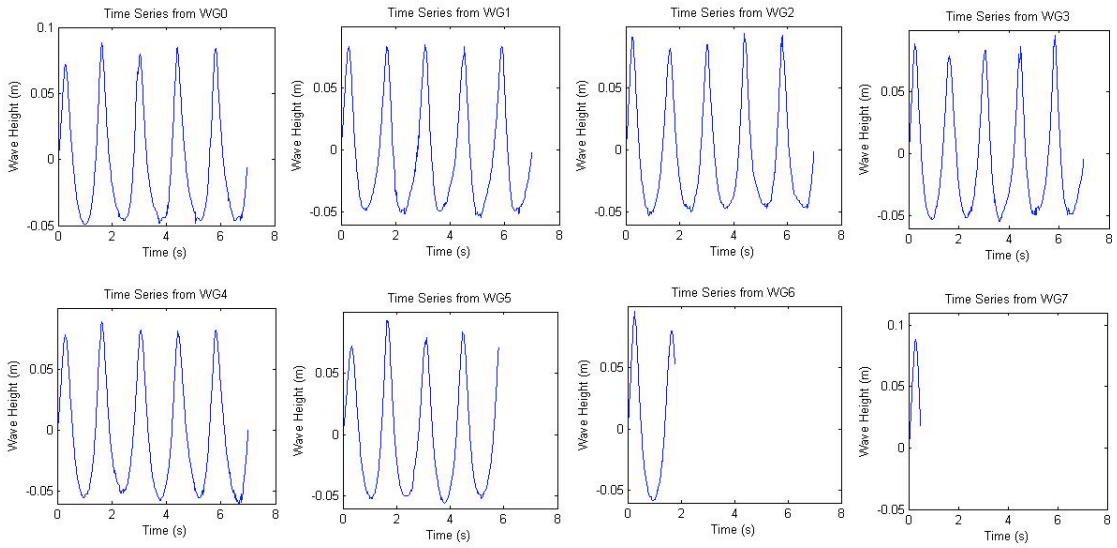

Figure 5.29. Utilized free surface elevation time series for first order simulation of Case 9.

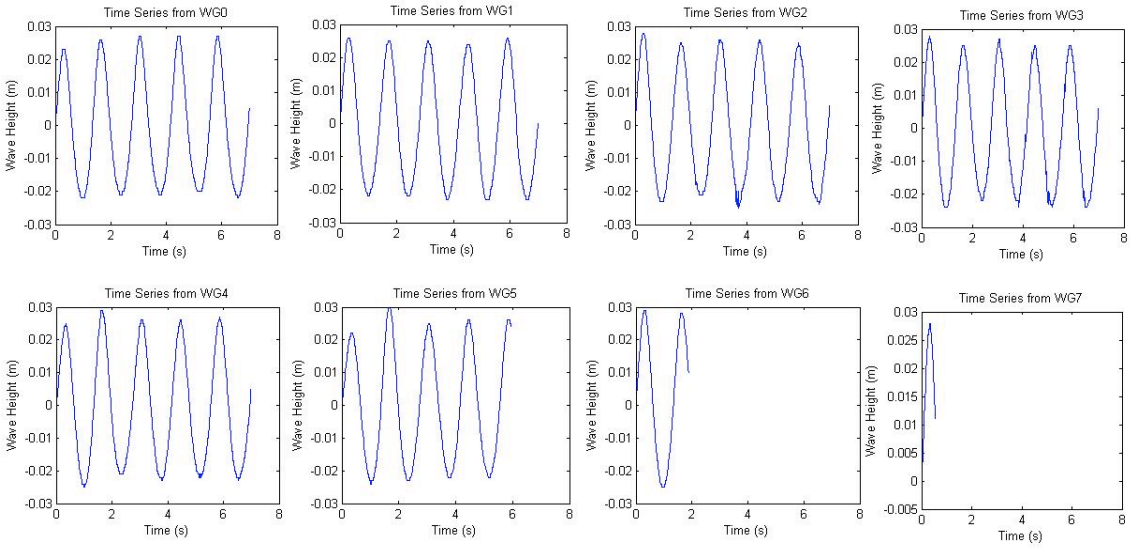

Figure 5.30. Utilized free surface elevation time series for first order simulation of Case 11.

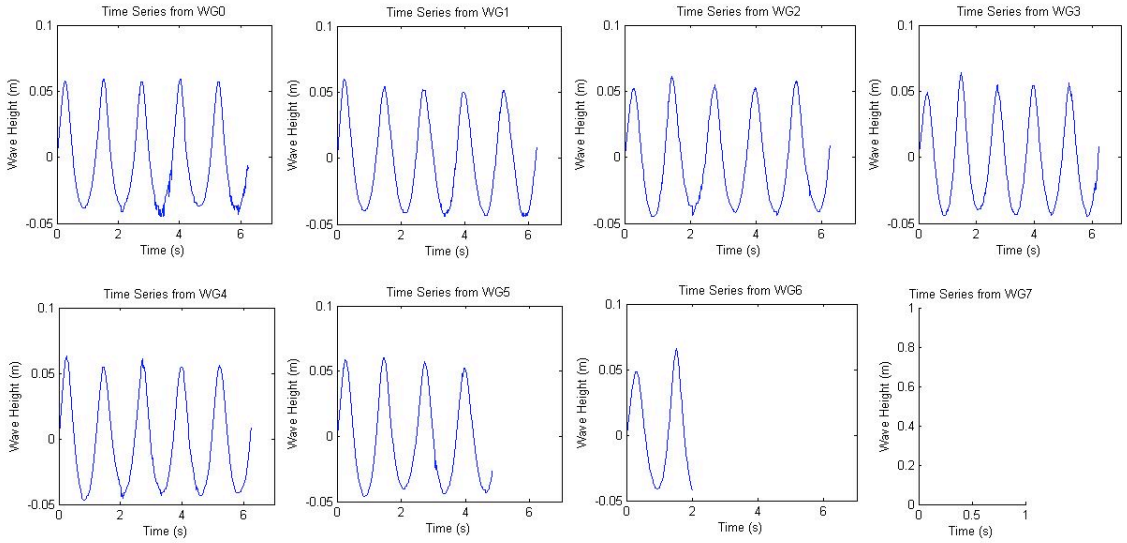

Figure 5.31. Utilized free surface elevation time series for first order simulation of Case 14.

5.2.3.2. Wave Height

The wave height found from the zero upcrossing method at each wave gauge, the generated wave height (the average), and the ratio between the generated wave height and the simulated wave height are summarized in Table 5.9. All the wave heights are given in meters.

From this table we see that the wave height varies as the wave travels along the wave flume. Also, we find that the generated wave height differs from the simulated wave height. The resulting wave height is larger than the simulated wave height. For Case 2 this difference was the largest, and for Case 14 it was the smallest.

Table 5.9. Wave height recorded at each wave gauge, average, and ratio of obtained wave height to simulated wave height.

Case	WG0	WG1	WG2	WG3	WG4	WG5	WG6	WG7	Avg.	H/H_{sim}
2	0.0918	0.1053	0.1093	0.1103	0.1094	0.1005	0.1040	-	0.1044	1.0872
9	0.1290	0.1084	0.1372	0.1365	0.1370	0.1345	0.1540	-	0.1338	1.0453
11	0.0472	0.0475	0.0492	0.0496	0.0494	0.0485	0.0540	-	0.0493	1.0280
14	0.0990	0.0960	0.0990	0.0990	0.1020	0.1020	0.0900	-	0.0981	1.0223

5.2.3.3. Harmonics

From the spectral analysis the frequency spectrums and the normalized frequency spectrums were found. Figure 5.32 and Figure 5.33, Figure 5.34 and Figure 5.35, Figure 5.36 and Figure 5.37, and Figure 5.38 and Figure 5.39 show the frequency spectrum and the normalized frequency spectrum for Case 2, Case 9, Case 11, and Case 14, respectively.

For Case 2 the peak frequency is 0.49 Hz, which is close to the desired 0.5 Hz. There is also a defined second peak at a frequency close to twice the peak frequency, 1 Hz, and a smaller third peak can be seen at wave gauges WG1, WG2, and WG3, which has a frequency of about three times the peak frequency, 1.5 Hz. This can also be seen in the normalized spectrum. The height of the second peak has a maximum of 0.3033 and an average of 0.1759. As stated in Section 5.1.3.3, this height gives the amount of energy that is found at the second peak relative to the energy in the primary peak. It may also be seen that the spectrum varies along the wave flume.

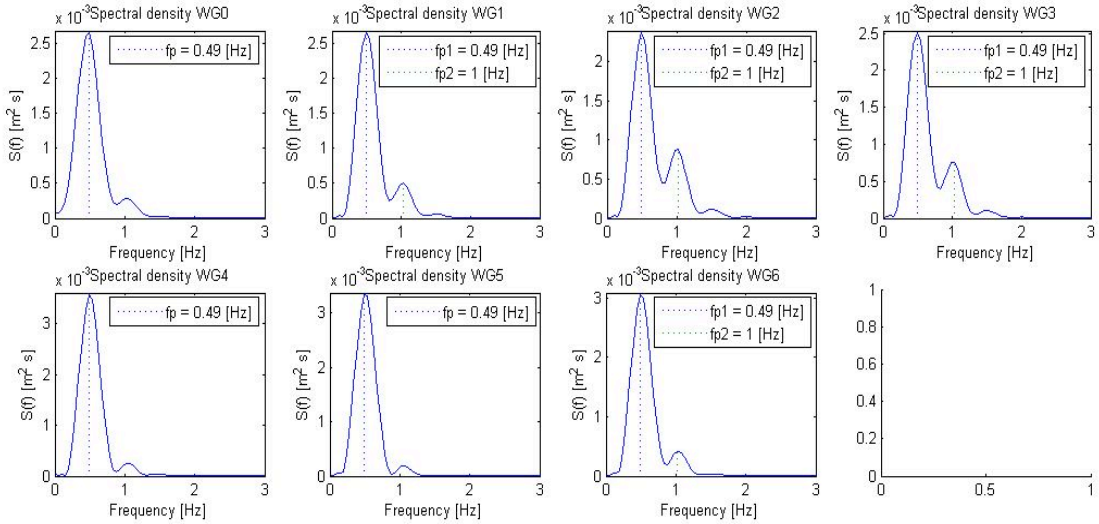

Figure 5.32. Spectral density plot for first order simulation of Case 2.

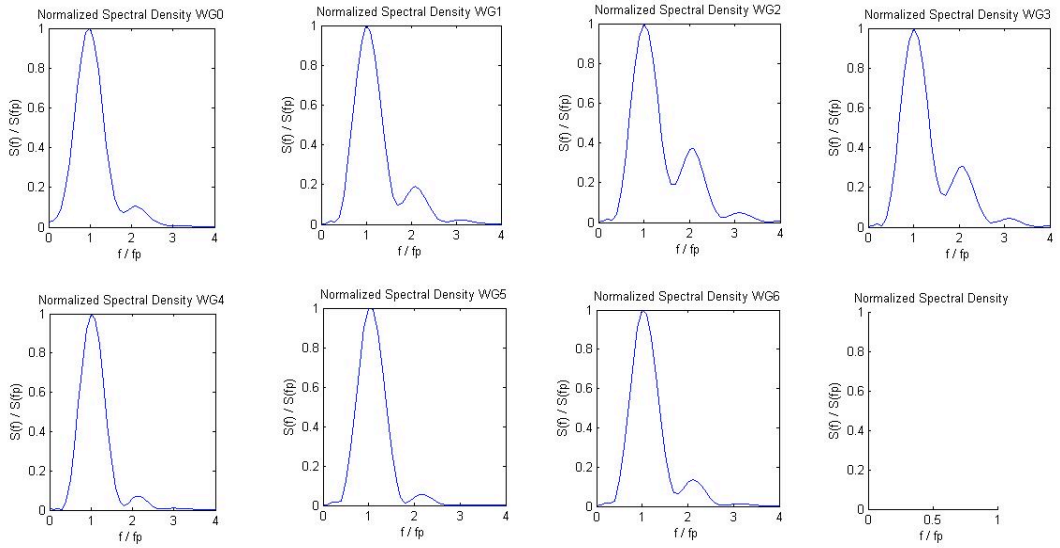

Figure 5.33. Normalized spectral density plot for first order simulation of Case 2.

From Case 9 we find the peak frequency to be 0.73 Hz, which is close to the simulated frequency of 0.714 Hz. Here there is also a second peak at about twice the peak frequency, 1.4 Hz. There is a very small third peak at about three times the peak frequency that may be seen in all the wave gauges. This is also seen in the normalized spectrum. The height of the second peak has a maximum of 0.1292 and an average of 0.1060.

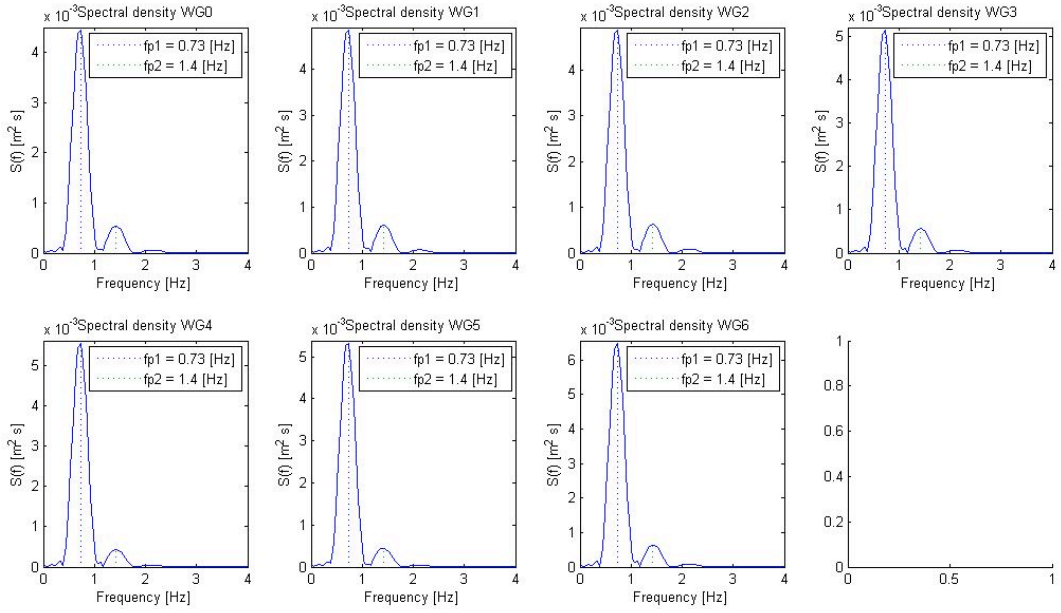

Figure 5.34. Spectral density plot for first order simulation of Case 9.

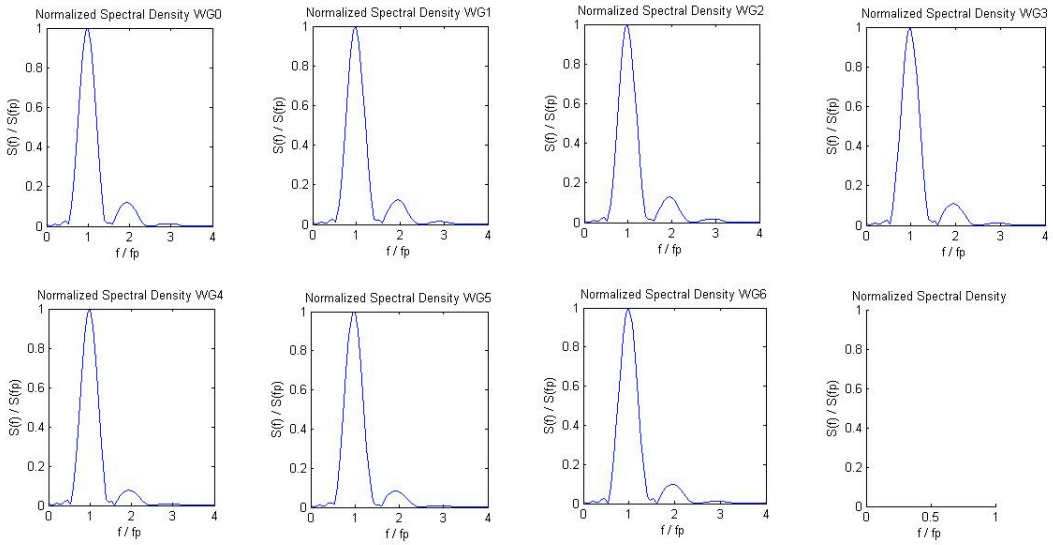

Figure 5.35. Normalized spectral density plot for first order simulation of Case 9.

For Case 11 we find a peak frequency of 0.73 Hz, which is close to the expected 0.714 Hz. There is no defined second peak in this case.

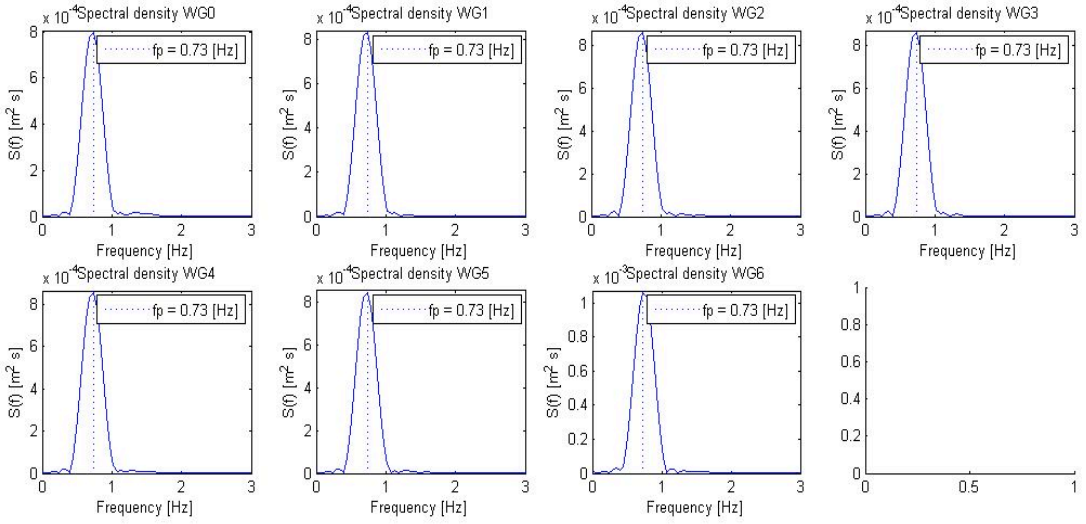

Figure 5.36. Spectral density plot for first order simulation of Case 11.

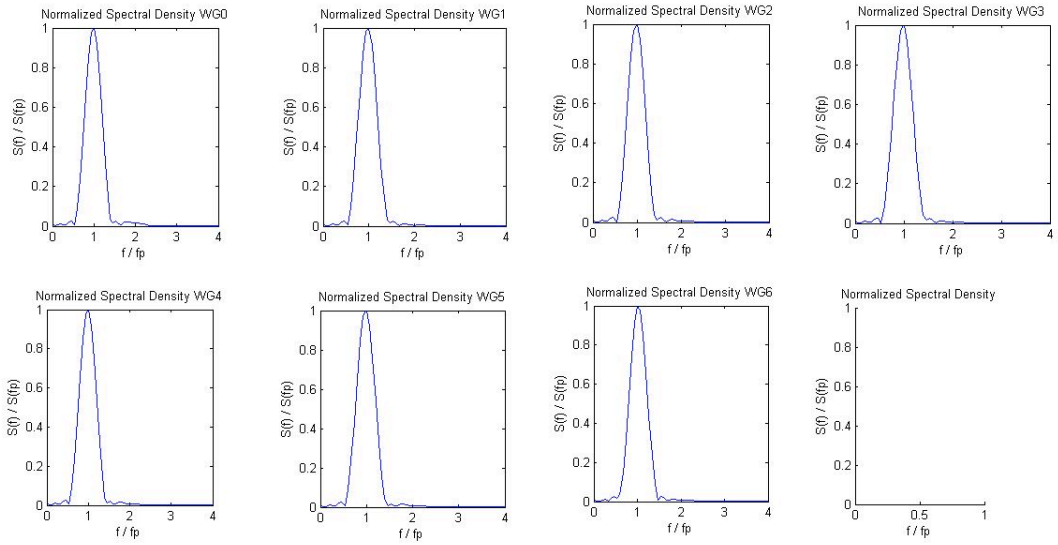

Figure 5.37. Normalized spectral density plot for first order simulation of Case 11.

For Case 14 the peak frequency found is of 0.78 Hz, except for wave gauge WG5 where it is 0.83 Hz. This peak frequency is close to the simulated frequency of 0.8 Hz. There is a small well-defined second peak at a frequency of about twice the peak frequency. This may be seen in the normalized spectrum as well. The height of the second peak has a maximum of 0.0621 and an average of 0.0372.

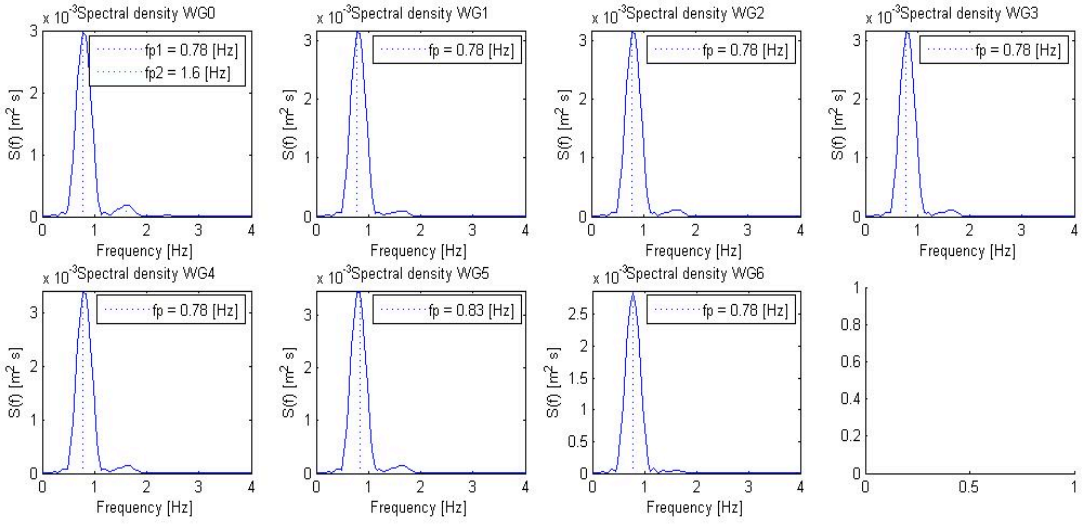

Figure 5.38. Spectral density plot for first order simulation of Case 14.

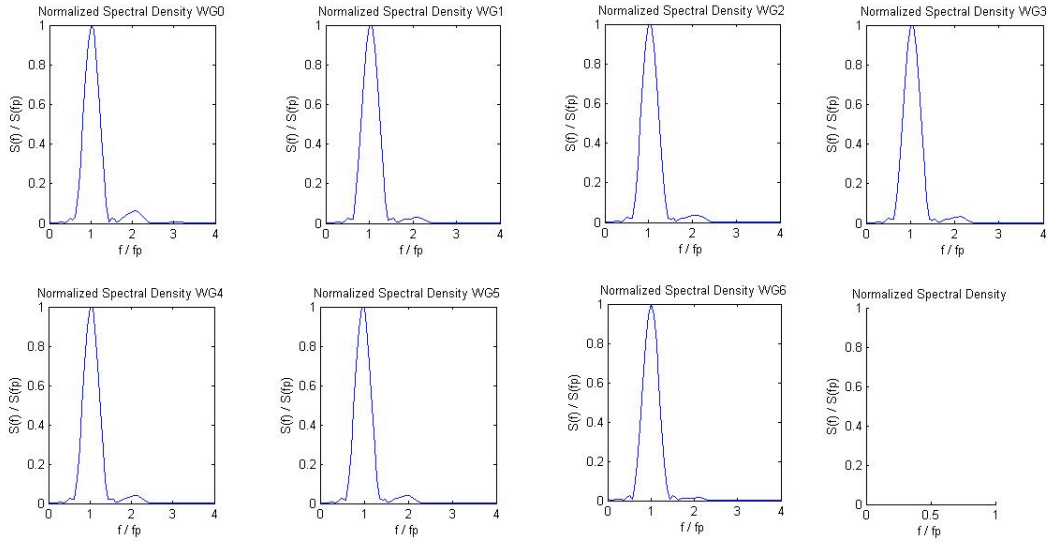

Figure 5.39. Normalized spectral density plot for first order simulation of Case 14.

The height of the second peak found at each wave gauge, and the average, for each case are summarized in Table 5.10.

Table 5.10. Height of the normalized secondary peak recorded at each wave gauge and average.

Case	WG0	WG1	WG2	WG3	WG4	WG5	WG6	WG7	Avg.
2	0.1046	0.1899	0.371	0.3033	0.0712	0.0552	0.1362	-	0.1759
9	0.1213	0.1239	0.1292	0.1094	0.077	0.0836	0.0976	-	0.1060
11	0.0201	0.0088	0.0109	0.0093	0.0127	0.0107	0.0127	-	0.0122
14	0.0621	0.031	0.0376	0.0332	0.0407	0.0406	0.0149	-	0.0372

5.3. COMPARISON OF PHYSICAL AND NUMERICAL RESULTS

In this section the results obtained from the numerical wave generation simulation will be compared to the results of the physical wave generation experiment. From this it will be seen if the PFEM numerical wave flume simulation actually represents the CIEMito wave flume.

5.3.1. WAVE PROFILE

Figure 5.40, Figure 5.41, Figure 5.42, and Figure 5.43 show the free surface elevation time series of both the physical experiment (the blue line) and the numerical simulation (the green line) of Case 2, Case 9, Case 11, and Case14, respectively. From these figures we may see that the waves simulated in the PFEM numerical model follow the waves generated in the CIEMito wave flume. There are some small differences, but overall the simulated waves have the same wave profile as the ones generated physically.

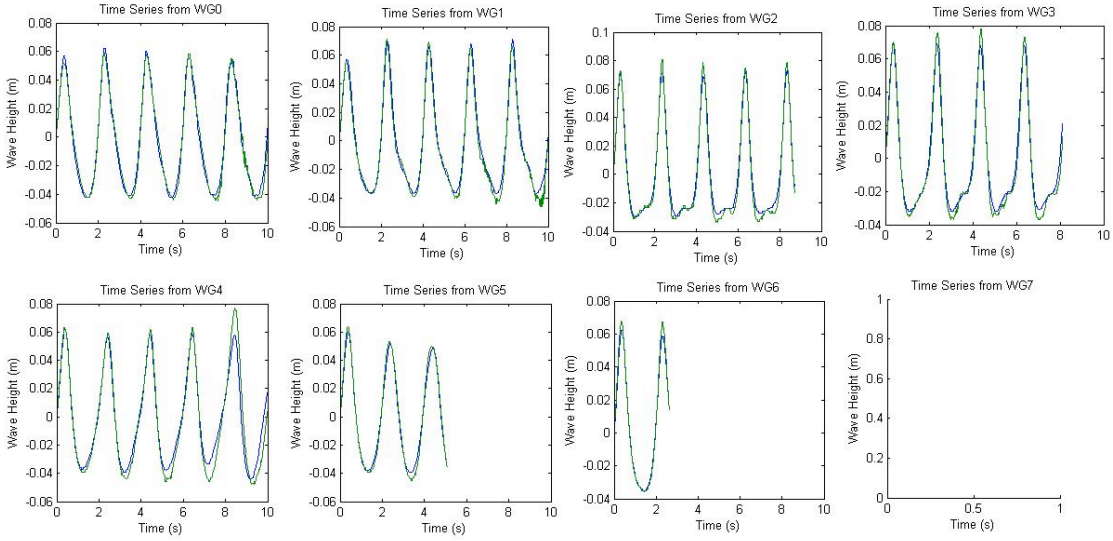

Figure 5.40. Physical (blue) and numerical (green) free surface elevation time series of Case 2.

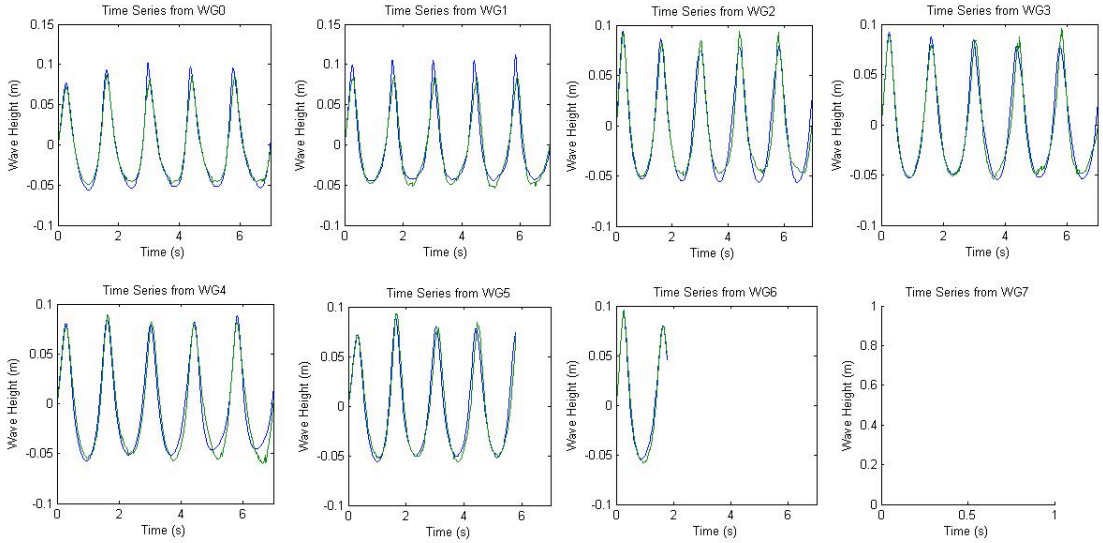

Figure 5.41. Physical (blue) and numerical (green) free surface elevation time series of Case 9.

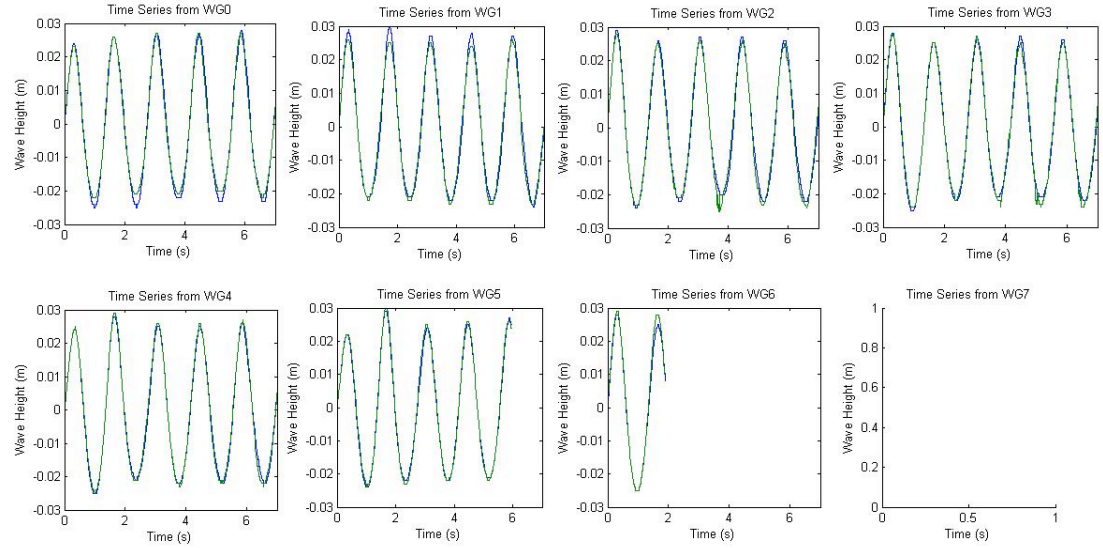

Figure 5.42. Physical (blue) and numerical (green) free surface elevation time series of Case 11.

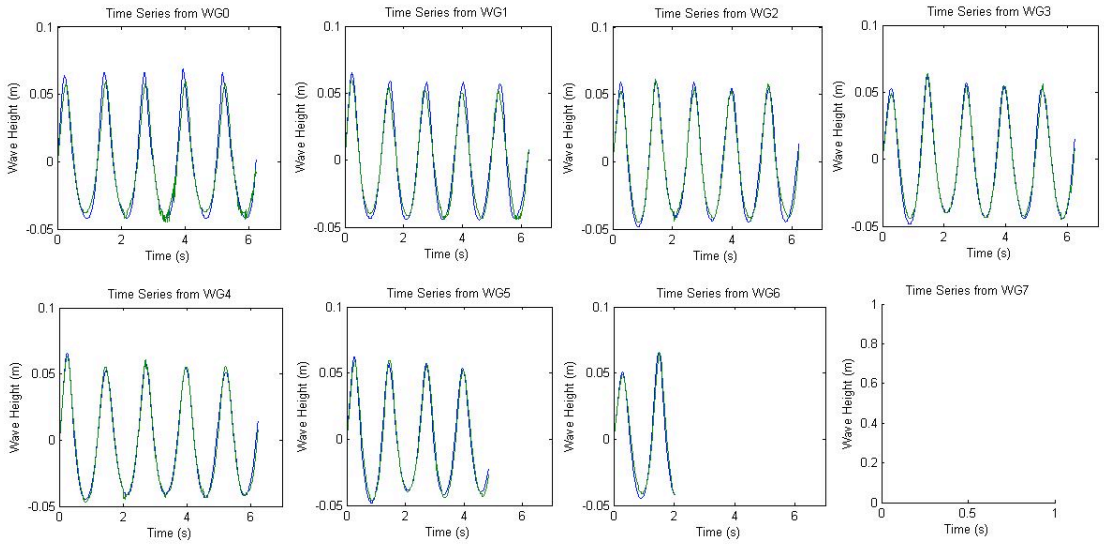

Figure 5.43. Physical (blue) and numerical (green) free surface elevation time series of Case 14.

5.3.2. WAVE HEIGHT

Table 5.11 shows a summary of the wave height found at each wave gauge, and the average wave height for both the physical wave generation experiment, and the numerical wave generation simulation. The wave heights are given in meters, and the results of the numerical simulation are highlighted in grey. From this table we may see that although the results of the simulation are not equal to the results of the physical experiment, they are very similar, and follow the same trend.

Table 5.11. Wave height recorded at each wave gauge, and the average wave height, for both the physical and numerical (highlighted in grey) wave generation test.

Case	WG0	WG1	WG2	WG3	WG4	WG5	WG6	WG7	Avg.
2	0.0994	0.1030	0.0992	0.1003	0.0972	0.0945	0.0980	-	0.0988
2	0.0910	0.1053	0.1093	0.1103	0.1094	0.1005	0.1040	-	0.1044
9	0.1462	0.1470	0.1378	0.1366	0.1338	0.1315	0.1460	-	0.1398
9	0.1290	0.1084	0.1372	0.1365	0.1370	0.1345	0.1540	-	0.1338
11	0.0500	0.0500	0.0490	0.0486	0.0480	0.0473	0.0530	-	0.0494
11	0.0472	0.0475	0.0492	0.0496	0.0494	0.0485	0.0540	-	0.0493
14	0.1082	0.1034	0.1016	0.0998	0.0988	0.1013	0.0960	-	0.1013
14	0.0990	0.0960	0.0990	0.0990	0.1020	0.1020	0.0900	-	0.0981

5.3.3. HARMONICS

Figure 5.44, Figure 5.45, Figure 5.46, and Figure 5.47 show the normalized spectrum found for both the physical experiment (the blue line) and the numerical simulation (the green line) for Case 2, Case 9, Case 11, and Case 14, respectively. Table 5.12 summarizes the height of the second peak and the average for these cases. From these figures and the table we may see that the normalized spectrums are not exactly the same, but they do have very similar results.

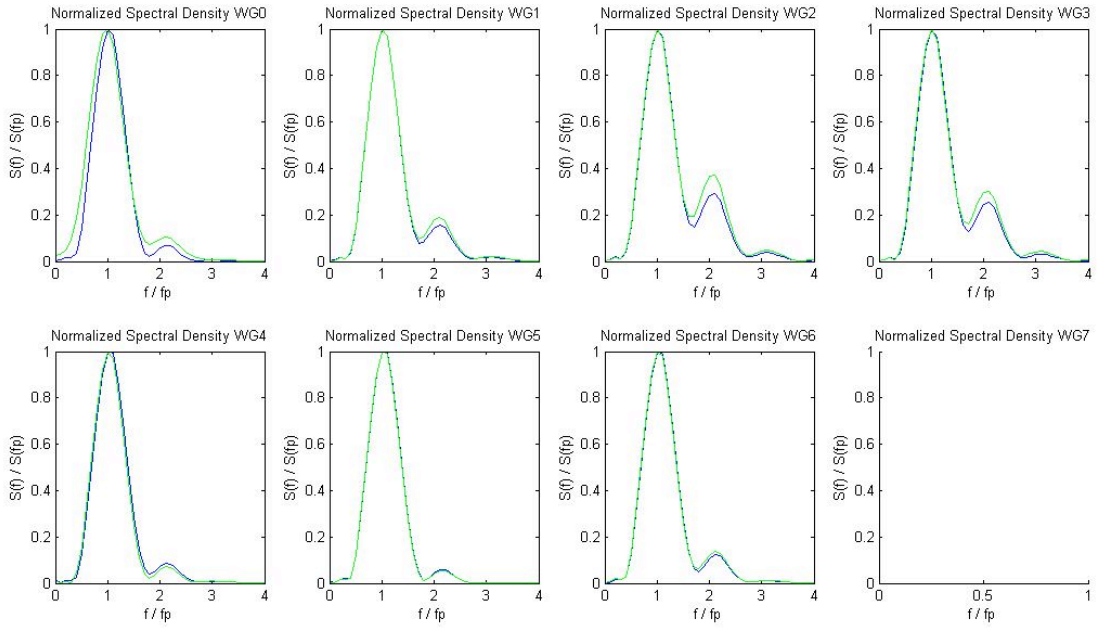

Figure 5.44. Physical (blue) and numerical (green) normalized spectral density plot of Case 2.

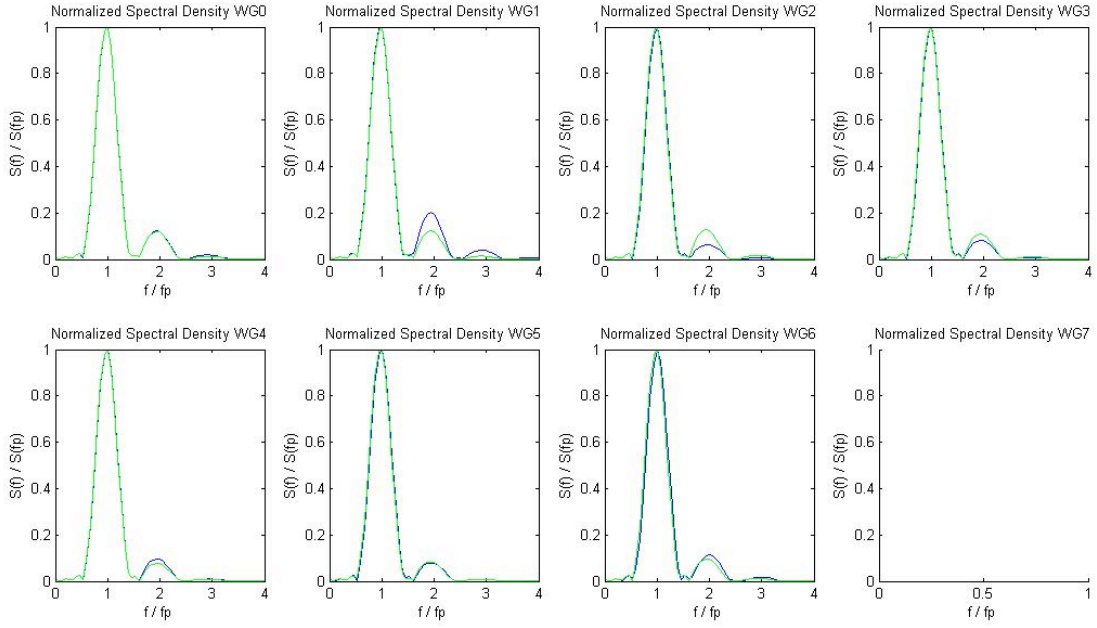

Figure 5.45. Physical (blue) and numerical (green) normalized spectral density plot of Case 9.

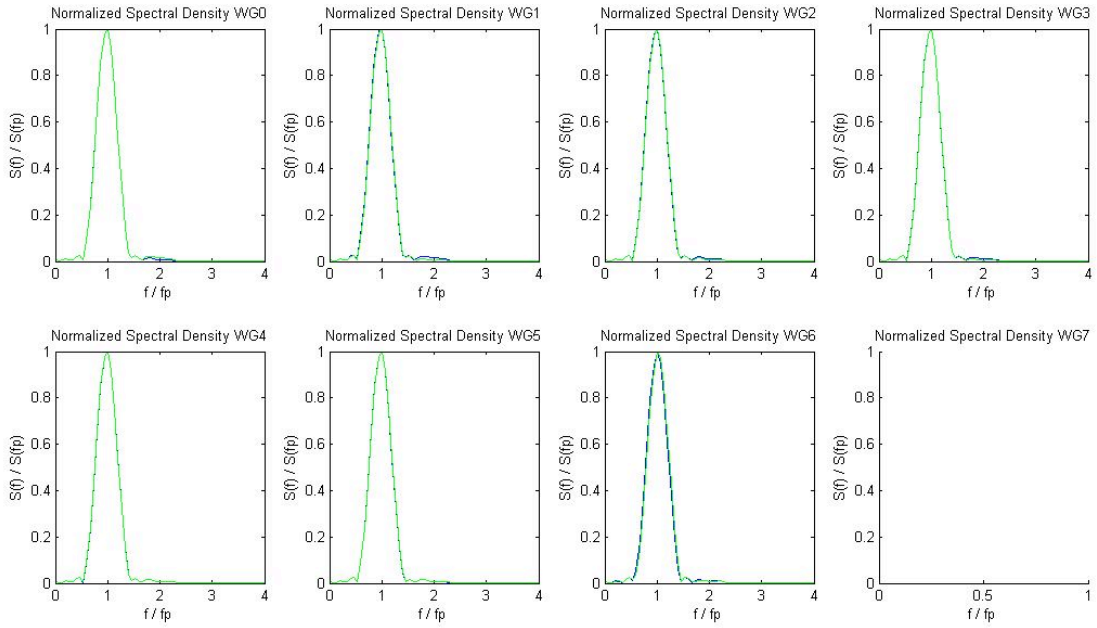

Figure 5.46. Physical (blue) and numerical (green) normalized spectral density plot of Case 11.

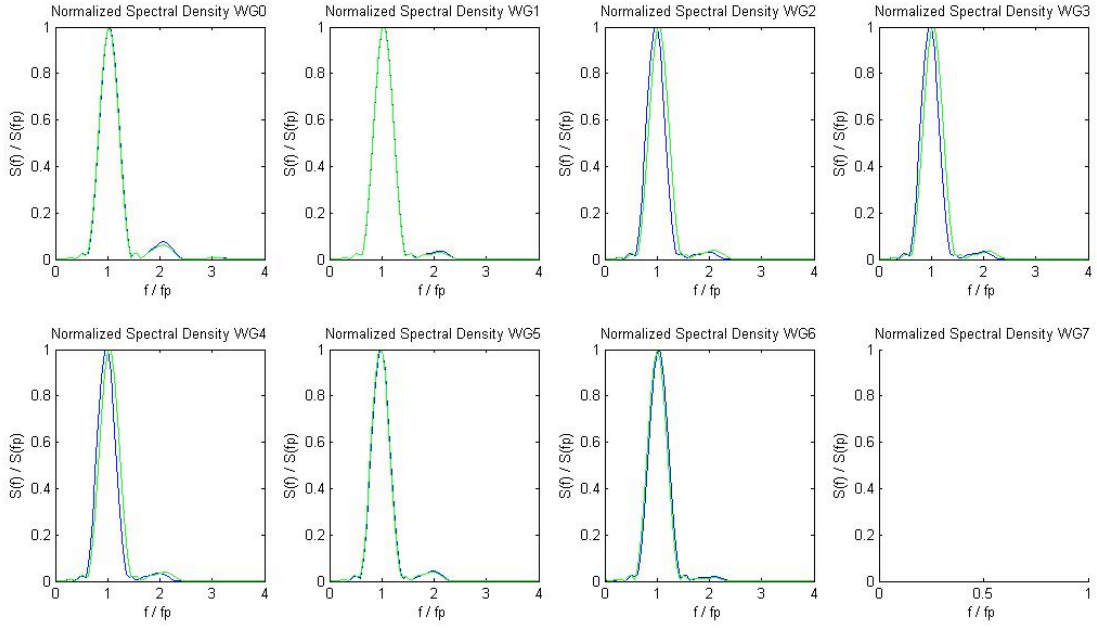

Figure 5.47. Physical (blue) and numerical (green) normalized spectral density plot of Case 14.

Table 5.12. Height of normalized secondary peak recorded at each wave gauge for the physical and the numerical (highlighted in grey) wave generation test.

Case	WG0	WG1	WG2	WG3	WG4	WG5	WG6	WG7	Avg.
2	0.0698	0.1573	0.2917	0.2556	0.0855	0.0607	0.1216	-	0.1489
2	0.1046	0.1899	0.371	0.3033	0.0712	0.0552	0.1362	-	0.1759
9	0.1241	0.2044	0.0621	0.0812	0.0977	0.0787	0.1148	-	0.1090
9	0.1213	0.1239	0.1292	0.1094	0.077	0.0836	0.0976	-	0.1060
11	0.0102	0.0200	0.0165	0.0156	0.0125	0.0103	0.0137	-	0.0141
11	0.0201	0.0088	0.0109	0.0093	0.0127	0.0107	0.0127	-	0.0122
14	0.0753	0.0372	0.0310	0.0330	0.0353	0.0442	0.0208	-	0.0395
14	0.0621	0.031	0.0376	0.0332	0.0407	0.0406	0.0149	-	0.0372

6. SECOND ORDER WAVE GENERATION EXPERIMENT

Second order wavemaker theories were developed in order to suppress the unwanted secondary waves that appear when using first order wavemaker theory. Since it was only possible to adapt Madsen's second order wavemaker theory to the CIEMito wave flume conditions, it will be this wavemaker theory that will be tested. As stated, it was not possible to test second order wavemaker theories in the CIEMito wave flume. As seen in Section 5.3, by simulating the CIEMito wave flume in the PFEM numerical wave flume it is possible to reproduce what would happen in the physical wave flume numerically.

The PFEM numerical wave flume was used to simulate the wave generation in the CIEMito wave flume using Madsen's second order wavemaker theory. This way it will be possible to find if this theory is capable of suppressing the unwanted secondary waves, and generate a stable wave profile along the flume. In this chapter all the details of the numerical wave generation simulation are given, from the simulation set-up, to the data analysis, and finally the results.

6.1. SIMULATION SET-UP

In this section all the considerations taken for the second order numerical wave generation simulation will be discussed. First, the selection of the wave conditions to be tested. Then, the required paddle motion to achieve these wave conditions, and how it was obtained. Finally, the means used to record and obtain the data from the simulation.

6.1.1. WAVE CONDITIONS

The chosen wave conditions to be simulated are the same as the ones given in Section 5.2.1.1. This will enable comparison between first and second order wave generation.

6.1.2. PADDLE MOTION

The simulated piston paddle motion was obtained from Madsen's second order wavemaker theory as described in Section 3.3. A routine as the one described in Section 3.3, which may be found in Appendix B, was used to generate the paddle motion time series. The paddle motion was found for the expected wave height, H, and the obtained time series was then multiplied by a factor of 0.8 in order to obtain the simulated wave height, H_{sim}. This was done in order to simulate the inefficiencies of the CIEMito wave flume.

Figure 6.1 shows the position of the piston paddle with respect to time for Case 2, which has an expected wave height, H, of 0.12 m, a simulated wave height, H_{sim}, of 0.096 m, and a wave period, T, of 2.0 s. As discussed in Section 3.3, the paddle motion given by Madsen's second order wavemaker theory is given by the summation of two paddle motions. A second order term, which is supposed to suppress the unwanted secondary waves, is added to the paddle motion found by the linear wavemaker theory. Figure 6.1 shows the two paddle motions that are summed, and the final resulting paddle motion given by Madsen's second order wavemaker theory.

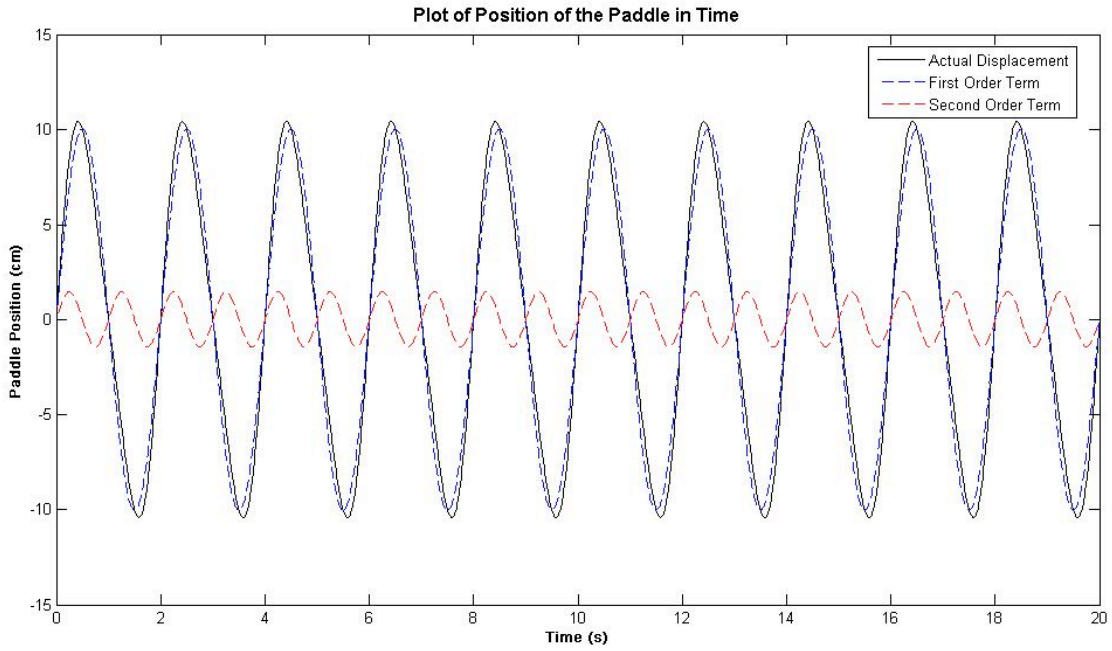

Figure 6.1. Time series of the paddle displacement to generate Case 2 using Madsen's theory.

Since this is a simulation and there is no danger of damaging a wavemaker system, then there is no need to introduce a ramp to the wavemaker motion.

6.1.3. PFEM MODEL SETTINGS

The same PFEM model settings used for the first order wave generation simulation, as described in Section 5.2.1.3, were used.

6.2. DATA ANALYSIS

The same data analysis performed to the first order numerical wave generation data, as described in Section 5.2.2, was done to the data obtained from these simulations.

6.3. RESULTS

In this section all the results found from the second order numerical wave generation simulation are given.

6.3.1. WAVE PROFILE

Figure 6.1, Figure 6.2, Figure 6.3, and Figure 6.4 show the resulting free surface elevation time series at each wave gauge for Case 2, Case 9, Case 11, and Case 14, respectively.

For Case 2 we can see that the wave profile changes as the wave travels along the wave flume. For Case 9 the wave profile also changes along the wave flume. The secondary crest in these two cases is not clearly visible. For Case 11 and Case 14 the wave profile does not change noticeably as the wave propagates, and no distinguishable secondary crest is visible.

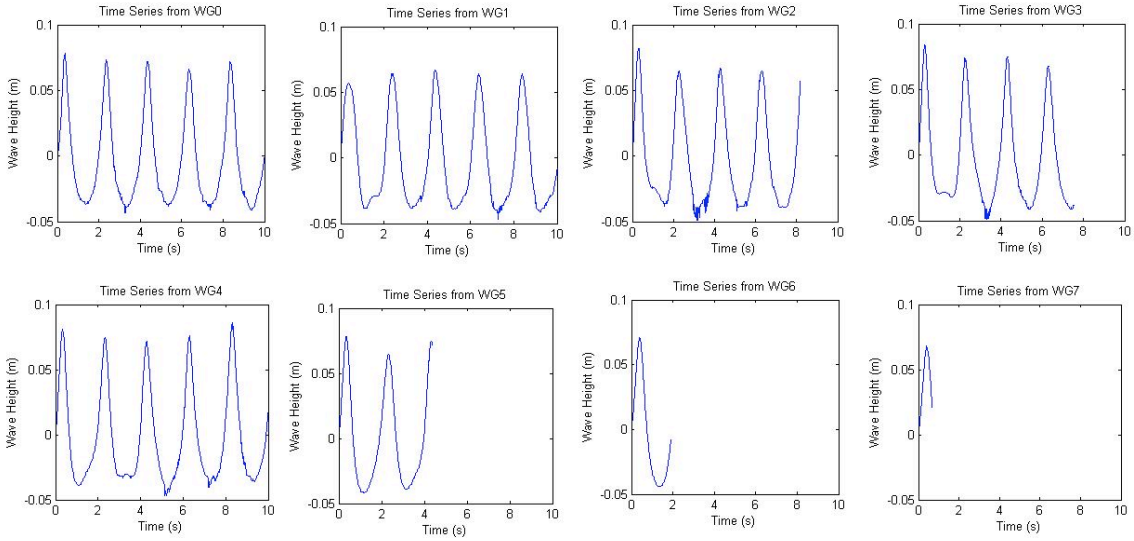

Figure 6.2. Utilized free surface elevation time series for second order Madsen simulation of Case 2.

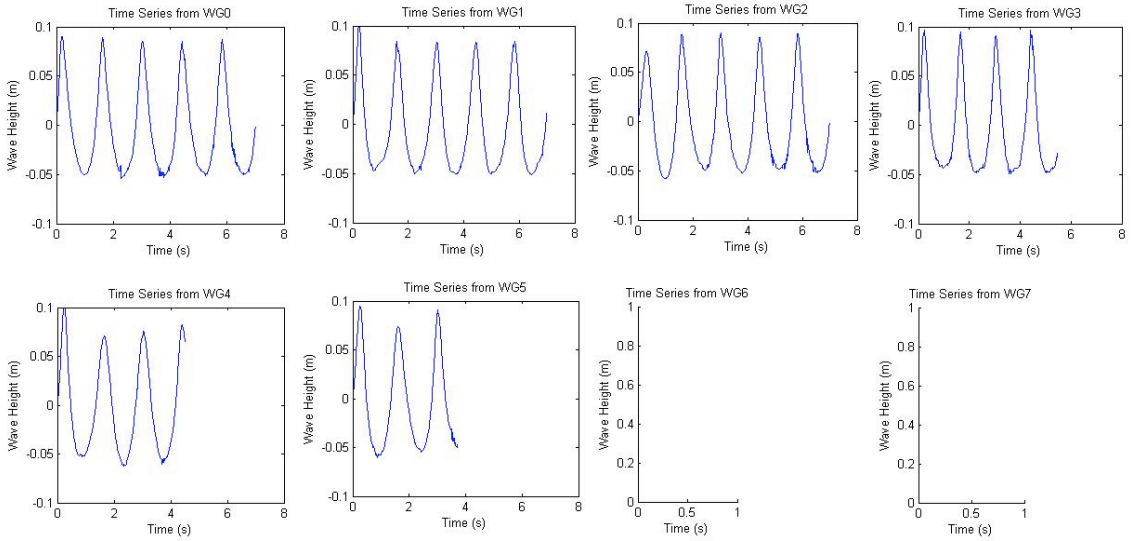

Figure 6.3. Utilized free surface elevation time series of second order Madsen simulation of Case 9.

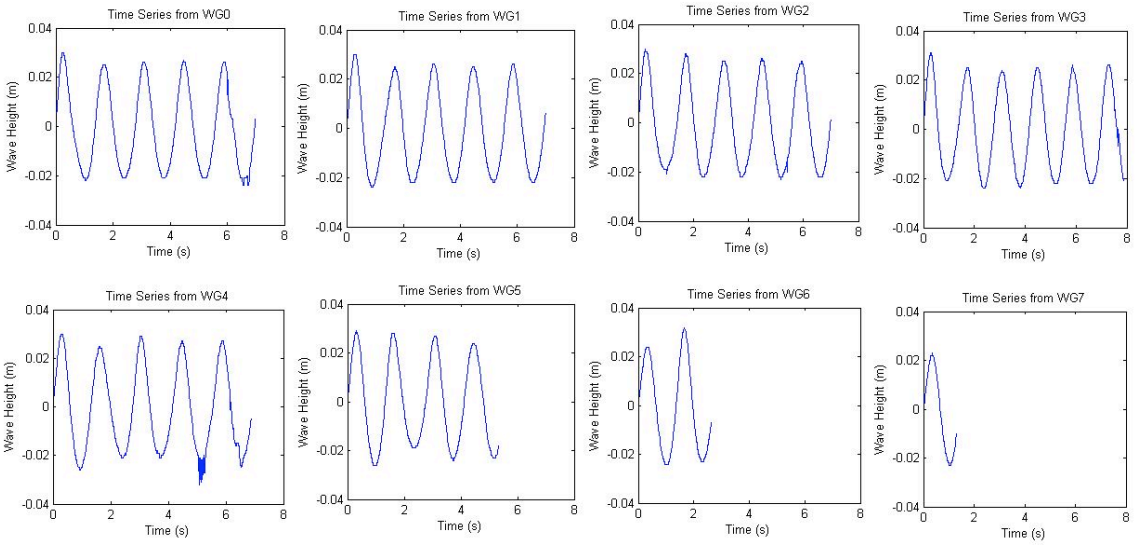

Figure 6.4. Utilized free surface elevation time series of second order Madsen simulation of Case 11.

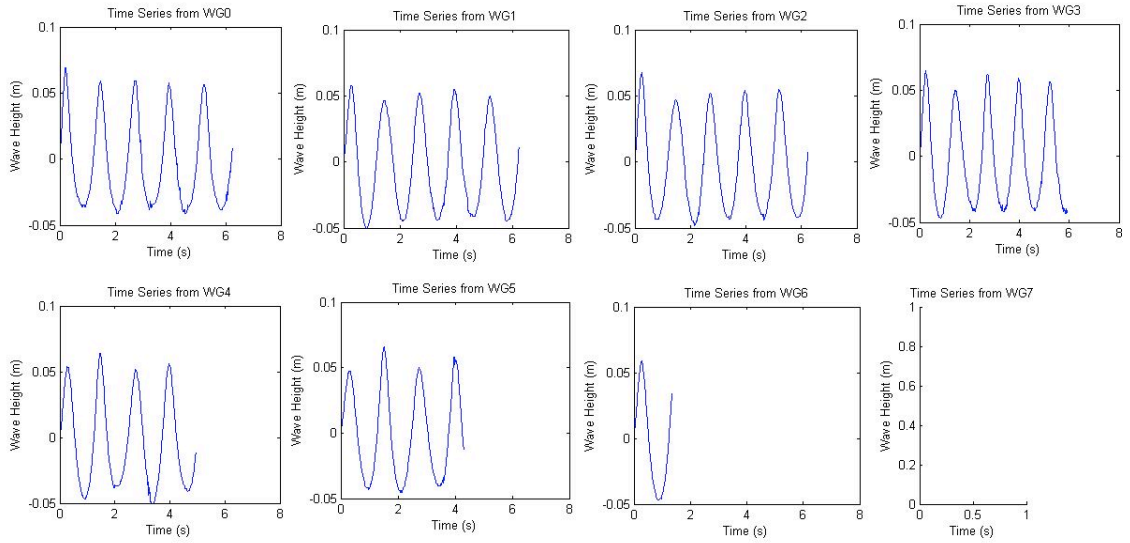

Figure 6.5. Utilized free surface elevation time series of second order Madsen simulation of Case 14.

6.3.2. WAVE HEIGHT

The wave height found from the zero upcrossing method at each wave gauge, the generated wave height (the average), and the ratio between the generated wave height and the simulated wave height are summarized in Table 6.1. All the wave heights are given in meters.

From this table we can see that the wave height changes as the wave propagates along the wave flume, in cases more noticeably than others. Also, the generated wave height exceeds the simulated wave height. For Case 2 this difference is the largest, for Case 11 it is the smallest.

Table 6.1. Wave height recorded at each wave gauge, average, and ratio of generated wave height to simulated wave height.

Case	WG0	WG1	WG2	WG3	WG4	WG5	WG6	WG7	Avg.	H/H_{sim}
2	0.1120	0.1038	0.1118	0.1187	0.1170	0.1120	-	-	0.1126	1.1714
9	0.1392	0.1374	0.1355	0.1413	0.1417	0.1420	-	-	0.1395	1.0900
11	0.0486	0.0488	0.0488	0.0488	0.0478	0.0510	0.0480	-	0.0488	1.0173
14	0.0992	0.0972	0.0992	0.1020	0.1017	0.0973	0.1060	-	0.1004	1.0455

6.3.3. HARMONICS

From the spectral analysis the frequency spectrums and the normalized frequency spectrums were found. Figure 6.5 and Figure 6.6, Figure 6.7 and Figure 6.8, Figure 6.10 and Figure 6.11, and Figure 6.12 and Figure 6.13 show the frequency spectrum and the normalized frequency spectrum for Case 2, Case 9, Case 11, and Case 14, respectively.

For Case 2 the peak frequency is 0.49 Hz, which is close to the desired 0.5 Hz. There is also a defined second peak at a frequency close to twice the peak frequency, 1 Hz, and a smaller third peak can be seen at all wave gauges, except WG1, which has a frequency of about three times the peak frequency, 1.5 Hz. This can also be seen in the normalized spectrum. The height of the second peak has a maximum of 0.1744 and an average of 0.1524. Also, we may see that the wave spectrum remains fairly constant throughout each wave gauge.

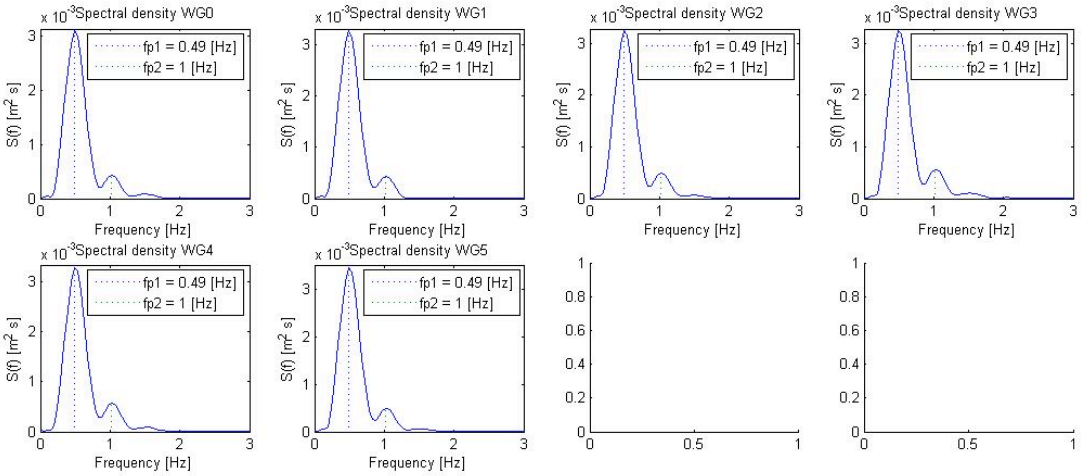

Figure 6.6. Spectral density plot of second order Madsen simulation of Case 2.

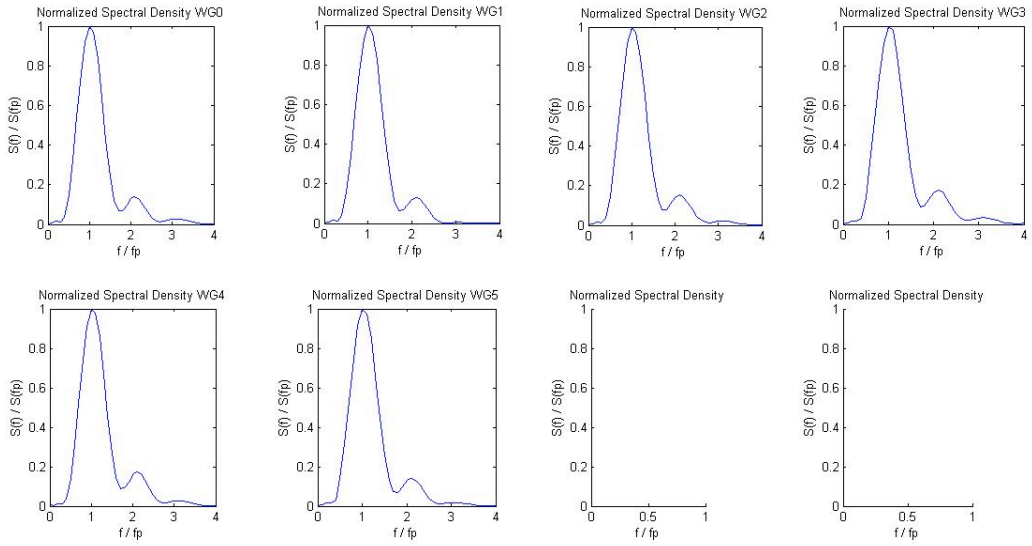

Figure 6.7. Normalized spectral density plot of second order Madsen simulation of Case 2.

For Case 9 we find a peak frequency of 0.73 Hz, which is close to the expected 0.714 Hz. There is also a second peak at a frequency of 1.4 Hz, which is close to twice the peak frequency. A third peak is also visible at a frequency about three times the peak frequency. This may also be seen in the normalized spectrum. The height of the second peak has a maximum of 0.1610, and an average of 0.1053. Here the spectrums also remain fairly similar.

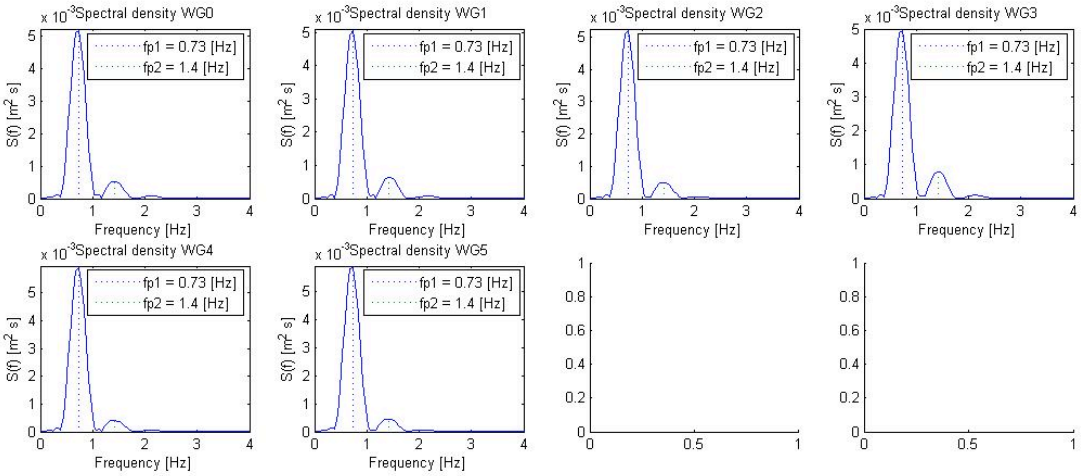

Figure 6.8. Spectral density plot of second order Madsen simulation of Case 9.

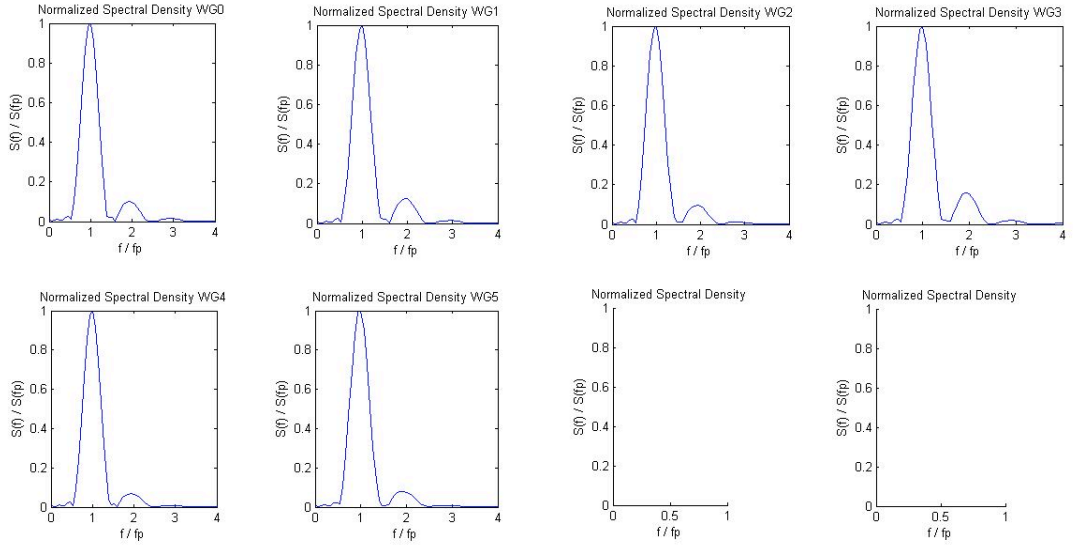

Figure 6.9. Normalized spectral density plot of second order Madsen simulation of Case 9.

For Case 11 we find a peak frequency of 0.73 Hz, except for at wave gauge WG4 where it is 0.68 Hz. This is close to the expected frequency, 0.714 Hz. In this case there is not a well defined second peak.

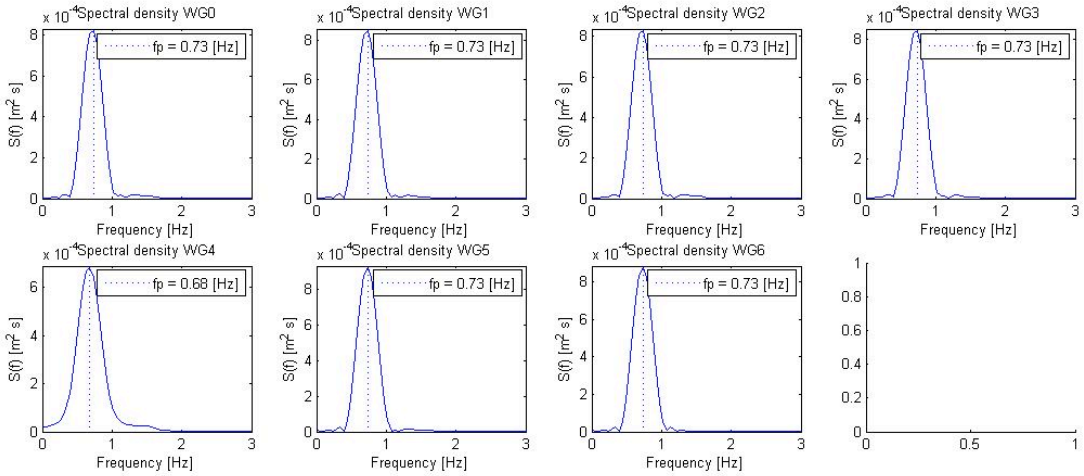

Figure 6.10. Spectral density plot of second order Madsen simulation of Case 11.

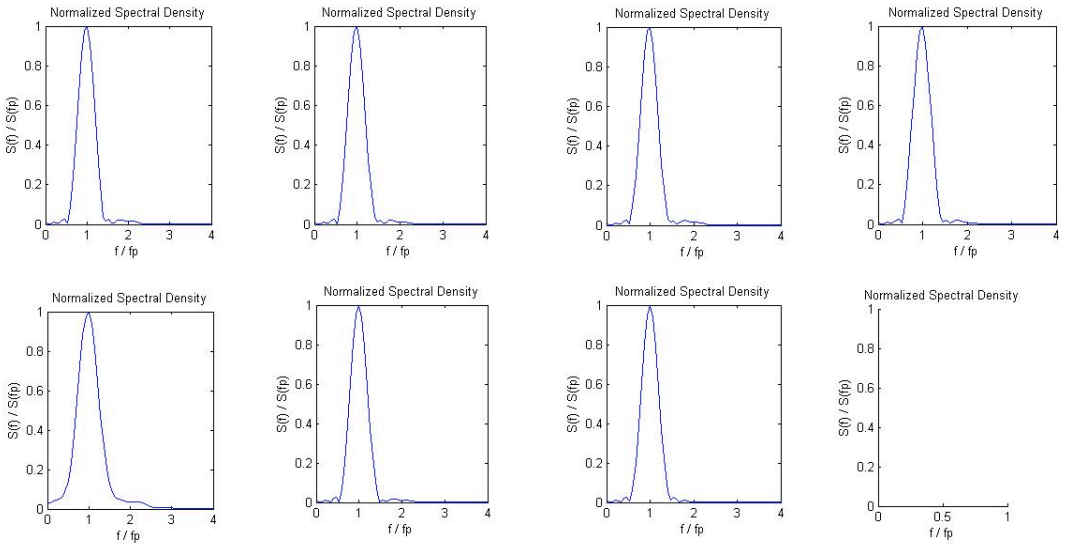

Figure 6.11. Normalized spectral density plot of second order Madsen simulation of Case 11.

For Case 14 we find a peak frequency of 0.78 Hz, except for at wave gauge WG6, where it is 0.83 Hz. This is close to the expected frequency, 0.8 Hz. There is also a small, but well-defined second peak at a frequency of 1.6 Hz, twice the peak frequency. The height of the second peak has a maximum of 0.0757, and an average of 0.0390. Here the spectrums remain fairly similar, with the exception of WG0.

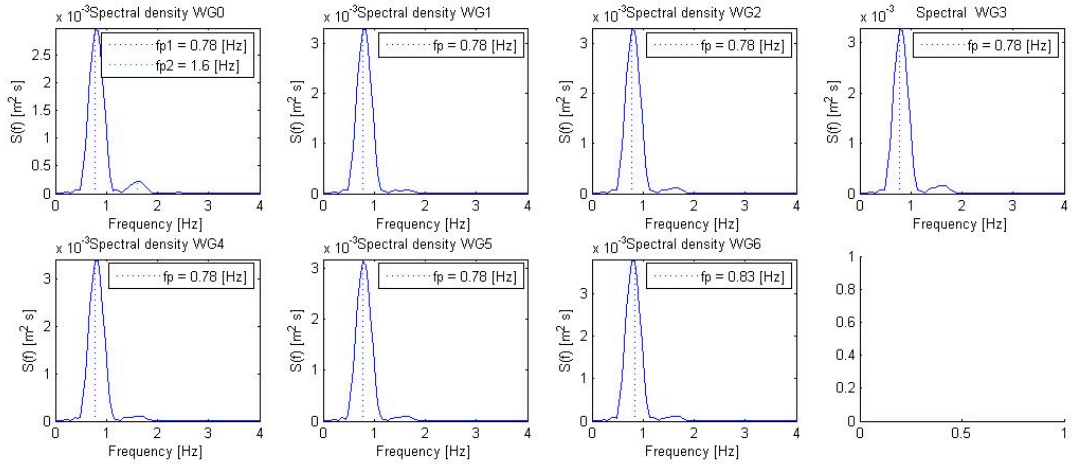

Figure 6.12. Spectral density plot of second order Madsen simulation of Case 14.

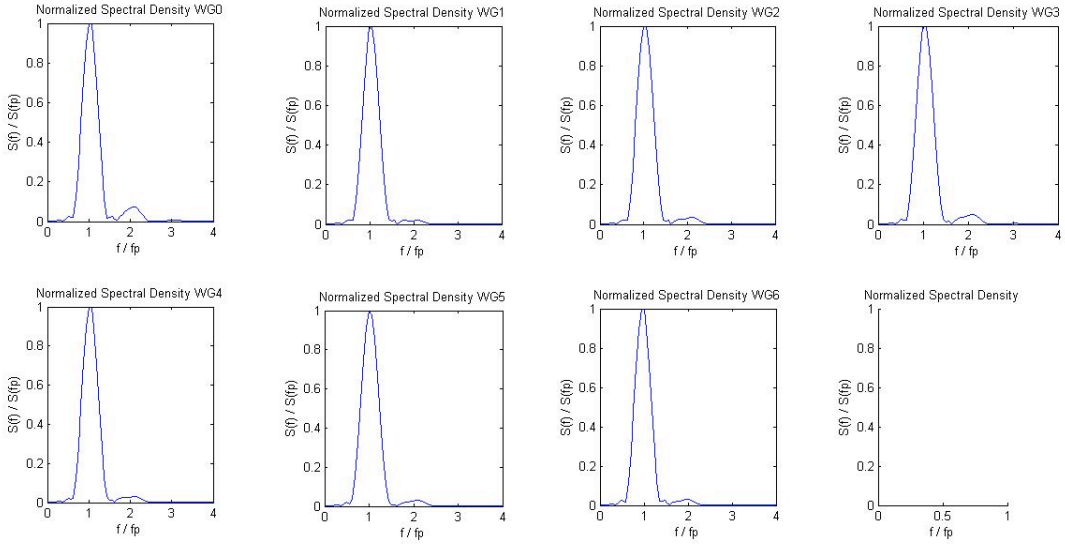

Figure 6.13. Normalized spectral density plot of second order Madsen simulation of Case 14.

The height of the second peak found at each wave gauge, and the average, for each case are summarized in Table 6.2.

Table 6.2. Height of normalized secondary peak recorded at each wave gauge and average.

Case	WG0	WG1	WG2	WG3	WG4	WG5	WG6	WG7	Avg.
2	0.1395	0.1318	0.1523	0.1740	0.1744	0.1426	-	-	0.1524
9	0.1022	0.1257	0.0963	0.1610	0.0680	0.0788	-	-	0.1053
11	0.0212	0.0177	0.0212	0.0146	0.0407	0.0154	0.0056	-	0.0195
14	0.0757	0.0212	0.0344	0.0497	0.0299	0.0308	0.0315	-	0.0390

6.4. COMPARISON TO FIRST ORDER WAVE GENERATION RESULTS

In order to find if the second order Madsen wavemaker theory was capable of reducing the appearance of the unwanted secondary waves the results of the second order Madsen numerical wave generation simulation will be compared to the results of the first order numerical wave generation simulation.

6.4.1. WAVE PROFILE

Figure 6.13, Figure 6.14, Figure 6.15, and Figure 6.16 show the free surface elevation time series of both the first order (the blue line) and the second order Madsen (the green line) numerical simulation of Case 2, Case 9, Case 11, and Case14, respectively.

For Case 2 we can see that the appearance of the second crest, which is significant in the first order time series, is reduced for the second order Madsen time series, and the wave profile becomes more constant. For the other cases, Case 9, Case 11, and Case 14, the difference between the two time series is not significant.

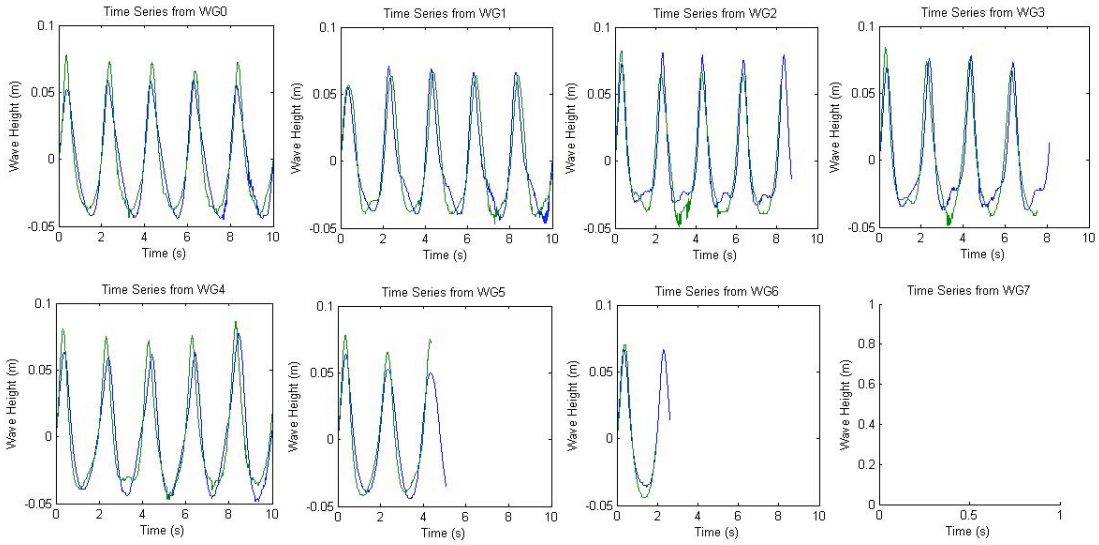

Figure 6.14. First order (blue) and second order Madsen (green) free surface elevation time series of Case 2.

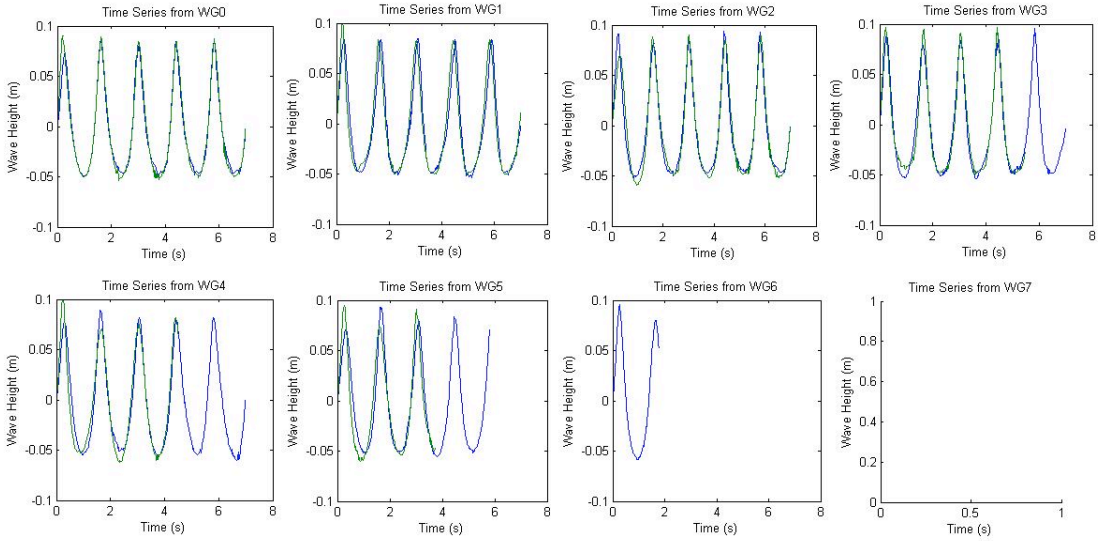

Figure 6.15. First order (blue) and second order Madsen (green) free surface elevation time series of Case 9.

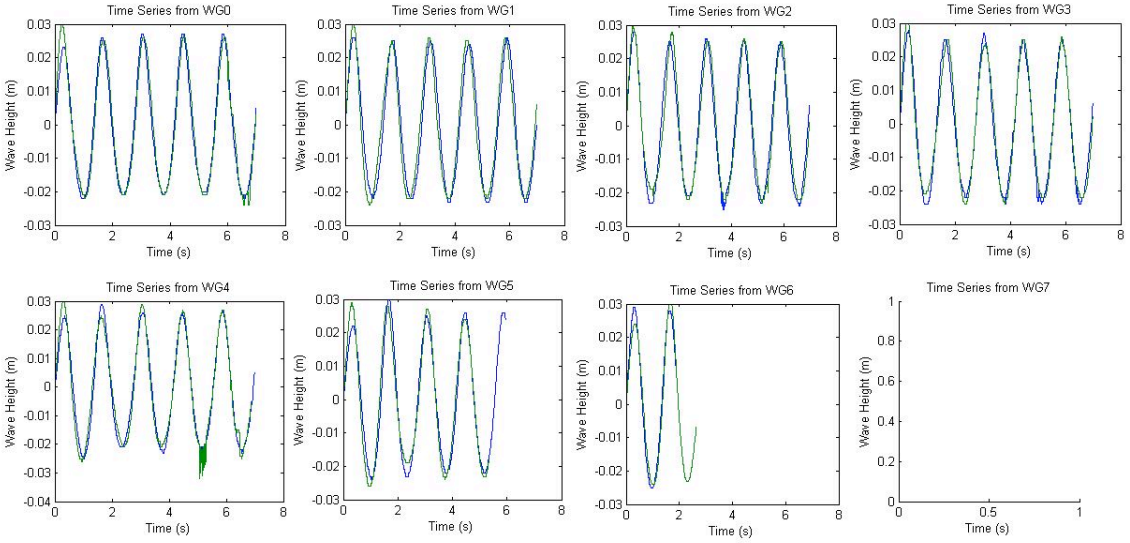

Figure 6.16. First order (blue) and second order Madsen (green) free surface elevation time series of Case 11.

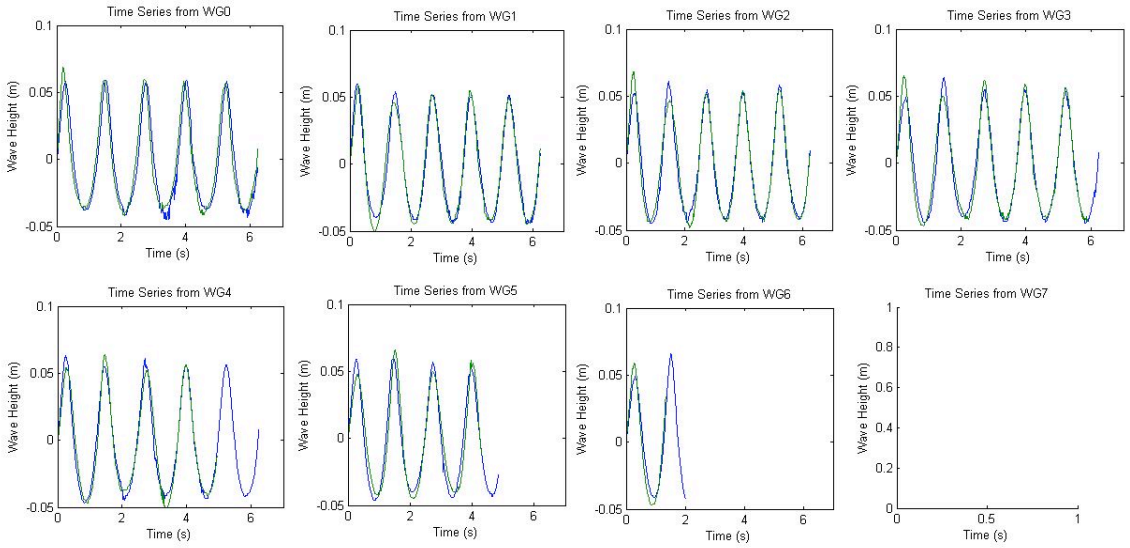

Figure 6.17. First order (blue) and second order Madsen (green) free surface elevation time series of Case 14.

6.4.2. WAVE HEIGHT

Table 6.3 shows a summary of the wave height found at each wave gauge, and the average wave height for both the first order and the second order Madsen numerical wave

generation simulation. The wave heights are given in meters, and the results of the second order Madsen simulation are highlighted in grey. From this table we may see that for both wavemaker theories the wave height changes along the wave flume. For Case 2 the generated wave height is increased when using second order Madsen wavemaker theory, and it is kept more constant. This is also true for Case 9 and Case 14, but to a smaller degree. For Case 14 the generated wave height decreases, but not very significantly.

Table 6.3. Wave height recorded at each wave gauge, and the average wave height, for both the first order and second order Madsen (highlighted in grey) numerical wave generation test.

Case	WG0	WG1	WG2	WG3	WG4	WG5	WG6	WG7	Avg.	H/H_{sim}
2	0.0918	0.1053	0.1093	0.1103	0.1094	0.1005	0.1040	-	0.1044	1.0872
2	0.1120	0.1038	0.1118	0.1187	0.1170	0.1120	-	-	0.1126	1.1714
9	0.1290	0.1084	0.1372	0.1365	0.1370	0.1345	0.1540	-	0.1338	1.0453
9	0.1392	0.1374	0.1355	0.1413	0.1417	0.1420	-	-	0.1395	1.0900
11	0.0472	0.0475	0.0492	0.0496	0.0494	0.0485	0.0540	-	0.0493	1.0280
11	0.0486	0.0488	0.0488	0.0488	0.0478	0.0510	0.0480	-	0.0488	1.0173
14	0.0990	0.0960	0.0990	0.0990	0.1020	0.1020	0.0900	-	0.0981	1.0223
14	0.0992	0.0972	0.0992	0.1020	0.1017	0.0973	0.1060	-	0.1004	1.0455

6.4.3. HARMONICS

Figure 6.17, Figure 6.18, Figure 6.19, and Figure 6.20 show the normalized spectrum found for both the first order (the blue line) and the second order Madsen (the green line) numerical simulation for Case 2, Case 9, Case 11, and Case 14, respectively.

For Case 2 we can see that the normalized spectrum has a more constant shape with the second order Madsen wavemaker theory. Also, the maximum height of the second peak is significantly reduced. For the other cases, Case 9, Case 11, and Case 14, the normalized spectrum is fairly similar for both wavemaker theories, with only slight variations.

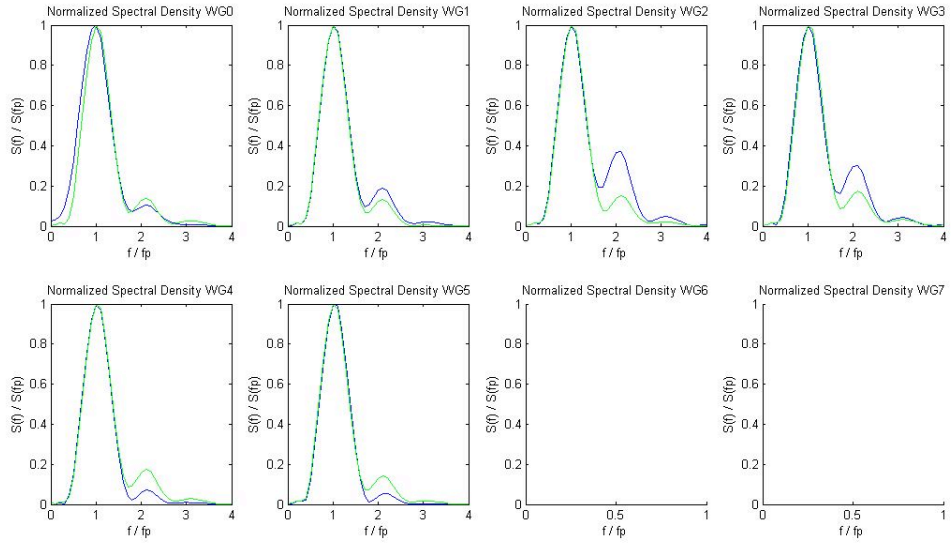

Figure 6.18. First order (blue) and second order Madsen (green) normalized spectral density plot of Case 2.

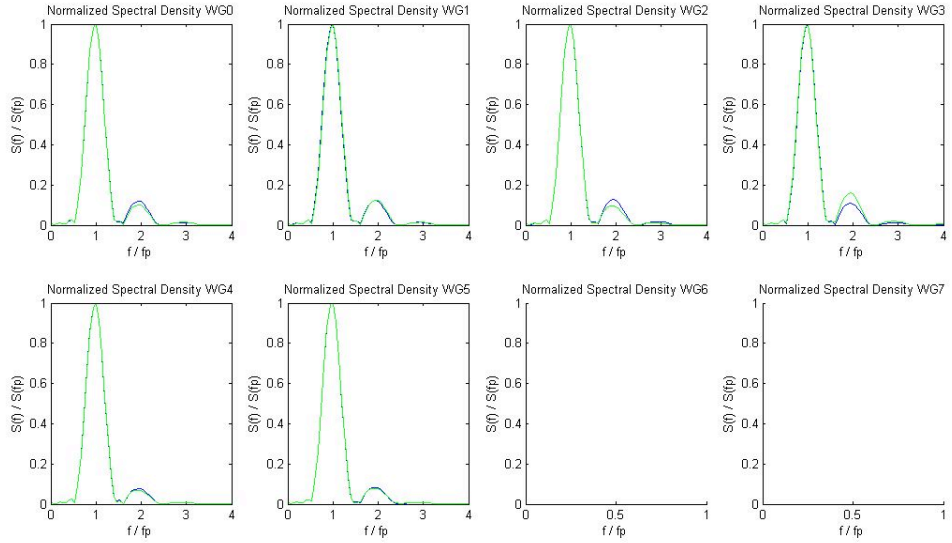

Figure 6.19. First order (blue) and second order Madsen (green) normalized spectral density plot of Case 9.

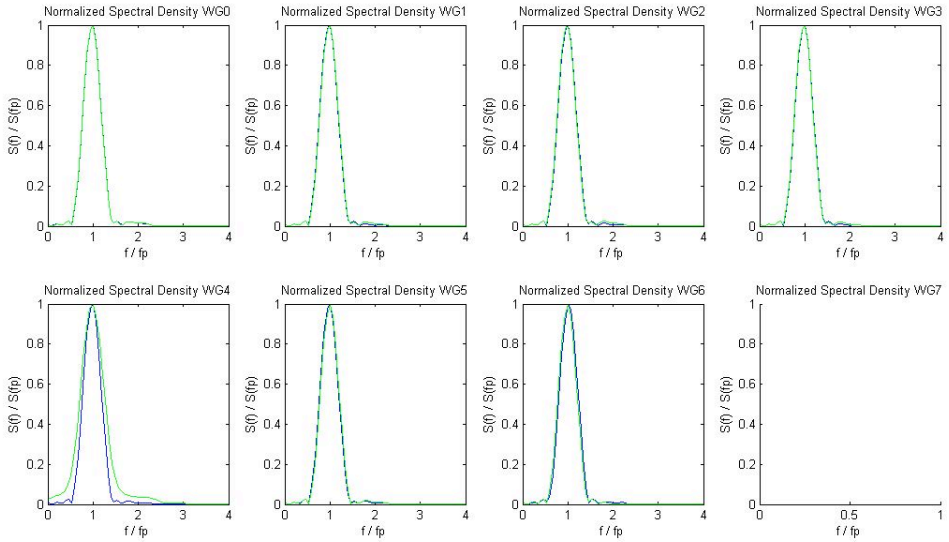

Figure 6.20. First order (blue) and second order Madsen (green) normalized spectral density plot of Case 11.

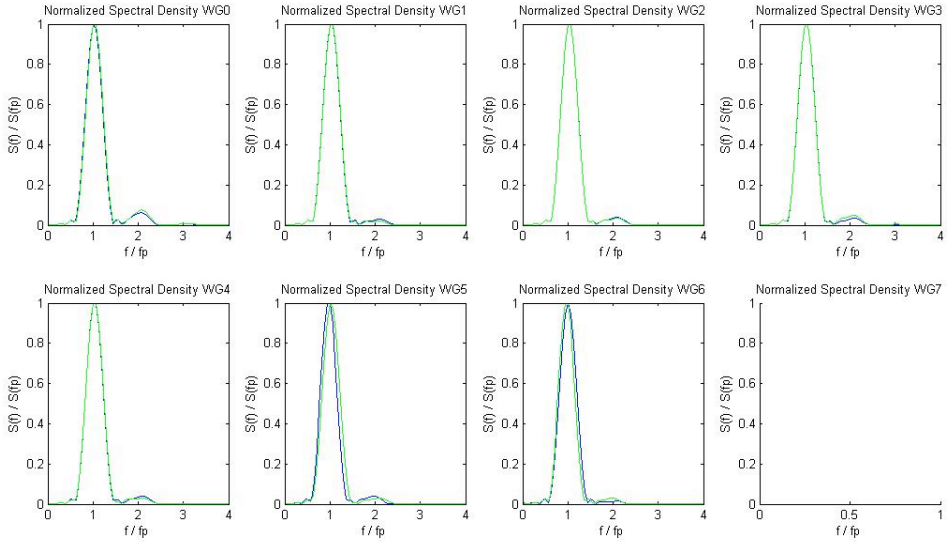

Figure 6.21. First order (blue) and second order Madsen (green) normalized spectral density plot of Case 14.

Table 6.4 summarizes the height of the second peak and the average for Case 2, Case 9, Case 11, and Case14. Here we can see that the average height or the second peak is reduced using the second order Madsen wavemaker theory in Case 2. This is also true

for Case 9, but to a smaller degree. For Case 11 and Case 14 the second order theory increased the height of the second peak slightly.

Table 6.4. Height of normalized secondary peak recorded at each wave gauge for the first order and the second order Madsen (highlighted in grey) numerical wave generation test.

Case	WG0	WG1	WG2	WG3	WG4	WG5	WG6	WG7	Avg.
2	0.1046	0.1899	0.371	0.3033	0.0712	0.0552	0.1362	-	0.1759
2	0.1395	0.1318	0.1523	0.1740	0.1744	0.1426	-	-	0.1524
9	0.1213	0.1239	0.1292	0.1094	0.077	0.0836	0.0976	-	0.1060
9	0.1022	0.1257	0.0963	0.1610	0.0680	0.0788	-	-	0.1053
11	0.0201	0.0088	0.0109	0.0093	0.0127	0.0107	0.0127	-	0.0122
11	0.0212	0.0177	0.0212	0.0146	0.0407	0.0154	0.0056	-	0.0195
14	0.0621	0.031	0.0376	0.0332	0.0407	0.0406	0.0149	-	0.0372
14	0.0757	0.0212	0.0344	0.0497	0.0299	0.0308	0.0315	-	0.0390

7. CONCLUSIONS AND RECOMMENDATIONS

7.1. CONCLUSIONS

7.1.1. FIRST ORDER WAVE GENERATION

From the results of the physical wave generation experiments, Section 5.1.3, we find that when generating waves with a low relative water depth, h/L_0, and/or high wave steepness, H/L, in the CIEMito wave flume using first order wavemaker theory, the desired waves are contaminated by unwanted secondary waves. This follows the description given by Goda (1967). The wave profile will vary as the wave propagates along the wave flume, and there is a visible secondary wave crest. The secondary wave crest will be at the trough of the primary wave at one point, and, since it travels at a slightly slower speed than the primary wave, it will then slowly recede so that the primary crest absorbs it, and then move to the trough of the primary wave again.

The actual wave height generated by the piston paddle was not the same as the expected wave height. There may be two reasons for this, the inefficiencies of the paddle, and the unwanted secondary waves. The piston paddle does not have a perfect seal along the edges, so that when it moves back and forth some water will seep through the sides, between the flume panel and the paddle. This is water that should have been set in motion, but since it escapes through the sides it causes the generated wave to be smaller than expected. It seems as though for a given wave period the efficiency of the paddle is increased for a larger wave height, but this could also be due to the second factor which affects the generated wave height, the unwanted secondary waves.

The secondary waves also produce a difference between the obtained wave height and the expected wave height. As can be seen from Section 5.2.3, the obtained wave height in the PFEM numerical wave flume simulations differs form the simulated wave height, even though the PFEM numerical wave flume does not have any inefficiency. The differences in wave height come from the generation of unwanted waves, which slightly increase the resulting wave height. Therefore, for a given wave period, the waves with a larger height, and because of this higher wave steepness, will appear to

have a higher efficiency, but in reality the generated wave has a higher contamination of secondary waves. This will be true as long as the waves conditions being generated have the issue of unwanted secondary waves. In Section 5.1.3, it can be seen that for Set 1, cases 1 through 12 agree with this, but cases 13 through 24 do not. Cases 13 through 24 have the higher relative water depth, above 0.13, and therefore lowest generation of unwanted secondary waves. Here the efficiency is higher for the waves with smaller height. For Set 1 the average efficiency of the generated wave height was of 83.5%, the maximum being 87.4% and the minimum 71.1%. For Set 2 the average efficiency of the generated wave height was of 85.0%, the maximum being 92.9% and the minimum 77.62%. Since the generated wave height differs from the expected wave height, the generated wave will have different characteristics than expected.

From the spectral analysis of the wave generation it was found that the generation of unwanted secondary waves is inversely related to the relative water depth, so that as the relative water depth increases the generation of unwanted waves decreases. Also, the generation of unwanted waves is directly related to the wave steepness, so that as the wave steepness decreases, the generation of unwanted secondary waves decreases as well. In Figure 5.26 we can see that for the CIEMito wave flume, for a relative water depth above 0.13 the unwanted secondary wave generation becomes much less significant. This agrees with Goda (1967) where it is stated that waves with a relative water depth above 0.15 will not generate unwanted waves. Still, it is seen that for the conditions with a higher relative water depth, if the wave height is large, therefore increasing the wave steepness, there will be more significant secondary wave generation. Using the Ursell number, which is used to measure the nonlinearity of a wave, may be a good way to include both the relative water depth and the wave steepness. From Figure 5.27 we find that as the Ursell number increases, the generation of secondary waves increases exponentially.

Also from the spectral analysis it was seen that the secondary waves have a frequency that is a multiple of the desired frequency. The secondary peaks appear at $2f_p$, $3f_p$, and so on. Still, in order for the second harmonic at $3f_p$ to appear, the relative water depth must be very low, and the wave steepness high. Only in a few cases did the third peak appear, and in most of these it was not very significant.

From the comparison of the results of the physical and numerical wave generation experiments, Section 5.3, we find that the PFEM numerical wave flume is a good tool for the simulation of wave generation in the CIEMito wave flume. The free surface elevation time series obtained from the PFEM numerical wave flume simulation of the CIEMito wave flume closely resembles the free surface elevation time series found in the actual CIEMito wave flume. Also, when finding the normalized spectrums, the results from the numerical model are very similar to the results from the physical model. The unwanted secondary waves are well simulated in the numerical model. There are some slight differences, but overall the PFEM numerical wave flume may be used with confidence to simulate the CIEMito wave flume.

The PFEM numerical wave flume simulations also provide an advantage to the actual physical wave generation. Other types of data than just free surface elevation may be obtained from the numerical model, such as particle velocities or pressure. This may be useful to study other characteristics of the waves generated in a wave flume.

7.1.2. SECOND ORDER WAVE GENERATION

From the study of the state of the art of second order wavemaker theories, Chapter 3, we can see that it is not easy to implement a second order wavemaker theory for the CIEMito wave flume. Some of the available theories do not provide a definition for all their variables, so it was not possible to program them. Then, the theories that did provide all the information, such as the one given by Schäffer (1996), are mathematically complex, which makes it very difficult to apply. Because of this it was only possible to implement the second order wavemaker theory given by Madsen (1971) to the CIEMito wave flume.

From the results of the wave generation simulations using the second order Madsen wavemaker theory, Section 6.1.3, we find that in general, for the CIEMito wave flume, this theory did not alleviate the generation of unwanted secondary waves. Only for one of the simulated wave conditions, Case 2, the results show improvement, even though it did not meet the criteria set forth by Madsen. For Case 2, even though the secondary waves are still present, the wave profile is more constant as the wave travels along the wave flume. Also, from the normalized spectrum we see that for Case 2 the

amount of energy in the first harmonic is reduced. The other wave conditions did not show significant improvements. Another second order wavemaker theory should be used to eliminate the unwanted secondary wave problem.

7.2. RECOMMENDATIONS

Further study is required in order to fully assess the ability of second order wavemaker theories to suppress the appearance of unwanted secondary waves. The second order Madsen wavemaker theory was only tested for four wave conditions, which may be very few to give a definitive result. Even though the results of this study were not very promising for this theory, it needs to be tested in other wave conditions to find if there are wave conditions where it is more efficient. Also, other second order wavemaker theories have to be adapted to the CIEMito wave flume and teste. The second order wavemaker theory given by Schäffer (1996) would be a good theory to investigate. If the use of the CIEMito wave flume is not possible for these experiments, the PFEM numerical wave flume may be used with confidence.

Another interesting study would be to perform experiments on a given process driven by waves, such as overtopping, by using both linear and second order wavemaker theories. This way it would be possible to find if the use of second order wavemaker theory would make a significant impact on the results.

Finally, it is important to test these theories for generating irregular waves. When generating irregular waves other issues may arise, and it is necessary to find how these theories would perform under these conditions.

BIBLIOGRAPHY

- **Bièsel, F., and Suquet, F. 1954.** "Laboratory Wave-Generating Apparatus." (Translation of French Articles from *La Houille Blanche),* Project Report No. 39, Anthony Falls Hydraulic Laboratory, University of Minnesota.

- **CEM, 2005.** "Chapter 1: Water Wave Mechanics." *Coastal Engineering Manual.* May 2009. Web. <http://chl.erdc.usace.army.mil/cem>.

- **CIEMLAB, 2010.** "CIEMito." *Canal d'Investigació i Experimentació Marítima (CIEMLAB)*. May 2010. Web. 13 May 2010. <http://ciemlab.upc.edu/facilities/ciemito>.

- **Calabrese, *et al*. 2009. "**The Generation of Periodic Shallow Water Waves in a Flume: Theory and Measurements." *Proc. 2nd Int. Conf. on the Application of Physical Modelling to Port and Coastal Protection (Coastlab)*, in print (2009).

- **Daugaard, E. 1952.** "Generation of Regular Waves in the Laboratory." Doctoral Dissertation, Institute of Hydrodynamics and Hydraulic Engineering, Technical University of Denmark.

- **Dean, R. G., Dalrymple, R. A. 1984.** "Water Wave Mechanics for Engineers and Scientists." Prentice-Hall, Inc., Englewood Cliffs, New Jersey.

- **Flick, R. E., and Guza, R. T. 1980.** "Paddle Generated Waves in Laboratory Channels." *Journal of the Waterway, Port, Coastal and Ocean Division,* ASCE, Vol 106, No, WW1, pp. 79-97.

- **Fontanet, P. 1961.** "Theorie de la Génération de la Houle Cylindrique par un Batteur Plan." *La Houille Blanche,* Vol. 16, No. 1, pp. 3-31.

- **Goda Y. 1967.** "Travelling Secondary Wave Crests in Wave Channels." Appendix to: "Laboratory Investigation on Wave Transmission Over Breakwaters." Report No. 13, Port and Harbor Research Institute, pp. 32-38

- **Goda, Y. 1997.** "Recurring Evolution of Water Waves Through Nonresonant Interactions." *Proc. 3rd Int. Symp. Ocean Wave Measurements and Analysis (WAVES '97)*, Virginia Beach, 1-23, ASCE (1997).

- **Goring, D. G. 1979.** "Tsunamis- The Propagation of Long Waves Onto a Shelf." Doctoral Dissertaion, Report No. KH-R-38, W.M. Keck Laboratory of Hydraulics and Water Resources, California Institute of Technology.

- **Havelock, T. H. 1929.** "Forces Surface Wave on Water." *Philosophical Magazine,* Series 7, Vol. 8, pp. 569-576.

- **Hudspeth, R. T., and Sulisz, W. 1991.** "Stokes Drift in Two-Dimensional Wave Flumes." *Journal of Fluid Mechanics,* Vol. 230, pp. 209-229.

- **Hughes, S. A. 1993.** "Physical Models and Laboratory Techniques in Coastal Engineering." World Scientific Publishing Co. Pte. Ltd., JBW Printers & Binders Pte. Ltd., Singapore.

- **Le Méhauté, B. 1976.** "Introduction to Hydrodynamics and Water Waves." Springer-Verlag, New York.

- **Madsen, O. S. 1971.** "On the Generation of Long Waves." *Journal of Geophysical Research,* Vol. 76, No. 36, pp. 8672-8683.

- **Moubayed, W. I. and Williams, A. N. 1994.** "Second-Order Bichromatic Waves Produced by a Generic Planar Wavemaker in a Two-Dimensional Wave Flume." *Journal of Fluids and Structures,* Vol. 8, pp. 73-92.

- **Nelson, R. C. 1994.** "Depth Limited Wave Heights in Very Flat Regions." *Coastal Engineering*, Vol. 23, pp. 43-59.

- **Oliveira, T. C. A. *et al.* 2009.** "Nonlinear Wave Generation in Numerical and Physical Flumes." *Journal of Coastal Research,* SI 56 (Proceedings of the 10th International Coastal Symposium), pp. 1025-1029, Lisbon, Portugal.

- **Oliveira, T. C. A. *et al.* 2009b.** "Absorption of water waves in a two-dimensional numerical flume." Computational Methods in Marine Engineering III, T. Kvamsdal, B. Pettersen, P. Bergan, E. Oñate and J. García eds., CIMNE, Barcelona, Spain, 105-108.

- **Schäffer, H. A., 1996.** "Second-Order Wavemaker Theory for Irregular Waves." *Ocean Engineering*, Vol. 23, No. 1, pp. 47-88.

- **Ursell, F., et al., 1960.** "Forced Small-Amplitude Water Waves: A Comparison of Theory and Experiment." *Journal of Fluid Mechanics,* Vol. 7, Part 1, pp. 3-52.

- **Zhang, H., and Schäffer, H. A., 2006.** "Approximate Stream Function Wavemaker Theory for Highly Non-Linear Waves in Wave Flumes." *Ocean Engineering*, Vol. 34, pp. 1290-1302.

APPENDIX A

Matlab routine to find the necessary paddle movement to obtain regular waves with given characteristics using first order wavemaker theory.

```
% 1st Order Regular Waves

clear all
close all

% 1.INPUT

% General
g=9.81;   %gravity in meters/second^2

% Wave data
H=0.16;   %wave height in meters
T=2.0;    %wave period in seconds

% Geometrical data
h=0.32;  %water depth in meters
gamma=1; %correction factor
Smax=0.27;  %maximun paddle movement in meters

% Sampling data
freq=100;  %frequency of paddle positon data in Hz
N=10;      %number of waves to be produced
time=0;   %duration of the wave generation in seconds

% 2.PROCESSING
```

```
% 2.1.Find the time from the number of waves
if time==0
   time=N*T;
end

% 2.2.Find wave characteristics (wave length, number, and frequency)

  % first find the wave lenght (iterative)
g=9.81;              %gravity in m/s^2
Lo=(g*(T^2))/(2*pi);  %deep water wave length
L1=Lo;               %wave length to be changed to find actual wavelength

a=0;       %variable used to stop the following loop
while a~=1
   b=Lo*tanh((2*pi*h)/L1);  %%%%revisar si tengo que pasar esto a radianes
   if L1-b<=0.00001
      L=b;
      a=1;
   else
      L1=L1-0.00001;
   end
end

  % from wave length can get the wave number
k=(2*pi)/L;  %wave length

  % could either get the wave frequency from period
  % or from the wave number
sigma1=(2*pi)/T;
sigma2=sqrt(g*k*tanh(k*h));    % check if they are the same
```

```
% 2.3.Values to determine created wave type
HdgT=H/(g*(T^2));
hdgT=h/(g*(T^2));   %To determine what wave theory would best describe the wave

hdL=h/L;     %Values taken from the CEM
WaveType='Transitional';
if hdL>=0.5
   WaveType='Deep Water';
elseif hdL<=0.04
   WaveType='Shallow Water';
end

% 2.4.Use transfer function for piston paddle (including correction factor)
So=H*((sinh(2*k*h)+(2*k*h))/(4*((sinh(k*h))^2)))*gamma;

% 2.5.Determine if possible to create wave
RelativeWaveHeight=H/h;
if RelativeWaveHeight>0.78
   Error1='Breaking Limit Exceeded';
elseif RelativeWaveHeight<=0.78
   Error1='Breaking Limit No Error';
end

WaveSteepness=H/L;
if WaveSteepness>0.142
   Error2='Steepness Limit Exceeded';
elseif WaveSteepness<=0.142
   Error2='Steepness Limit No Error';
end

if So>Smax
```

```
   Error3='Smax Exceeded';
elseif So<=Smax
   Error3='Smax No Error';
end

% 2.6.Find position of the paddle in time
dt=1/freq;    % duration of each time step (uniform)
t=0:dt:time;
lt=length(t);

for i=1:1:lt
   X(i,1)=(So/2)*sin(sigma1*((1/freq)*(i-1)));
end

% 3.OUTPUT

% 3.1.Create output file with paddle position, and hedder with frequency
for i=2:1:lt+1
   Xo(1,1)=freq;  %Header to indicate the frequency (Hz) of the data given
   Xo(i,1)=(So/2)*sin(sigma1*((1/freq)*(i-2))); %Paddle position (m)
end

save FirstOrderRegularT05H04.txt Xo -ASCII;

% 3.2.Graph of paddle position in time
plot(t,X*100)
xlabel('Time (s)')
ylabel('Paddle Position (cm)')
title('Plot of Position of the Paddle in Time')
```

APPENDIX B

Matlab routine to find the necessary paddle movement to obtain regular waves with given characteristics using Madsen's second order wavemaker theory.

```
% 2nd Order Madsen Regular Waves

clear all
close all

% 1.INPUT

% General
g=9.81;   %gravity in meters/second^2

% Wave data
H=0.12;   %wave height in meters
T=2.0;    %wave period in seconds

% Geometrical data
h=0.32;  %water depth in meters
gamma=1; %correction factor
Smax=1;  %maximun paddle movement in meters

% Sampling data
freq=100;  %frequency of paddle positon data in Hz
N=10;      %number of waves to be produced
time=0;   %duration of the wave generation in seconds

% 2.PROCESSING
```

```
% 2.1.Find the time from the number of waves
if time==0
   time=N*T;
end

% 2.2.Find wave characteristics (wave length, number, and frequency)

  % first find the wave lenght (iterative)
g=9.81;              %gravity in m/s^2
Lo=(g*(T^2))/(2*pi);  %deep water wave length
L1=Lo;               %wave length to be changed to find actual wavelength

a=0;       %variable used to stop the following loop
while a~=1
   b=Lo*tanh((2*pi*h)/L1);  %%%%revisar si tengo que pasar esto a radianes
   if L1-b<=0.00001
      L=b;
      a=1;
   else
      L1=L1-0.00001;
   end
end

  % from wave length can get the wave number
k=(2*pi)/L;  %wave length

  % could either get the wave frequency from period
  % or from the wave number
sigma1=(2*pi)/T;
sigma2=sqrt(g*k*tanh(k*h));    % check if they are the same
```

```
% 2.3.Values to determine created wave type
HdgT=H/(g*(T^2));
hdgT=h/(g*(T^2));   %To determine what wave theory would best describe the wave

hdL=h/L;     %Values taken from the CEM
WaveType='Transitional';
if hdL>=0.5
   WaveType='Deep Water';
elseif hdL<=0.04
   WaveType='Shallow Water';
end

% 2.4.Determine if Madsen theory applies
if Ur<(8*(pi^2))/3
   Error4='Madsen Applies';
elseif Ur>=(8*(pi^2))/3
   Error4='Madsen Does Not Apply';
end

% 2.5.Use transfer function for piston paddle (including correction factor)
m1=(4*((sinh(k*h))^2))/(sinh(2*k*h)+(2*k*h));
So=(H/m1)*gamma;

% 2.6.Determine if possible to create wave
RelativeWaveHeight=H/h;
if RelativeWaveHeight>0.78
   Error1='Breaking Limit Exceeded';
elseif RelativeWaveHeight<=0.78
   Error1='No Error';
end
```

```
WaveSteepness=H/L;
if WaveSteepness>0.142
   Error2='Steepness Limit Exceeded';
elseif WaveSteepness<=0.142
   Error2='No Error';
end

if So>Smax
   Error3='Smax Exceeded';
elseif So<=Smax
   Error3='No Error';
end

% 2.8.Find position of the paddle in time
dt=1/freq;    % duration of each time step (uniform)
t=0:dt:time;
lt=length(t);

for i=1:1:lt
   X1(i,1)=(So/2)*sin(sigma1*((1/freq)*(i-1)));
   X2(i,1)=((H^2)/(32*h))*(((3*cosh(k*h))/((sinh(k*h))^3))-
(2/m1))*sin(2*sigma1*((1/freq)*(i-1)));
   X(i,1)=X1(i,1)+X2(i,1);
end

% 3.OUTPUT

% 3.1.Create input file with paddle position, and hedder with frequency
for i=2:1:lt+1
   Xo(1,1)=freq;  %Header to indicate the frequency (Hz) of the data given
   Xo(i,1)=X(i-1,1); %Paddle position (m)
```

```
end

save FirstOrderRegularX.txt Xo -ASCII;

% 3.3.Graph of paddle position in time
plot(t,X*100,'k-',t,X1*100,'b:',t,X2*100,'r:')
xlabel('Time (s)')
ylabel('Paddle Position (cm)')
title('Plot of Position of the Paddle in Time')
legend('Actual Displacement','First Order Term','Second Order Term')
```

APPENDIX C

Complete results of the wave generation experiments are included in the attached CD.